

<sup>1</sup> The dating and correlation of an eastern  
<sup>2</sup> Mediterranean lake sediment sequence: a 46 – 4 ka  
<sup>3</sup> tephrostratigraphy for Ioannina (NW Greece)

<sup>4</sup> Amy M. McGuire<sup>1</sup>, Christine S. Lane<sup>1</sup>, Katherine H. Roucoux<sup>2</sup>, Paul G. Albert<sup>3</sup>, and  
<sup>5</sup> Rebecca Kearney<sup>4</sup>

<sup>6</sup> <sup>1</sup>Department of Geography, University of Cambridge, Downing Place, Cambridge, CB2  
<sup>7</sup> 3EN, UK

<sup>8</sup> <sup>2</sup>School of Geography and Sustainable Development, Irvine Building, University of St  
<sup>9</sup> Andrews, North Street, St Andrews, KY16 9AL, UK

<sup>10</sup> <sup>3</sup>Department of Geography, College of Science, Swansea University, Singleton Park,  
<sup>11</sup> Swansea, SA2 8PP, UK

<sup>12</sup> <sup>4</sup>GeoForschungsZentrum Potsdam, Climate Dynamics and Sediments, Telegrafenberg,  
<sup>13</sup> D-14473 Potsdam, Germany

<sup>14</sup> **ABSTRACT**

<sup>15</sup> Terrestrial archives from the Mediterranean have been crucial to expanding our under-  
<sup>16</sup> standing of past environmental variability on a range of timescales. Dating Quaternary  
<sup>17</sup> sequences in the Mediterranean is, however, often challenging, and age models often  
<sup>18</sup> have large chronological uncertainties. Tephra deposits can provide crucial age con-  
<sup>19</sup> trol for detailed environmental reconstructions on sub-centennial timescales. Here,  
<sup>20</sup> tephra analysis is undertaken for the first time on a sediment core (I-08) from Lake  
<sup>21</sup> Ioannina, northwest Greece, for the interval spanning 46 to 4 ka BP. Detailed visible  
<sup>22</sup> and ‘crypto-’ tephra analysis identifies deposits associated with explosive volcanism at  
<sup>23</sup> Italian volcanic sources, including Campi Flegrei, Pantelleria, and the Aeolian Islands.  
<sup>24</sup> We identify two visible tephra layers, the Campanian Ignimbrite (CI/Y-5; ca. 39.8  
<sup>25</sup> ka BP) and Pantelleria Green Tuff (PGT/Y-6; ca. 45.7 ka), as well as the Holocene  
<sup>26</sup> Vallone del Gabellotto cryptotephra marker (VG/E-1; ca. 8.3 ka BP). Evidence for  
<sup>27</sup> repeated remobilisation and redeposition of CI tephra material is outlined, and the  
<sup>28</sup> potential mechanisms and effects of sediment reworking in lake environments are  
<sup>29</sup> examined. Bayesian modelling, which incorporates the new tephra ages with earlier  
<sup>30</sup> radiocarbon dates, extends the I-08 core chronology back to ca. 46 ka BP, facilitating  
<sup>31</sup> direct correlation of the Ioannina sequence to others in the Mediterranean region.

<sup>32</sup> Keywords: tephrochronology, last glacial cycle, Ioannina, Mediterranean, palaeolim-  
<sup>33</sup> nology

## <sup>34</sup> 1 Introduction

<sup>35</sup> Millennial and centennial-scale climate oscillations during the last glacial cycle, such  
<sup>36</sup> as Dansgaard-Oeschger (D-O) oscillations, were first identified in the Greenland ice  
<sup>37</sup> core records (e.g. Dansgaard et al., 1982; Johnsen et al., 1992; Dansgaard et al., 1993;  
<sup>38</sup> Andersen et al., 2004) and, subsequently, in terrestrial and marine sequences throughout  
<sup>39</sup> the North Atlantic realm and into the Mediterranean (e.g. Bond et al., 1993; Allen et al.,  
<sup>40</sup> 1999; Goñi et al., 2000; Roucoux et al., 2001; Tzedakis et al., 2004). Detailed studies of  
<sup>41</sup> last glacial sequences have provided important insights into the heterogeneity of climate  
<sup>42</sup> and environmental responses to abrupt climate change. During the last glacial period  
<sup>43</sup> oscillations between cold D-O stadial and warm D-O interstadial conditions occurred on  
<sup>44</sup> timescales of decades or shorter, and are argued to reflect the interplay between internal  
<sup>45</sup> atmospheric, glacial, and ocean dynamics (Li and Born, 2019; Men viel et al., 2020).  
<sup>46</sup> Detailed proxy studies with secure chronologies are necessary to examine temporal and  
<sup>47</sup> spatial variation in the expression of D-O cycles in the Mediterranean region (e.g. Allen  
<sup>48</sup> et al., 1999).

<sup>49</sup> Developing robust and independently derived chronologies to facilitate accurate  
<sup>50</sup> inter-site comparisons is a necessary, but complex, task (Lowe et al., 2008; Blaauw et al.,  
<sup>51</sup> 2018). Two main dating approaches are typically used to develop chronologies for long  
<sup>52</sup> terrestrial sedimentary records from the Mediterranean. Radiocarbon dating is frequently  
<sup>53</sup> applied to develop chronologies spanning the last 50 ka (e.g. Lawson et al., 2004; Staff  
<sup>54</sup> et al., 2019). Beyond the 50 ka BP upper dating limit of radiocarbon, pollen records  
<sup>55</sup> from terrestrial sites can be correlated to their marine equivalents, and, in turn, to the sea  
<sup>56</sup> surface temperature (SST) and  $\delta^{18}\text{O}$  records therein, which provide age constraints based  
<sup>57</sup> on alignment to the Greenland ice cores and orbital parameter, (e.g. Tzedakis, 2002;  
<sup>58</sup> Tzedakis et al., 2004; Müller et al., 2011; Roucoux et al., 2011). Refining chronologies  
<sup>59</sup> through correlation, however, inhibits our ability to interrogate relative leads and lags in  
<sup>60</sup> environmental responses to climate drivers (Blaauw, 2012). Moreover, the large (often  
<sup>61</sup> millennial-scale) uncertainties inherent in the chronologies to which the records are tuned,  
<sup>62</sup> such as the layer-counting uncertainty in the Greenland ice core records (e.g. Rasmussen  
<sup>63</sup> et al., 2014) are rarely factored into tuned age models.

<sup>64</sup> The central and eastern Mediterranean region is home to numerous active and extant  
<sup>65</sup> volcanic centres and explosive volcanism has produced widespread tephra layers that  
<sup>66</sup> comprise a well-dated and interconnected tephrostratigraphic framework (see Blockley  
<sup>67</sup> et al., 2014; Bronk Ramsey et al., 2015; Lowe and Walker, 2015, and references therein),  
<sup>68</sup> providing scope to test and improve the existing age-depth models of palaeoenvironmental  
<sup>69</sup> records in the region (e.g. Giaccio et al., 2017; Leicher et al., 2016). Furthermore,  
<sup>70</sup> tephra markers form time-parallel event horizons (e.g. Lane et al., 2013; Neugebauer  
<sup>71</sup> et al., 2017) that allow the direct comparison of sequences at and between precise  
<sup>72</sup> moments in time. By integrating palaeoclimate records from different sites, tephra studies  
<sup>73</sup> avoid the often large chronological uncertainties associated with other dating approaches.

74 Analytical advances over the last two decades have improved our ability to extract,  
75 identify, and fingerprint the geochemical composition of glass shards which are not  
76 visible within the sedimentary sequence (known as cryptotephra; Blockley et al., 2005;  
77 Hayward, 2012). Consequently, tephra deposits can be detected at ever-larger distances  
78 from volcanic source regions, increasing the spatial scope of existing tephrostratigraphic  
79 frameworks to continental and, in some cases, hemispheric scales (Davies, 2015; van der  
80 Bilt et al., 2017).

81 This paper presents the first tephra study of last glacial and Holocene sediments  
82 from the key Mediterranean palaeoecological site of Lake Ioannina, NW Greece. In  
83 constructing a last glacial and Holocene tephrostratigraphy for Lake Ioannina, we create  
84 opportunities for direct correlation of the valuable proxy record of millennial- and  
85 centennial-scale change contained within the Ioannina sequence (see Lawson et al., 2004;  
86 Tzedakis et al., 2004; Jones et al., 2013) to other key sites in the central and eastern  
87 Mediterranean region. In doing so, we allow for an interrogation of the sequencing of  
88 local climate and environmental responses to Dansgaard-Oeschger cycles at the periphery  
89 of the North Atlantic climate system.

## 90 2 Study site

91 Lake Ioannina is located in the interior of the Epirus region of northwest Greece, in the  
92 western foothills of the Pindus mountain range (Fig. 1a). The Ioannina basin, ca. 470 m  
93 a.s.l., is situated within a tectonic depression bounded by the gently sloping Tomarochoria  
94 mountains to the west and the steep-sided Mitsikeli mountain to the east. The growth  
95 of the basin has been attributed to karst solution and subsidence (Lawson, 2001, *and*  
96 *references therein*). The lake itself (also known as Lake Pamvotis) has undergone  
97 extensive artificial drainage, culminating in 1959 when the northerly Lapsista sub-basin  
98 (previous water depth 1 to 3 m) was converted to agricultural land (Romero et al., 2002).  
99 Whilst the 'natural' (pre-drainage) scale of the lake basin is not known, it may have been  
100 as large as 20 km (Conispolatis et al., 1986) The longest retrieved sediment record is core  
101 I-284, recovered by the Greek Institute of Geology and Mineral Exploration (IGME),  
102 which records continuous sedimentation back >250 ka BP (Tzedakis, 2002; Lawson  
103 et al., 2004; Roucoux et al., 2008, 2011).

104 The present-day lake (Fig. 1b) is located near the foot of Mitsikeli mountain, in  
105 the southeast of the original basin, is 11 km on its longest axis, with a surface area of  
106 ca. 23 km<sup>2</sup>. The modern lake is shallow, with a maximum water depth of 10 m, and is  
107 a closed system with no major fluvial inputs, although ephemeral streams have been  
108 identified within the basin (Lawson, 2001). The lake is primarily fed by springs, most  
109 notably at the foot of the Mitsikeli Ridge (Fig. 1b; Higgs et al., 1967). Drainage occurs  
110 through sinkholes, termed *katavothrai*, located throughout the basin (Higgs et al., 1967).

111 Previous work at Ioannina has identified millennial-scale expansions and contractions

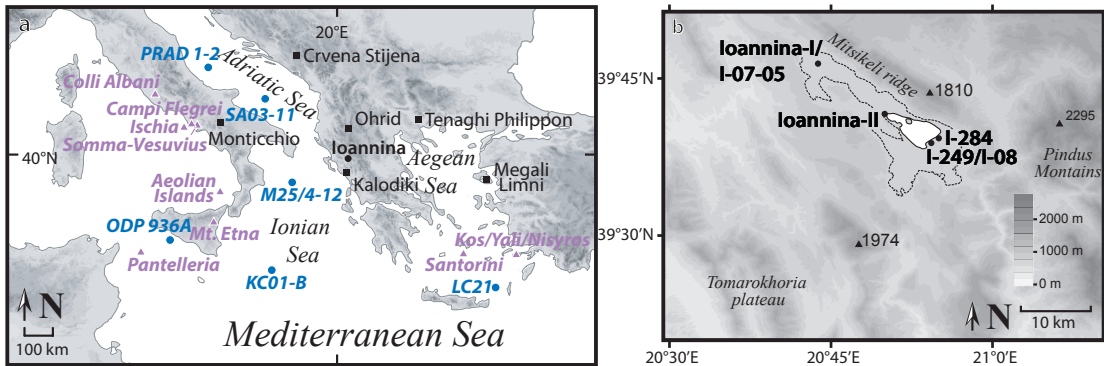


Figure 1. Maps showing (a) the location of the Ioannina site, along with Quaternary terrestrial (black squares) and marine (blue circles) sediment sequences featured in the text, alongside volcanic centres with known last glacial and Holocene activity (purple triangles) and (b) the Ioannina catchment, showing local topography, the present day lake (solid line), the limit of lake sediment deposits (dotted line), and the location of I-08 and earlier core sites.

of tree populations which have been linked to climate oscillations recorded in Greenland and throughout the North Atlantic, however, tuned chronologies inhibit interrogation of the timing of these responses between sites (Tzedakis et al., 2004). More recent studies have sought to generate independent, well-resolved age models for the site (e.g. Jones et al., 2013), however, chronological limitations continue to complicate inter-site comparison of the environmental response to abrupt last glacial climate change between Ioannina and other terrestrial sites in the Central and Eastern Mediterranean. In particular, the hard-water effect, whereby  $^{14}\text{C}$  ages are artificially inflated by unquantifiable amounts of old, inert carbon derived from the karstic bedrock (Shotton, 1972), coupled with the absence of terrestrial macrofossils and macrocharcoal, limit the utility of radiocarbon dating at the site. Through integrating the Ioannina site into the wider Mediterranean tephra framework, we seek to open up opportunities for direct correlation, providing new insights into how the relative timing of proxy responses to climate forcing vary spatially.

There is significant potential for locating tephra layers in the Ioannina sediment record. Ioannina lies to the east of several Italian volcanoes which have been active throughout the Quaternary (Fig. 1a), and thus the site is located downwind of these volcanoes assuming the present-day prevailing westerlies were dominant during the last glacial. Widespread tephra layers, found in sedimentary sequences across the Central and Eastern Mediterranean basin, have been generated by eruptions from the Campanian and Roman Volcanic Zones (Tomlinson et al., 2012; Marra et al., 2020), the Aeolian Island volcanoes (Albert et al., 2017), and Pantelleria Island (Jordan et al., 2018). The Aegean Arc volcanoes, e.g., Santorini, Nisyros, Yali and Kos, lie  $<1,000$  km southeast of Ioannina and were also active during the last glacial and tephra layers have been found

135 in both terrestrial and marine sedimentary archives (e.g. Eastwood et al., 1999; Karkanas  
136 et al., 2014; Wulf et al., 2020).

### 137 **3 Methods and Materials**

#### 138 **3.1 Core recovery**

139 The I-08 core site ( $39^{\circ}39.0350'N$ ,  $20^{\circ}54.8990'E$ ; Fig. 1b) lies near the earlier I-249  
140 core site (Tzedakis, 1994), towards what would have been the centre of the lake prior to  
141 drainage. Core I-08 was recovered in 2008 from a single borehole using a truck-mounted  
142 drill, which maintained the vertical integrity of samples, with a core recovery  $>90\%$ .  
143 Cores were stored in steel tubing at temperatures  $<6^{\circ}C$ . Coarse sand dominates between  
144 21.00 and 19.71 m, and the remainder of the sequence consists mainly of carbonate clays  
145 and silts.

146 Jones et al. (2013) developed a chronology for the upper 21 m of the I-08 sequence  
147 through radiocarbon dating using a novel approach which combined radiocarbon dates  
148 from microcharcoal concentrates with dates determined through compound-specific  
149 radiocarbon analysis (CSRA). More specifically, Jones et al. (2013) measured of the  $^{14}C$   
150 content of long-chain, odd-numbered n-alkanes which originate from epicuticular waxes  
151 of terrestrial higher plants, thus circumventing the impact of local lake reservoir effects.  
152 Here we build on this chronology through tephra study from 12 m depth (early Holocene)  
153 to the base of the core at 37 m, which covers part of the last glacial (coeval with Marine  
154 Isotope Stages 3 and 2).

#### 155 **3.2 Sediment analyses**

156 Sediment logging was undertaken throughout the I-08 core sequence to detect any visible  
157 changes in sedimentology which may reflect changes in the sedimentary regime at  
158 the core site. Visible tephra layers were identified on visual inspection of the core, and  
159 confirmed using low-powered microscopy to identify volcanic glass shards. Visible tephra  
160 deposits were wet-sieved to remove  $<25 \mu m$  particles, allowing the characterisation of  
161 glass shard morphology and subsequent geochemical analysis.

162 Particle size analysis was undertaken to supplement sediment logging on a complex  
163 unit between 28 and 32 m depth where multiple changes in grain size were observed. 323  
164 contiguous 1 cm (ca. 1 g) sediment samples were treated with sodium pyrophosphate  
165 to deflocculate clays and analysed using a Malvern Mastersizer in the Department of  
166 Geography, University of Cambridge.

167 X-ray fluorescence scanning was used to analyse the chemical composition of I-08  
168 core sediments. Measurements span the entire 38 m sequence, undertaken at 2 mm

169 intervals using the Avaatech core scanner in the Godwin Laboratory for Palaeoclimate  
170 Research, Department of Earth Sciences, University of Cambridge.

### 171 **3.3 Cryptotephra extraction and identification**

172 Cryptotephra investigations were carried out in two stages. An initial range-finding  
173 investigation analysed contiguous 10 cm long (ca. 5 g) samples of sediment, and was  
174 followed by contiguous 1 cm analyses through sections of the core that were identified  
175 as containing peaks in tephra glass shard concentrations.

176 Samples were dried, weighed, and soaked in 3% hydrochloric acid to remove car-  
177 bonates. For sections of the core where the initial 10 cm samples had glass shard  
178 concentrations of  $>10,000$  shards  $\text{g}^{-1}$ , *Lycopodium* tablets of known concentration were  
179 added to subsequent 1 cm (ca. 1 g) samples (Gehrels et al., 2006).

180 Samples were wet sieved at 25  $\mu\text{m}$ , with the  $>25 \mu\text{m}$  remainder density separated  
181 using a heavy liquid (sodium polytungstate) solution at 1.95 and 2.55  $\text{g cm}^{-3}$  (Blockley  
182 et al., 2005). After extraction the 1.95 - 2.55  $\text{g cm}^{-3}$  fraction was sieved again at 25  $\mu\text{m}$   
183 to remove any residues and mounted onto microscope slides using Canada Balsam.

184 Glass shards were identified at  $400\times$  using a high-powered, polarizing optical mi-  
185 croscope. In samples where marker spores were added glass shard concentrations were  
186 calculated in shards  $\text{g}^{-1}$  dry weight calculated by multiplying the number of *Lycopodium*  
187 spores in the tablet by the ratio of glass shards counted to *Lycopodium* marker spores  
188 counted. Peaks in glass shard concentration were identified as potential ash fall layers  
189 and assigned depth codes based on the lower bound of the sediment unit containing the  
190 peak.

### 191 **3.4 Geochemical analysis of tephra samples**

192 Intervals with distinct peaks in glass shard concentration at 1 cm resolution, identified as  
193 containing potential primary airfall deposits, were re-extracted using the above protocols  
194 and prepared for geochemical analysis. Low concentration tephra horizons ( $<500$  shards  
195  $\text{g}^{-1}$ ) were concentrated by picking out individual glass shards using a gas chromatography  
196 syringe mounted on a micromanipulator (Lane et al., 2014). Both visible and cryptotephra  
197 samples were mounted in epoxy resin, then ground and polished to expose flat internal  
198 glass shard surfaces for electron microprobe analysis.

199 Samples from 12 – 20 m depth were analysed for major and minor element concen-  
200 trations using the JEOL-8600 wavelength-dispersive electron microprobe (WDS-EPMA)  
201 at the Research Laboratory for Archaeology and History of Art, University of Oxford. A  
202 15 keV accelerating voltage and 6nA beam current were used, along with a defocused  
203 (10  $\mu\text{m}$ ) beam. Secondary glass standards Atho-G and StHs6/80-G were used as a  
204 check on accuracy and precision of the EPMA data. All other samples were analysed  
205 using a Cameca SX100 WDS EPMA at the Department of Earth Sciences, University of

206 Cambridge. Analyses utilised a 15keV accelerating voltage, a 10nA beam current, with  
207 a 10  $\mu\text{m}$  diameter unfocused beam. Secondary standards KL2-G, T1-G, GOR 128-G,  
208 ATHO-G and STHS6/180G (Jochum and Willbold, 2006) were analysed before, between,  
209 and after batches of analyses to ensure consistency between sessions.

210 Trace element analyses used the Agilent 7500es ICP-MS coupled to a Resonetcs 193  
211 nm ArF excimer laser-ablation in the Department of Earth Sciences, Royal Holloway,  
212 University of London following analytical procedures outlined in Tomlinson et al. (2010).  
213 The repetition rate was 5 Hz and the count time 40 seconds on the sample and 40 seconds  
214 on the gas blank to determine the background signal. Blocks of eight sample/shards of  
215 glass and one MPI-DING reference glass were bracketed by NIST612 glass calibration  
216 standard (GeoREM 11/2006). The internal standard applied was  $^{29}\text{Si}$ , as determined by  
217 grain-specific EPMA analysis. ATHO-G, StHs6/80-G, and GOR128-G were used as  
218 secondary standards (Jochum and Willbold, 2006).

219 Full EPMA, LA-ICP-MS, and associated secondary standard data can be found in  
220 Supplementary Information 1.

### 221 **3.5 Age-depth model**

222 The new I-08 age-depth model incorporates new dates imported through the application  
223 of tephrochronology alongside previously-published radiocarbon dates (Jones et al.,  
224 2013). An updated I-08 age-depth model was constructed using a Bayesian approach  
225 implemented in OxCal v4.4 (Bronk Ramsey, 2020), using the IntCal20 calibration curve  
226 (Reimer, 2020). The P\_Sequence deposition model was used, with a low rigidity ( $k = 10$ )  
227 applied, allowing for increased uncertainty ranges in the sections of core between dates  
228 (Ramsey, 2008; Ramsey and Lee, 2013). A 'general' outlier model, with a 5% prior  
229 probability of any individual date being a statistical outlier, was applied (Bronk Ramsey,  
230 2009). See Supplementary Information 2 for radiocarbon dates and OxCal code.

## 231 **4 Results**

232 In this section we present the results of both visible and crypto- tephra study of the  
233 I-08 core, as well as the our correlations to published proximal and distal glass shard  
234 geochemical data from sites in the Mediterranean region.

### 235 **4.1 Visible tephra deposits**

236 The I-08 core contains two visible tephra deposits. The lower tephra deposit, from 31.93  
237 to 31.92 m depth, henceforth I08T\_31.93, forms a clearly defined 1 cm layer in the  
238 stratigraphy with an abrupt contact at the base. The much larger upper tephra deposit  
239 29.91 to 30.14 m depth, I08T\_30.14, shows some fining towards the surface, however,

240 the base is less clearly delineated as it falls at the end of a core section. Microscopic  
241 inspection of sediments within these lighter horizons revealed that they contained a high  
242 concentration of volcanic glass shards.

243 **4.1.1 I08T\_31.93 - Y-6/Pantelleria Green Tuff**

244 I08T\_31.93 is a <1 cm thick layer that is visible within the stratigraphy due to its lighter,  
245 beige colour compared to the surrounding olive-coloured sediments. The bottom of  
246 the I08T\_31.93 unit is marked by an abrupt contact with the underlying lake sediments.  
247 Tephra glass shards in I08T\_31.93 have varied morphologies; primarily they are platy  
248 and fluted, with fewer cuspatate shapes. Maximum long axis lengths are 110 µm. Tephra  
249 glass shards in I08T\_31.93 are predominantly light olive in colour under plane polarised  
250 light.

251 The geochemical composition of I08T\_31.93 glass shards is predominantly rhyolitic  
252 ( $n=20$ ) with a limited number ( $n=2$ ) of trachytic shards (Fig. 3a).  $\text{SiO}_2$  ranges from 64.2  
253 to 72.5 wt.% and  $\text{Na}_2\text{O}$  (4.7-6.9 wt.%) is generally greater than  $\text{K}_2\text{O}$  (4.2-4.8 wt.%). The  
254 rhyolitic glass shards are pantelleritic following a peralkaline classification, where  $\text{FeO}_t$   
255 (7.9-8.7 wt.%) and  $\text{Al}_2\text{O}_3$  (7.7-8.6 wt.%) are near equal in their abundance (Fig. 3b).  
256 The two trachytic shards have lower  $\text{FeO}_t$  (6.3-6.5 wt.%) and increased  $\text{Al}_2\text{O}_3$  (11.6-14.0  
257 wt.%) than the rhyolitic glass shards (Tab. 1).

258 The major and minor element composition of I08T\_31.93 (Tab. 1) corresponds in full  
259 to the proximal glass compositions of the Pantelleria Green Tuff (PGT; Civetta et al. 1984;  
260 Tomlinson et al. 2015), correlated to the Y-6 tephra marker identified in marine sequences  
261 from the Ionian Sea (Keller et al., 1978, Tab. S7). Eruptions from anorogenic volcanism  
262 on Pantelleria Island are clearly distinguished from other Mediterranean sources by their  
263 high  $\text{SiO}_2$  and low  $\text{Al}_2\text{O}_3$  content (Tomlinson et al., 2015). Whilst other widespread  
264 Pantellerian tephra markers have been identified in the Mediterranean, the Green Tuff is  
265 easily discriminated on the basis of  $\text{FeO}_t$  concentrations (Hardiman, 2012). I08T\_31.93  
266  $\text{FeO}_t$  concentrations (Fig. S1b) closely match both proximal PGT (Tomlinson et al.,  
267 2015) and distal Y-6 (Vogel et al., 2010; Tamburrino et al., 2012).

268 The Pantelleria Green Tuff was produced during a caldera-forming eruption of the  
269 Island of Pantelleria in the Sicily channel, dated to  $45.7 \pm 1.0$  ka using the  $^{40}\text{Ar}/^{39}\text{Ar}$   
270 method (Scaillet et al., 2013, Tab. S7). We incorporate this best age for the Pantelleria  
271 Green Tuff eruption into the I-08 age-depth model at 31.93 m (Fig. 2).

272 **4.1.2 I08T\_30.14 - Y-5/Campanian Ignimbrite**

273 The I08T\_30.14 tephra unit (Fig. 2) appears ca. 18 cm thick, however, as 7 cm of material  
274 is missing between 30.21 and 30.14 m depth, due to the core extraction process, the  
275 true thickness of this tephra deposit is uncertain. As the underlying core section, with  
276 its surface at 30.21 m, contains a ca. 5 cm drop-stone of agglomerated ash it is likely

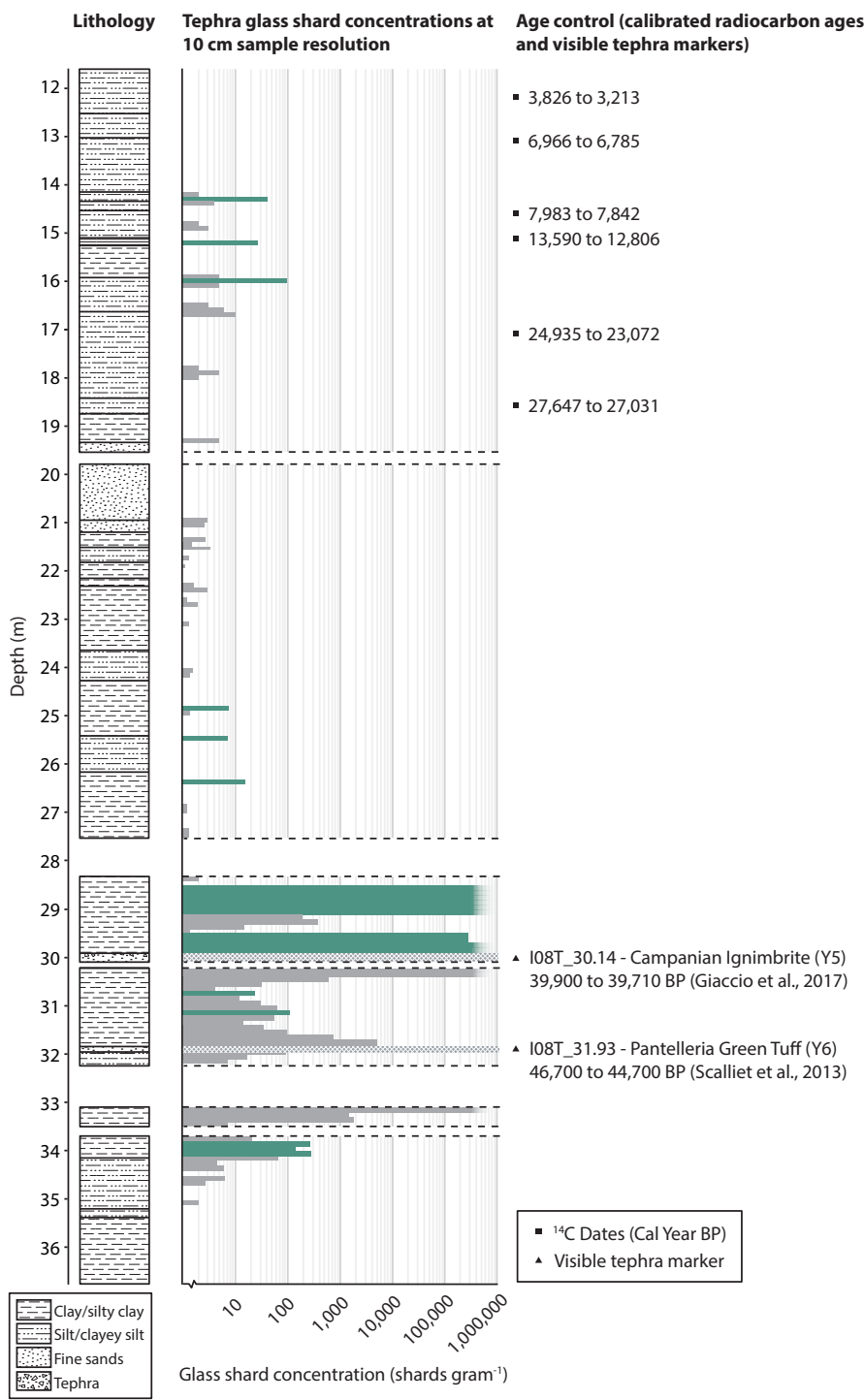


Figure 2. Results of low resolution (10 cm) rangefinder investigations of the I-08 core shown alongside  $^{14}\text{C}$  dates from Jones et al. (2013), recalibrated using the IntCal20 calibration curve (Reimer, 2020). Green bars represent horizons selected for high resolution analysis. Note glass shard concentrations are displayed on a logarithmic axis.

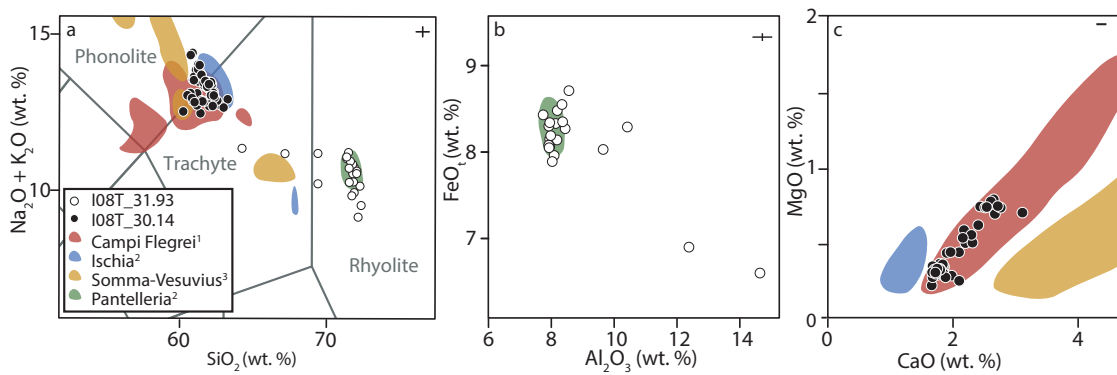


Figure 3. Major element geochemistry of tephra glass shards from visible tephra layers I08T\_31.93 and I08T\_30.14 compared to summary compositional envelopes from Italian volcanic centres that erupted trachytes, phonolites, and rhyolites during the last glacial cycle, including (a) total alkali vs. silica plot (Le Bas et al., 1986). Geochemical fields are based on proximal data from (1) Tomlinson et al. (2012), (2) Tomlinson et al. (2015) and (3) Tomlinson et al. (2015), for distal comparisons see Figs. S1 and S3. Errors are 2 s.d. calculated using replicate analyses of MPIDING StHs6/80 glass.

that the missing section of the lake sequence was predominantly tephra. Overlying and underlying sediments are generally well compacted clays and silts, less likely to be lost during core extraction than disaggregated, coarse grained tephra. Therefore, it is possible that the thickness of the I08T\_30.14 deposit is as much as 25 cm, indicative of an eruption that generated a significant amount of ash-fall and potential secondary thickening from re-deposition at the upper contact.

The I08T\_30.14 tephra deposit primarily consists of colourless glass shards with varied morphologies, however, the majority of shards are either platy or fluted. Particle size distributions of tephra glass shards are unimodal, with some evidence of fining

	SiO <sub>2</sub>	TiO <sub>2</sub>	Al <sub>2</sub> O <sub>3</sub>	FeO <sub>t</sub>	MnO	MgO	CaO	Na <sub>2</sub> O	K <sub>2</sub> O	P <sub>2</sub> O <sub>5</sub>	Cl
<b>I08T_30.14</b>											
Average	61.08	0.41	18.45	3.00	0.19	0.41	1.97	5.52	8.02	0.07	0.90
2sd	1.22	0.09	0.55	0.44	0.13	0.32	0.70	2.48	2.01	0.09	0.55
<b>I08T_31.93</b>											
Average	70.20	0.52	8.65	7.99	0.35	0.11	0.47	6.03	4.39	0.04	1.24
2sd	3.50	0.24	3.42	0.92	0.12	0.18	0.49	1.14	0.30	0.08	0.67

Table 1. Representative shard-specific normalised major and minor element (WDS-EMPA) glass data for visible tephra units I08T\_30.14 and I08T\_31.93. Errors are 2 s.d. calculated using replicate analyses of MPIDING StHs6/80 glass. A full grain-specific glass data set is presented in Supplementary Information 1.

286 upwards through the deposit (Fig. S2).

287 I08T\_30.14 glass shard major and minor element compositions straddle the phonolite-  
288 trachyte boundary with  $\text{SiO}_2$  ranging from 60.9 to 62.3 wt.% and total alkalis ranging  
289 from 13.8 to 14.0 wt.%. Glass compositions are potassium rich ( $\text{K}_2\text{O}$ : 7.1-10.3 wt.%)  
290 with lower sodium ( $\text{Na}_2\text{O}$ : 3.05-7.15 wt.%; Tab. 1), consistent with magma erupted from  
291 the Campanian Volcanic Zone (Fig. 3).

292 I08T\_30.14 glass compositions are consistent with glass compositions of the Cam-  
293 panian Ignimbrite (CI) generated from a caldera forming eruption of the Campi Flegrei  
294 volcano, Italy, ca. 40 ka BP and correlated to the widely-recognised Y-5 marine tephra in  
295 the Mediterranean tephrostratigraphy (Keller et al., 1978). The Campanian Ignimbrite  
296 eruption is one of the largest known Quaternary eruptions, with tephra deposits correlated  
297 to the eruption found thousands of kilometers from source (Pyle et al., 2006).

298 On the basis of the correlation of I08T\_30.14 to the CI (Y-5) tephra isochron (Tab.  
299 S7), the widely used  $^{40}\text{Ar}/^{39}\text{Ar}$  and  $^{14}\text{C}$  age of the CI  $39.85 \pm 0.14$  ka BP (Giaccio et al.,  
300 2017) is imported at the upper bound of the Campanian Ignimbrite visible tephra deposit,  
301 at 30.04 m depth in the I-08 core chronology (Fig. 2).

## 302 4.2 Cryptotephra

303 Rangefinder (10 cm contiguous sampling) investigations revealed 11 intervals of in-  
304 creased volcanic glass concentration which warranted further 1 cm resolution study (Fig.  
305 2). Sections of the core were selected for high resolution study by identifying significant  
306 increases in the tephra glass shard concentration profile.

307

The depths selected for high resolution study in the I-08 core were:

- 308
- 34.11 to 33.81 m      Section 4.2.1
  - 31.21 to 31.11 m      } Section 4.2.2
  - 30.71 to 30.81 m      } Section 4.2.3
  - 29.88 to 29.40 m      }
  - 29.00 to 28.51 m      }
  - 16.10 to 16.00 m      }
  - 15.30 to 15.20 m      }
  - 14.40 to 14.30 m      }

309 Three further small peaks at ca. 26.3, 25.5, and 24.9 m depth were also studied at 1  
310 cm resolution, however, the results of these investigations are not included here as the  
311 shape of a shard concentration profiles and inconsistent morphologies of glass shards  
312 within these sections suggest post-depositional reworking rather than primary airfall of  
313 tephra. Due to a gap in the core between 32 and 33 m, associated with core extraction,  
314 the increase in glass shard concentration at ca. 33.1 m was not interrogated.

315    **4.2.1 Pre-Pantelleria Green Tuff (> 30.93 m depth; > ca. 46 ka BP)**

316    Tephra glass shards were found in all but seven of the 1 cm samples studied between  
317    34.11 and 33.81 m depth, albeit at low concentrations (<1,500 shards g<sup>-1</sup>). Throughout  
318    this interval, glass shards were generally light olive in colour and of varying relief, with  
319    both fluted and cuspatate forms. Shards were generally small, <40 µm on the longest axis,  
320    however, at 34.03 m depth larger shards (ca. 80-100 µm) accounted for ca. 5% of the  
321    total shards counted. In the sample at 33.85 m depth, a few shards containing microcrysts  
322    were identified. The highest concentration of tephra glass shards in this section of the  
323    core, with ca. 1,600 shards g<sup>-1</sup>, was found at 33.97 m depth.

324    Considering the distribution, appearance and size of the glass shards in each sample,  
325    five peaks in cryptotephra concentration were targeted for geochemical analysis (Fig. 4a)  
326    at 34.07, 34.03, 33.99, 33.97, and 33.85 m depth. WDS-EPMA analysis of shards in this  
327    section of core was challenging due to their small size, however, at least one analysis was  
328    possible for shards in three of samples, hereon I08T\_34.02, I08T\_33.97, and I08T\_33.85.

329    I08T\_34.02, I08T\_33.97, and I08T\_33.85 all have a tephra glass shard concentration  
330    ca. 200 shards g<sup>-1</sup>. Glass shards in all three layers are geochemically similar (Fig.  
331    4a), with a rhyolitic ( $\text{SiO}_2 > 70\%$ ) composition (Fig. 4b). All three tephra layers are  
332    peralkaline rhyolites, characterised by low  $\text{Al}_2\text{O}_3$  between 8 and 12 wt.%. The  $\text{FeO}$   
333    values ( $\text{FeO}_t$  ca. 8 wt.%) rule out Pantellerites from known eruptions of Nemrut Volcano  
334    in Eastern Turkey (Peretyazhko et al., 2015), and thus the layers are likely derived from  
335    last glacial volcanism of Pantelleria.

336    There are three known widespread Mediterranean tephra isochrons of Pantellerian  
337    origin (Tab. S7), the ca. 46 ka BP Pantelleria Green Tuff (Y-6; Scaillet et al. 2013),  
338    the ca. 77 ka BP P-10 (Paterne et al., 1988) and the older, ca. 131 ka BP, P-11 tephra  
339    marker (Paterne et al., 2008). The P-10 tephra marker identified by Paterne et al. (1988),  
340    subsequently identified in Lago Grande di Monticchio (TM-22; Wulf et al. 2004), Adriatic  
341    Sea core PRAD 1-2 (PRAD-2375; Bourne et al. 2015) and correlated to the ca. 85 ka  
342    BP Proximal Ignimbrite Z of Pantelleria (Rotolo et al., 2013), is typically associated  
343    with a NNW dispersal axis. Correlation to the P-10 tephra marker can be ruled out  
344    as these deposits are, at all sites, associated with higher  $\text{Al}_2\text{O}_3$  and lower  $\text{FeO}_t$  values  
345    (Fig. 4) than the Ioannina tephra layers. The P-11 tephra marker has been identified  
346    in Greece, at Theopetra Cave (Karkanas et al., 2014) and, putatively, at Megali Limni  
347    (Lesvos; Margari et al. 2007; Vogel et al. 2010). Correlation of the ML-5 tephra layer at  
348    Megali Limni to the P-11 tephra marker is uncertain as, whilst geochemically similar,  
349    the age of the P-11 eruption is difficult to reconcile with its stratigraphic position within  
350    the Megali Limni pollen record. Both the P-11 and ML-5 tephra deposits can be ruled  
351    out as correlatives as the  $\text{FeO}_t$  concentrations found in I08T\_34.02, I08T\_33.97 and  
352    I08T\_33.85 fall considerably above the range of  $\text{FeO}_t$  in glass shards from the P-11 and  
353    ML-5 deposits (Fig. 4).

354    The geochemical affinity of glass shards in layers I08T\_34.02, I08T\_33.97, and

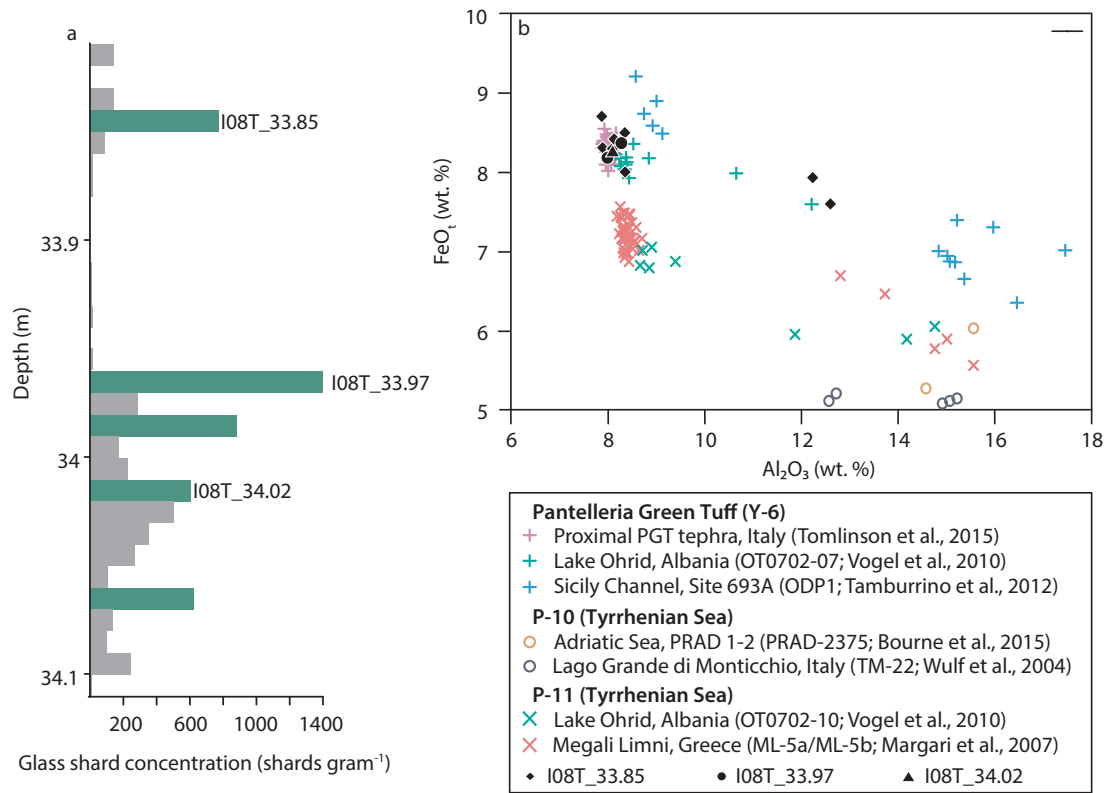


Figure 4. Tephra glass shard concentrations identified in sediments below the visible I08T\_31.93 tephra marker (correlated to the Pantelleria Green Tuff). (a) Glass shard concentration against depth, horizons in green reflect depths prioritised for geochemical analysis and (b) Al<sub>2</sub>O<sub>3</sub> vs FeO<sub>t</sub> biplot for the analysed Ioannina cryptotephra layers from this interval, alongside proximal and distal tephra layers associated with the Pantelleria Green Tuff eruption (+; pink) /Y-6 distal tephra (+; blue and green) and the P-11 distal tephra (x). Note: Margari et al. (2007) originally correlated ML-5 to the Y-6 eruption, however, here we utilise the revised correlation of Vogel et al. (2010); Hardiman (2012). Errors are 2 s.d. calculated using replicate analyses of MPIDING StHs6/80 glass.

355 I08T\_33.85 leaves open the possibility that these layers are stratigraphically displaced  
356 contamination from the visible I08T\_31.93 tephra layer either through post-depositional  
357 reworking, or coring-related displacement. The absence of tephra glass shards from  
358 a number of samples, for example, between 33.96 and 33.86 m depth, as well as the  
359 absence of tephra from the blank samples run during the extraction process rules out  
360 laboratory contamination during cryptotephra extraction and analysis.

361 Alternatively, tephra layers I08T\_34.02, I08T\_33.97, and I08T\_33.85 may be coring  
362 artefacts, given that the borehole from which cores were retrieved would still have  
363 contained tephra from the I08T\_31.93 visible deposit which may have been retrieved in  
364 subsequent core drives. Similar stratigraphic displacement of tephra glass shards has  
365 been identified in the TP-2005 core from Tenaghi Philippon, with glass shards associated  
366 with the Campanian Ignimbrite identified 22.78 m below the visible CI deposit, attributed  
367 by Wulf et al. (2018) to coring-related contamination. Particularly, following retrieval  
368 of a core drive the load of the water column in the borehole is suggested to have forced  
369 glass shards to depths of 20 cm or more into the upper part of the subsequent drive (Wulf  
370 et al., 2018). In contrast to the peat-dominated Tenaghi Philippon sequence, the sediment  
371 matrix of the Ioannina I-08 core primarily consists of silts and clays, and thus the denser,  
372 more cohesive Ioannina cores should have reduced porewater, making the sediments less  
373 susceptible to such displacement. Furthermore, the glass shard distribution profiles (Fig.  
374 4) do not support the coring-associated displacement hypothesis. If tephra glass shards  
375 were coring artefacts, it would be expected that from the top of the 70 cm core segment  
376 at 33.81 m depth water load should disperse shards throughout the stratigraphy. Instead,  
377 distinct peaks in glass shard concentration are observed at 21, 16, and 4 cm below the  
378 top of the core drive (I08T\_34.02, I08T\_33.97, and I08T\_33.85 respectively).

379 The I08T\_34.02, I08T\_33.97, and I08T\_33.85 cryptotephra peaks may represent  
380 smaller, previously unknown eruptions of Pantelleria. Much of our understanding of  
381 Pantellerian volcanism is based on the proximal stratigraphy and smaller eruptions from  
382 Pantelleria predating the large P-11 and Green Tuff (Y-6) deposits may not have been  
383 observed due to subsequent burial by more voluminous deposits. Whilst distal tephra  
384 study has been undertaken on visible units identified in marine sequences from the  
385 nearby Sicily Channel, very few detailed cryptotephra studies have been undertaken  
386 in the southern Mediterranean. Correlation of these tephra deposits to known volcanic  
387 events or tephra isochrons identified in other sequences is not possible at present.

388 Therefore, we suggest that tephra layers between 34.11 and 33.81 m depth in the  
389 I-08 core to genuine but previously unrecognised eruptions of Pantelleria, however,  
390 confirmation is needed by replication at another site.

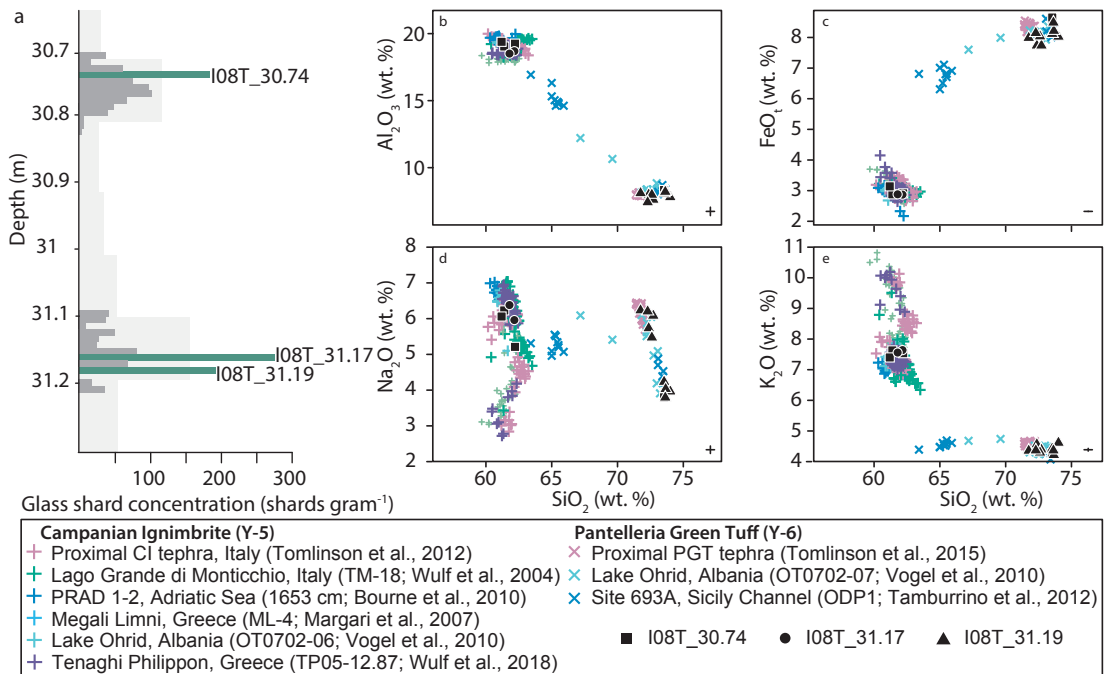


Figure 5. Cryptotephra peaks identified in sediments bracketed by the I08T\_31.93 and I08T\_30.14 tephra deposits (correlated to the Pantelleria Green Tuff and Campanian Ignimbrite respectively). (a) Glass shard concentration against depth and (b-e) major element biplots for Ioannina cryptotephra layers, alongside proximal and distal tephra layers associated with the Pantelleria Green Tuff and Campanian Ignimbrite eruptions. Errors are 2 s.d. calculated using replicate analyses of MPIDING StHs6/80 glass.

391    **4.2.2 Post-Pantelleria Green Tuff and Pre-Campanian Ignimbrite (31.93 to 30.14**  
392    **m depth; ca. 46 to 40 ka BP)**

393    Two intervals of increased glass shard concentration were identified for further study in  
394    the section of core bracketed by the visible I-08 tephra layers, I08T\_31.93 and I08T\_30.14,  
395    which are correlated to the ca. 46 ka Pantelleria Green Tuff and 40 ka BP Campanian Ig-  
396    nimbrate respectively. Three depths within which glass shard concentrations peaked well  
397    above background, were identified and selected for geochemical analysis: I08T\_31.19,  
398    I08T\_31.17, and I08T\_30.74 (Fig. 5a).

399    I08T\_31.19 primarily of low relief, olive-coloured shards, with a concentration ca.  
400    200 shards g<sup>-1</sup>. Glass shards in I08T\_31.19 are rhyolitic (SiO<sub>2</sub> from 72.3 to 74.1 wt.%) in  
401    composition, and demonstrate the diagnostic low Al<sub>2</sub>O<sub>3</sub> associated with distal deposits  
402    from Pantelleria (Fig. 5b). Within this grouping there is some variation in Na<sub>2</sub>O with  
403    values between 3.2 and 6.8 wt.%, however, values for FeO<sub>t</sub> and K<sub>2</sub>O are well clustered  
404    (Fig. 5c-e).

405    Whilst evidence exists for post-PGT eruptive activity at Pantelleria, a period of  
406    quiescence has been suggested following the PGT, ending at 35 ka BP with the eruption  
407    of the Serra di Ghirlanda tephra (Civetta et al., 1984). In contrast, Mahood and Hildreth  
408    (1986) suggest that volcanism at Pantelleria resumes rapidly after the PGT eruption,  
409    identifying trachyte lavas from a vent at Monte Gibebe which they date using K/Ar to  
410    ca. 44-37 ka BP, which would indicate that some eruptive activity occurred between the  
411    PGT and CI eruptions. However, no distal studies have yet identified tephra deposits  
412    associated with post-PGT Pantellerian volcanism that could provide a correlative for  
413    I08T\_31.19.

414    Alternatively, I08T\_31.19 may be the result of remobilisation of tephra glass shards  
415    associated with the I08T\_31.93 tephra marker some 70 cm deeper in the core. Mechan-  
416    isms that may have caused post depositional reworking in the Ioannina cores will be  
417    discussed in greater detail in Section 5.

418    I08T\_31.17 (just 2 cm above I08T\_31.19) and I08T\_30.74 contain low relief, colour-  
419    less shards in concentrations ca. 275 and 180 shards g<sup>-1</sup> respectively. Tephra glass shards  
420    from both layers are phono-trachytic (SiO<sub>2</sub> ca. 62 wt. %) and have a geochemical signa-  
421    ture that matches eruptions of the Campanian Volcanic Field (Fig. 5). The I08T\_31.17  
422    and I08T\_30.74 compositions are indistinguishable from that of the Campanian Ign-  
423    imbrate tephra layer (I08T\_30.14), which occurs 60 cm above I08T\_30.74 and ca. 1 m  
424    above I08T\_31.17 in the Ioannina core (Fig. S4).

425    Multiple pre-CI eruptions have been recorded in both proximal and distal archives,  
426    including marine cores from the Adriatic (S7; Tomlinson et al. 2012; Bourne et al.  
427    2010; Matthews et al. 2015). Most notably, the tephra record from Lago Grande di  
428    Monticchio identifies at least four smaller-scale tephra markers associated with pre-CI  
429    volcanism from Campi Flegrei which occur ca. 600 varve years prior to the CI (Wulf  
430    et al., 2004, 2008; Wutke et al., 2015). The pre-CI LGdM tephra markers, termed the

431 TM-18 tephras, are geochemically difficult to distinguish from the CI without high-  
432 precision trace element glass data (Wutke et al., 2015). Of these markers Wulf et al.  
433 (2018) identify medial distal tephras TM-18-1d, TM-18-4, TM-18-9e as the most likely  
434 correlatives for pre-CI Campi Flegrei tephra horizons identified in distal settings. Tephra  
435 deposits associated with the TM-18 pre-CI sequence have been identified in a limited  
436 number of distal archives. TM-18-1d, for example, has been identified in the Tenaghi  
437 Philippon sequence (Wulf et al., 2018). The geochemical fingerprint of the Ioannina  
438 tephra deposits can, however, be separated from many of these pre-CI deposits on the  
439 basis of  $K_2O/Na_2O$  (Fig. S4).

440 As with the ca. 33 m depth tephra markers, it is also possible that I08T\_31.17  
441 and I08T\_30.74 are related to downcore displacement of tephra shards associated with  
442 the coring process. All the tephra deposits identified fall within the major element  
443 composition of the I08T\_30.14 tephra deposit (Fig. S4), this explanation cannot be ruled  
444 out at present.

445 I08T\_31.19, I08T\_31.17, and I08T\_30.74 are, at present, uncorrelated, however, they  
446 may represent distal deposits of 46-40 ka BP activity at Pantelleria (I08T\_31.19) and  
447 Campi Flegrei (I08T\_31.17 and I08T\_30.74). Given their close geochemical match with  
448 the visible I08T\_31.93 and I08T\_30.14 tephra markers, however, it seems most likely that  
449 these layers represent post-depositional reworking of tephra glass shards (I08T\_31.19).

#### 450 4.2.3 Post-Campanian Ignimbrite (29.88 to 28.51 m depth; ca. 40 to 30 ka BP)

451 High resolution (1cm) cryptotephra investigations were undertaken between 29.88 and  
452 29.51 m depth and 29.01 to 28.51 m depth. The section of core between 29.51 and  
453 29.01 m depth, where glass shard concentrations fell below 100 shards  $g^{-1}$  in rangefinder  
454 investigations, was not studied further (Fig. 2). The hiatus in tephra deposition between  
455 29.51 to 29.01 m, observed via cryptotephra analyses, is verified by the XRF scanning  
456 data. XRF-derived elemental ratios for bulk sediment, most notably the K/Ti ratio,  
457 closely tracks tephra glass shard concentration throughout this section of the core (Fig.  
458 6b).

459 Three abrupt increases in glass shard concentration relative to the underlying sample  
460 were observed at 29.72, 29.65, and 29.62 m depth, which is above the I08T\_30.14 CI  
461 tephra marker but below the hiatus in shard deposition at 29.51 m depth (Fig. 6a). Whilst  
462 peaks in glass shard concentration at 29.65 and 29.62 m depth are lower than peaks at  
463 29.83 and 29.72 m depth, tephra glass shard concentrations at 29.65 and 29.62 m depth  
464 (ca.  $5 \times 10^5$  and  $11 \times 10^5$  shards  $g^{-1}$  respectively) represent large increases relative to the  
465 underlying samples (Fig. 6a). Glass shards at all depths generally measured between 60  
466 and 100  $\mu m$  on the longest axis. At 29.72 m depth, however, shards were much larger,  
467 typically ca. 100  $\mu m$  on the longest axis (Fig. 6c).

468 A fourth sample at 29.83 m depth, was investigated as a potential primary ash-fall  
469 horizon on the basis of shard morphology as, similarly to the sample from 29.72 m

470 depth, shards in this sample were far larger than in surrounding tephra samples, typically  
471 > 100 µm on the longest axis (Fig. 6c). Glass shards throughout this section of core  
472 were generally colourless, of low relief, and largely consisted of platy forms, however,  
473 shards with a range of other morphologies, including fluted and cuspatate shards, were  
474 also present.

475 A distinct increase in tephra glass shard concentration is observed at 28.98 m depth  
476 and is also identifiable through a peak in the K/Ti XRF ratio as well as a coarsening in  
477 the particle size data. Above 28.98 m there is a return to glass shard concentrations ca.  
478  $1 \times 10^5$  shards g<sup>-1</sup> until 28.83 m depth, at which point concentrations begin to increase,  
479 albeit with a number of sharp jumps and oscillations in glass shard concentration. The  
480 increase in tephra glass shard concentration throughout this section of the core correlates  
481 with an increase in K/Ti ratio (Fig. 6b), reflected in the particle size data as an increase  
482 in the frequency of particles in the 100 to 200 µm fraction (Fig. 6c).

483 Above the peak at 28.98 m depth, a further six samples were investigated since they  
484 show a large increase in glass shard concentration relative to their underlying sample  
485 (Fig. 6a). Observed glass shard morphologies are broadly consistent in samples between  
486 29.01 and 28.51 m depth, with shards largely low relief, colourless, and dominated by  
487 platy, curvilinear, and cuspatate forms. A change in glass shard morphology is observed in  
488 at 28.66 m depth, where shards display an increase in ventricular features, microcryst  
489 inclusions with a limited number of shards (n=2) with pumicious forms. Due to a  
490 return to platy, low relief shards in samples above 28.66 m depth, this influx of new  
491 morphologies may reflect primary airfall, henceforth the I08T\_28.66 tephra deposit. Most  
492 shards observed in the 29.88 to 28.51 m interval were between 30 and 50 µm on their  
493 longest axis, however, occasional larger shards (up to 200 µm on the longest axis) were  
494 noted throughout the section.

495 Geochemical analysis of the 11 potential primary airfall tephra layers between 29.99  
496 and 28.51 m depth characterises glass shards as phono-trachytic, with limited variability  
497 in SiO<sub>2</sub> (between 60 and 63 wt. %). CaO (1.6–2.8 wt. %) and MgO (0.2 to 0.9 wt. %)  
498 values are consistent (Fig. 6b). Glass shards from all 11 depths are phono-trachytic (Fig.  
499 6a). Post-CI (<40 ka BP) Mediterranean tephra deposits with phono-trachytic glass  
500 compositions may correlate to eruptions from the Campanian Volcanic Zone (trachytic  
501 and phonolitic; Tomlinson et al. 2015), Gölcük (trachytic and phonolitic; Tomlinson et al.  
502 2015) and Mt. Etna (trachytic; Albert et al. 2013). The MgO and CaO concentrations of  
503 all 11 Ioannina tephra deposits between 29.99 and 28.51 m depth indicate that they are  
504 all associated with eruptive activity from Campi Flegrei (Fig. 6e).

505 Two possible explanations for the unusual stratigraphic distribution of tephra glass  
506 shards through this section of the core are suggested. The first is that the peaks, which  
507 are often characterised by abrupt increases in glass shard concentration relative to the  
508 underlying deposits, are primary air-fall deposits associated with post-CI eruptions in  
509 the Mediterranean. The second is that these peaks represent a complex process of post-

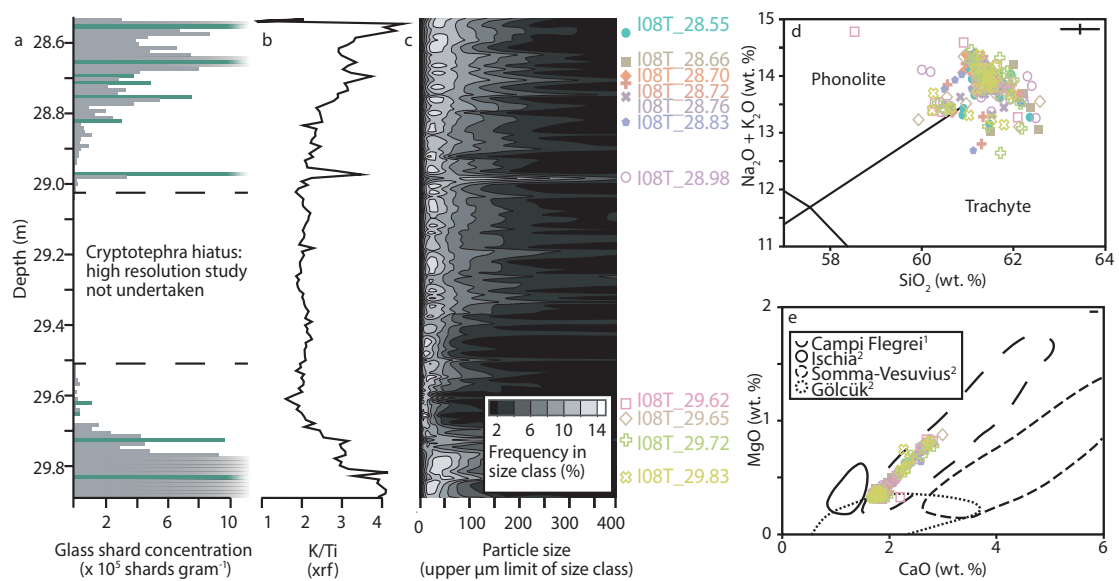


**Figure 6.** Results of high-resolution (1 cm) cryptotephra analysis between 29.88 and 28.51 m depth, showing: stratigraphic plot of (a) glass shard concentrations, (b) XRF-derived K/Ti ratio, and (c) bulk particle size distribution of the I-08 core. Also shown are major and minor element geochemistries of tephra glass shards from cryptotephra peaks, including (d) total alkali vs. silica plot (Le Bas et al., 1986) and (e) CaO vs. MgO showing geochemical fields based on data from (1) Tomlinson et al. (2012) and (2) Tomlinson et al. (2015). Errors are 2 s.d. calculated using replicate analyses of MPIDING StHs6/80 glass.

510 depositional reworking of the Campanian Ignimbrite tephra deposit in the Ioannina basin.  
511 It should be noted that the two explanations presented here are not mutually exclusive  
512 and it is possible that both reworking and the complex eruptive history of Campi Flegrei  
513 act in concert to produce the complex tephra record in this section of the I-08 core. Both  
514 possible interpretations of the I-08 tephra record are further discussed in Section 5.

515 **4.2.4 Last Glacial to Interglacial Transition (16.20 to 14.20 m depth; ca. 25 to 7  
516 ka BP)**

517 Three discrete peaks in cryptotephra glass shard concentration (I08T\_16.07, I08T\_15.23,  
518 and I08T\_14.39) are located between 16.20 and 14.20 m depth in the I-08 core. This  
519 section overlies the coarse sand deposits associated with low lake levels during the last  
520 full glacial (MIS2, ca. 22 ka BP) and shown by Jones et al. (2013) to cover the Last  
521 Glacial-Interglacial Transition (LGIT). In contrast to tephra peaks between 29.88 and  
522 28.51 m depth peaks I08T\_16.07, I08T\_15.23, and I08T\_14.39 are isolated, with no  
523 tephra glass shards found in the overlying and underlying sediments. We can rule out  
524 coring-related displacement for I08T\_16.07 and I08T\_14.39 as these isochrons are 17  
525 and 59 cm from the top of their core sections respectively. We are also confident that the  
526 isolated peak at I08T\_15.23 does not represent coring-related stratigraphic displacement  
527 as, whilst glass shards are identified in the 1 cm samples above and below the core,  
528 no shards are present in the samples which bound these, suggesting cryptotephra glass  
529 shards form a distinct layer within the stratigraphy. Therefore, we are confident that  
530 these are independent isochrons.

531 Shards from I08T\_16.07, I08T\_15.23, and I08T\_14.39 are highly evolved rhyolites  
532 (Fig. 7b) characterised by high SiO<sub>2</sub> values from 75.1 to 75.7 wt.% and total alkalis from  
533 8.3 to 9.3 wt.%. Mediterranean volcanic centres which produce highly evolved rhyolites  
534 include the Aeolian Islands (notably Lipari and Salina; Albert et al. 2017), Santorini  
535 (Tomlinson et al., 2015) and Acigöl (Tryon et al., 2009). Reference compositional data  
536 from these volcanic centres are compared to the Ioannina LGIT tephra compositions  
537 in Fig. 7. The Ioannina LGIT tephra correlate well to high-K calc-alkaline activity  
538 at Aeolian Island volcano Lipari. Multiple eruption phases have been identified in the  
539 proximal Lipari record during the last glacial cycle, some of which are indistinguishable  
540 based on their major element geochemistry (Albert et al., 2017). However, the Vallone  
541 del Gabellotto eruptive cycle (*sensu* Albert et al. (2017)), which is dated to ca. 8 ka BP  
542 (Caron et al., 2012; Siani et al., 2004), provides the only likely LGIT correlative for the  
543 Ioannina tephra markers (Fig. 7).

544 Of particular note is the widespread Vallone del Gabellotto (VG/E-1) tephra dated to  
545 8,630 to 8,430 cal yrs BP using the IntCal20 calibration curve (Fig. S7). The VG/E-1  
546 tephra has been correlated to horizons present in Tyrrhenian, Ionian, and Adriatic marine  
547 cores (Albert et al., 2017) as well as Tenaghi Philippon in NE Greece (Wulf et al., 2018).  
548 Of the three Ioannina LGIT tephra deposits the most likely correlative for this widespread

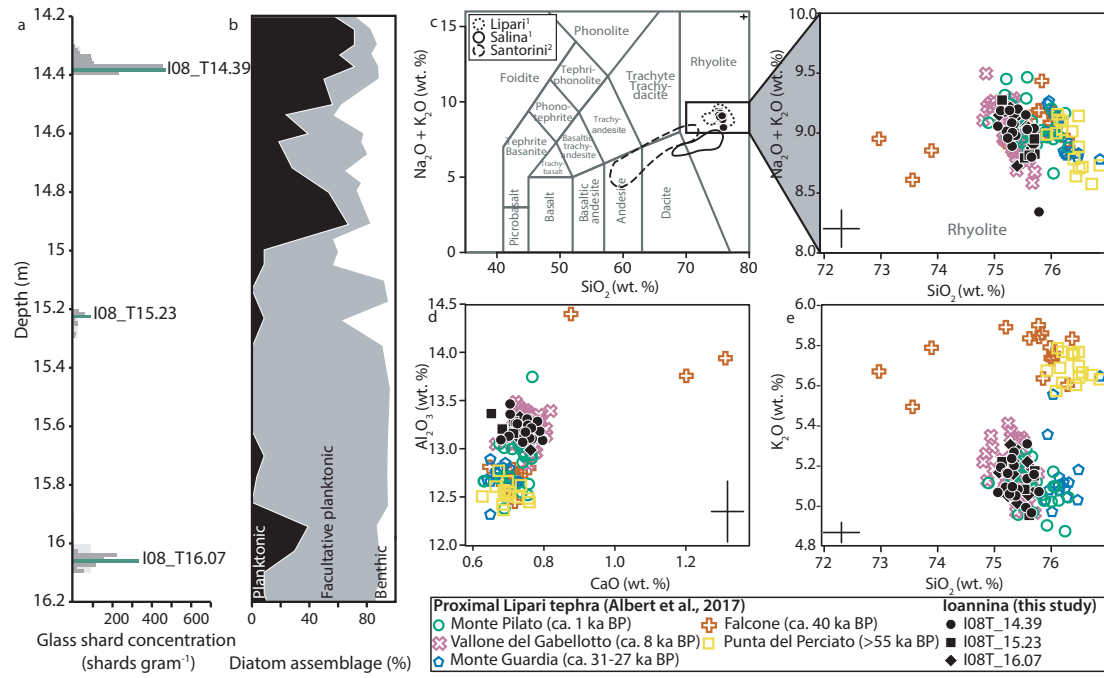


Figure 7. Identified cryptotephra peaks between 16.20 and 14.20 m depth in the I-08 core, showing (a) glass shard concentration against depth, (b) diatom assemblages from Jones et al. (2013) showing the Late Glacial to Early Holocene transition in the I-08 core, (c) total alkali vs. silica plot (Le Bas et al., 1986), geochemical fields are based on data from (1) Albert et al. (2017) and (2) Satow et al. (2015) (d-e) major element biplots for Ioannina Late Glacial cryptotephra layers alongside the major element compositions of proximal deposits associated with Lipari volcanism (Albert et al., 2017).

549 Holocene tephra marker is the uppermost I-08 tephra layer, I08T\_14.39, the only tephra  
550 deposit that sits within the Holocene section of the core (Fig. 7b). The correlation of  
551 I08T\_14.39 with the Vallone del Gabellotto (E-1) isochron is further supported by new  
552 trace element analysis, Supplementary Information 1. Fig. 8 shows good correspondence  
553 between I08T\_14.39, three proximal deposits of the Vallone del Gabellotto, and its distal  
554 correlative M25/4-12-28cm tephra from the Ionian Sea (Albert et al., 2017).

555 The proximal Lipari record does contain eruptive deposits of LGIT age, however,  
556 these are ‘localised’ and not traced widely across the island (Albert et al., 2017). In  
557 the distal realm an older layer with a Gabellotto-like Lipari composition has been  
558 recorded at 44 cm depth in the Ionian Sea core M25/4-12 (Albert et al., 2013). The  
559 lowermost Ioannina LGIT tephra layer, I08T\_16.07, has a trace element geochemistry  
560 that corresponds well to the distal Ionian Sea tephra marker M25/4-12-44cm, which has  
561 yet to be linked to a proximal deposit. Therefore, we propose a tentative correlation  
562 of I08T\_16.07 to Ionian Sea tephra marker M25/4-12-44cm, which does not yet have a  
563 correlative in the proximal tephrostratigraphy. The identification of this tephra marker ca.  
564 500 km from source is currently the most distal deposit and the first outside of Italy and  
565 the surrounding seas.

566 The intermediate Ioannina LGIT tephra, I08T\_15.23, has yet to be correlated to a  
567 proximal or distal isochron, however, has distinctly lower Th, La, Eu, and Ce concen-  
568 trations (Fig. 8a) than the other tephra layers and is thus likely to be the product of  
569 a separate eruption. Therefore, I08T\_15.23 has the potential to provide an additional  
570 stratigraphic marker in the future.

571 On the basis of the correlation of I08T\_14.39 to the E-1 tephra isochron, the uncali-  
572 brated  $^{14}\text{C}$  age of this marker,  $7.77 \pm 0.04$  ka BP (Caron et al., 2012; Albert et al., 2017),  
573 is imported to this depth in the I-08 core chronology and recalibrated as part of the OxCal  
574 P\_Sequence.

## 575 5 Discussion

### 576 5.1 The Campanian Ignimbrite tephra marker

577 The I08T\_30.14 tephra deposit, which we correlate to the 39.85 ka BP campanian  
578 Ignimbrite eruption of Campi Flegrei caldera, Italy, is interesting as it contains the full  
579 major and minor element variation observed in the CI proximal deposit (Fig. S3; Tab.  
580 S7). Two closely-related compositional groups can be recognised within the I08T\_30.14  
581 tephra deposit, illustrated by differences in CaO, MgO and K<sub>2</sub>O at overlapping SiO<sub>2</sub>  
582 concentrations (Fig. S3). The two composition groups in I08T\_30.14 closely correspond  
583 to the end member associated with the lower and intermediate fall deposits of the CI  
584 eruption in the proximal deposits (CaO <2; K<sub>2</sub>O <8; Na<sub>2</sub>O > 5), as well as as the  
585 higher CaO and K<sub>2</sub>O and lower Na<sub>2</sub>O end member associated with the upper flow

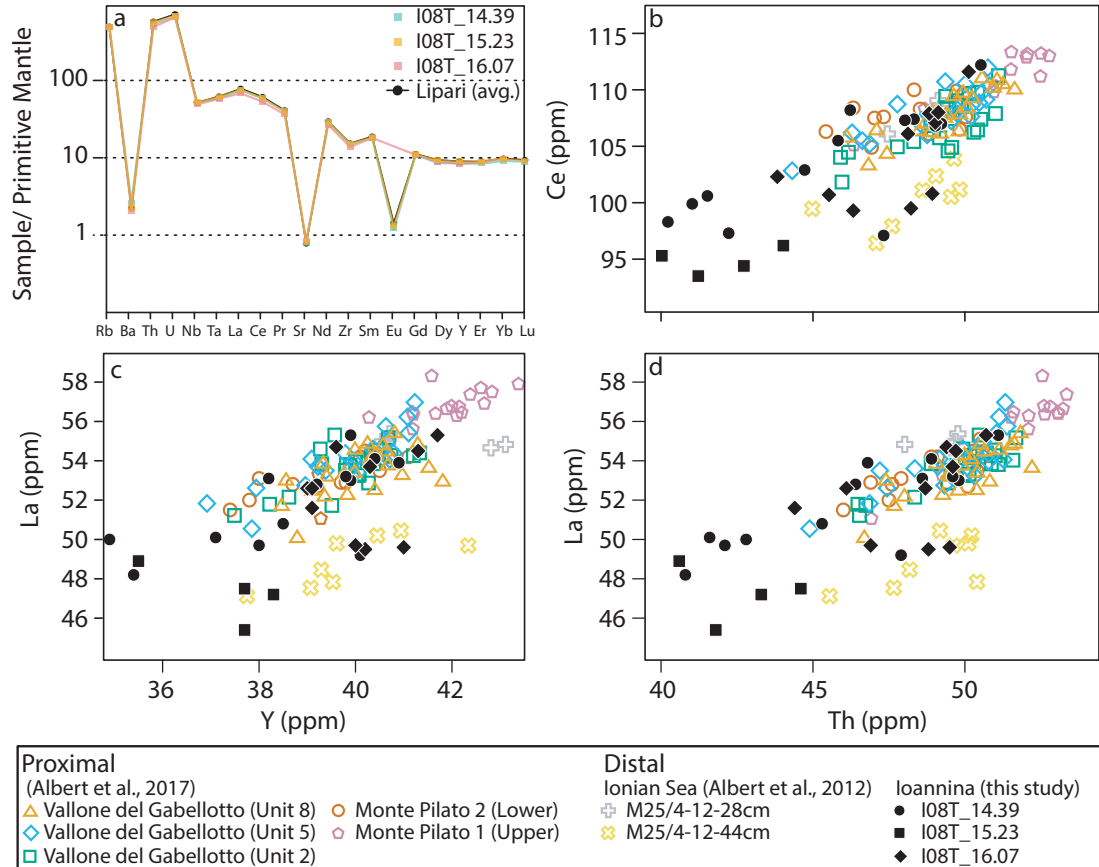


Figure 8. Trace element analysis of I-08 tephra layers I08T\_16.07, I08T\_15.23, and I08T\_14.39 plotted against Lipari proximal and Ionian Sea distal tephra deposits from (Albert et al., 2017), including: (a) average mantle normalised (Sun and McDonough, 1989) trace element profiles and (b-d) trace element biplots.

586 (Tomlinson et al., 2012). Of the distal occurrences of the CI/Y-5 tephra this upper  
587 flow end member is only identified in Megali Limni, Tenaghi Philippon, and Kalodiki  
588 (Greece; Margari et al. 2007; Wulf et al. 2018; Pyle et al. 2006) and the archaeological  
589 site of Crvena Stijena (Montenegro; Morley and Woodward 2011). Elsewhere tephra  
590 deposits associated with the CI eruption, for example, in PRAD 1-2 (Adriatic Sea; Bourne  
591 et al. 2010) and Lake Ohrid (Albania/Montenegro; Vogel et al. 2010), have chemical  
592 compositions which more closely match the lower and intermediate fall deposits. The  
593 offset in glass geochemical composition of the CI/Y-5 tephra layer between these different  
594 sites may arise from a variety of factors, including the height of the volcanic plume at  
595 different stages of the eruption, the prevailing wind direction, and the varying atmospheric  
596 transport and deposition of tephra glass shards due to differences in the eruption dynamics  
597 (e.g. injection height, wind speed, volume) and physical properties between glass shards  
598 generated in different phases of the eruption.

599 With regards to the thickness of the Ioannina I08T\_30.14 (CI/Y-5) deposit, estimates  
600 from the Costa et al. (2012) ash fall out model for the Campanian Ignimbrite suggest  
601 that a ca. 10 cm deposit is expected at the site. That the deposit in the I-08 sequence, at  
602 even the lowest estimate for layer thickness, exceeds the model estimate is likely related  
603 to site-specific factors. The increased thickness of the I-08\_30.14 layer is not without  
604 precedent. In their work mapping the thickness of the CI/Y-5 tephra marker Engwell et al.  
605 (2014) argue that in distal subaerial environments deposits are typically thicker than for  
606 equivalent deep sea deposits. Primarily, the large scale of the Ioannina catchment means  
607 large volumes of tephra would have been deposited into the lake environment through  
608 subsequent in-wash processes. Post-depositional reworking of unconsolidated tephra  
609 deposits from the surrounding landscape, facilitated by the steep topography, seems  
610 likely in the Ioannina basin and may have led to the redeposition of sediments in the lake.

## 611 5.2 Interpreting the post-CI tephra record

612 Here we consider two interpretations of the tephra distributions outlined in Section 4.2.3,  
613 in sediments from 29.88 to 28.51 m depth which postdate the 39.85 ka Campanian  
614 Ignimbrite eruption. Firstly we consider the evidence that peaks in tephra glass shards  
615 represent primary air-fall of post-CI eruptive activity at Campi Flegrei. Secondly, we  
616 argue that they may represent reworking of tephra within the Ioannina catchment as well  
617 as within the lake basin itself.

618 **Primary air-fall** Multiple post-CI last glacial tephra layers have been identified in the  
619 proximal Campi Flegrei stratigraphy, often termed the ‘Tufi Biancastri’ sequence (Tab.  
620 S7). Discriminating these eruptions in distal archives is challenging, however, given their  
621 close, often overlapping, glass shard geochemical compositions (e.g Paterne et al., 1988).  
622 Within the caldera, Tufi Biancastri tephra deposits have been identified at Verdolino (the

ca. 28 ka BP VRb and ca. 30 ka BP VRa; Pappalardo et al. 1999), and Trefola (the <38 ka BP TLo; Tomlinson et al. 2012). At Ponti Rossi, to the northeast of the caldera, the Masseria del Monte Tuff (MdM), associated with a large VEI 6 eruption ca. 30 ka BP, has recently been correlated with the widespread Y-3 marine tephra (Albert et al., 2019). The MdM/Y-3 tephra marker has been identified at a range of sites throughout the Mediterranean, including at Tenaghi Philippon (Wulf et al., 2018), to the east of the Ioannina site. Additionally, a number of extra-caldera outcrops linked to post-CI activity at Campi Flegrei have also been identified; most notably the SMP1-e and CE-1 deposits (Sulpizio et al., 2003; Albert et al., 2015).

In the distal realm, a range of post-CI tephra markers associated with eruptions of Campi Flegrei have been described that have not been correlated to an eruption identified within the proximal stratigraphy (Tab. S7). At the nearby Lago Grande di Monticchio the TM-17-2 tephra, associated with post-CI volcanism at Campi Flegrei, is dated at  $35,530 \pm 1780$  varve yrs BP. Further afield, sediment cores from the Adriatic Sea Matthews et al. (2015) highlight a layer consisting of both trachytic and rhyolitic shards, termed SA03-11-T1535 (Tab. S7). The trachytic component of SA03-11-T1535 is chemically trachytic component is chemically identical to the Campanian Ignimbrite, but the stratigraphic position and association to the rhyolitic component of the marker lead (Matthews et al., 2015) to argue a link to the CI eruption is implausible. The SA03-11-T1535 tephra marker correlates with a post-CI tephra marker reported in the Ionian Sea and the replication of the bimodal rhyolitic and trachytic chemical signature indicate it to be a distinctive layer from a single eruption event. The absence of any rhyolitic component in the post-CI cryptotephra peaks observed in the I-08 record mean that we can not identify a correlative with SA03-11-T1535.

The I08T\_30.14 visible tephra marker has a broad geochemical composition, containing not only the low CaO, MgO, and FeO<sub>t</sub> and high Na<sub>2</sub>O end members of the CI fall and the lower and intermediate flow units, but also the raised K<sub>2</sub>O, lower Na<sub>2</sub>O end member associated with the upper flow in the proximal stratigraphy (Tab. S7; citetTomlinson2012). All of the analysed tephra deposits which postdate the I08T\_30.14 tephra marker have major and minor element geochemical compositions which fall within the envelope of the I08T\_30.14 (Fig. S5) and, therefore, may represent reworked material from this deposit. Perhaps the most diagnostic component of the Campanian Ignimbrite tephra marker, which helps to discriminate it from other post-CI eruptions, is the upper flow end member (Tomlinson et al., 2012). Thus, I-08 tephra layers which contain glass shards with upper flow-like compositions are likely to be reworked CI from the catchment (Fig. S5).

As a result of the broad geochemical composition of the I08T\_30.14 tephra marker, identifying subsequent eruptions is challenging. For example, second to the CI, the most widespread last glacial tephra marker from Campi Flegrei is the ca. 30 ka BP Y-3 stratigraphic marker correlated by Albert et al. (2019) to the proximal Masseria

663 del Monte Tuff. Across the full range of major and minor elements the geochemical  
664 fingerprint of the Y-3 tephra marker falls within the envelope of the I08T\_30.14 (Fig. S6).  
665 It is possible to differentiate the markers, however, through  $\text{FeO}_t$  wt.% and the bimodal  
666  $\text{K}_2\text{O}$  distribution associated with the MdM/Y-3 deposit (Fig. S6).

667 The geochemical composition of the I08T\_28.98 tephra horizon does not match the  
668 MdM/Y-3 across the full major element geochemical assemblage of the Y-3 (Fig. S6)  
669 yet nor does the I08T\_28.98 perfectly match the geochemistry of I08T\_30.14. Given the  
670 difference in composition between the I08T\_28.98 cryptotephra layer and the I08T\_30.14  
671 (CI/Y-5) deposit, the I08T\_28.98 is suggested to represent a post-CI primary air-fall  
672 deposit, although correlation is not possible at this stage. Future trace element analysis  
673 may provide a means of discriminating primary tephra inputs associated with post-  
674 CI volcanism from reworked material associated with the Campanian Ignimbrite and  
675 I08T\_30.14 tephra markers.

676 **Reworking** The presence of glass shards with geochemical compositions unique to  
677 the CI is the primary indicator that peaks in glass shard concentration overlying the  
678 I08T\_30.14 (CI/Y-5) are most likely the products of the remobilisation of this tephra  
679 marker (Fig. S5). Specifically, glass shard compositions that match the products of the  
680 lower and intermediate flow (*sensu* Tomlinson et al. 2012), characterised by low  $\text{CaO}$ ,  
681  $\text{MgO}$ , and  $\text{FeO}_t$  and high  $\text{Na}_2\text{O}$  concentrations are unique identifiers of the reworked  
682 material.

683 The profile of glass shard concentrations against depth further suggests reworking,  
684 particularly in the upper layers (<28.8 m depth). In low energy lake sediment sequences  
685 primary air-fall tephra inputs are typically associated with a distinct peak followed by  
686 a decrease in the overlying sediments (Davies, 2015). The gradual increase in glass  
687 shard concentration between 28.97 and 28.66 m depth in the I-08 core does not suggest a  
688 primary input and could instead be interpreted as a gradual change in the sedimentary  
689 regime in the catchment.

690 A particular feature of this section of the core is the presence of shell layers absent  
691 from the underlying sediments. The presence of intervals within the Ioannina sediment  
692 sequence that contain molluscan faunal remains are argued to reflect lake-level variation  
693 (Frogley et al., 2009). Molluscan shells are preserved in the sediment above ca. 29.9 m,  
694 suggesting that water levels were decreasing at the time of deposition. Tephra material  
695 at the lake margins would have been subaerially exposed following lake level lowering,  
696 then remobilised and deposited further into the lake basin, including to the I-08 core  
697 site. Such a process is consistent with the trend of gradual increase in tephra glass shard  
698 concentrations between 29.88 and 28.51 m depth (Fig. 9).

699 Alternatively, the recurrent nature of tephra remobilisation suggested by the stratig-  
700 raphy of glass shard distributions (Fig. 6a), which shows pulses of increased glass  
701 shard concentration, may reflect surface run-off from a continuously eroding catchment.

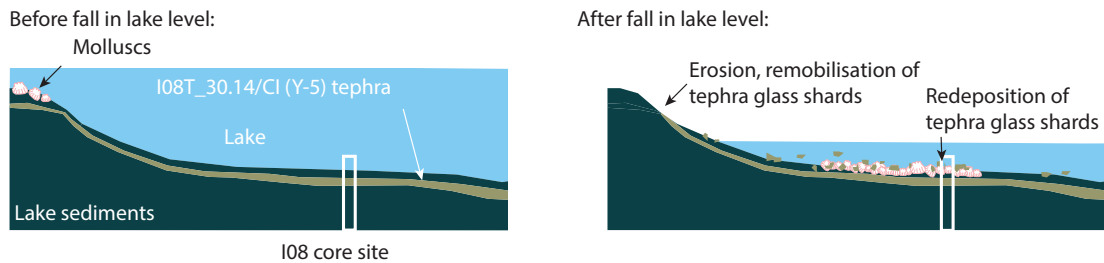


Figure 9. A schematic showing how a fall in lake level, also suggested by the presence of molluscan fauna within the I-08 core at the same depths, may have facilitated tephra reworking within the Ioannina catchment.

702 Lake Ioannina is primarily groundwater-fed and located in a basin largely bounded by  
 703 steep slopes; thus it seems unlikely that processes of alluvial erosion and deposition are  
 704 responsible for the recurrent inputs of reworked tephra.

705 A final mechanism which may explain the remobilisation of tephra deposits associated  
 706 with the Campanian Ignimbrite eruption in the I-08 core may be that the redeposited  
 707 tephra layers reflect a regional, extra-basin, erosional signal. Reworking of the Campanian  
 708 Ignimbrite tephra layer has been identified in both the Tenaghi Phillipon (Wulf et al.,  
 709 2018) and Kopais (Hardiman, 2012) Greek cryptotephra records. Remobilisation of  
 710 tephra deposits is becoming increasingly recognised as an important stage in the taphonomy  
 711 of volcanic ash (Dominguez et al., 2020; Buckland et al., 2020) and the Campanian  
 712 Ignimbrite deposit, widespread and deposited contemporaneously to the dry stadial  
 713 conditions associated with Heinrich stadial 4, would likely have been frequently eroded  
 714 and remobilised from the land surface. Indeed, tephra associated with the Campanian  
 715 Ignimbrite eruption is found in aeolian sequences as far afield as Ukraine (Melekestsev  
 716 et al., 1984) and Romania where deposits of the tephra >1 m thick have been identified  
 717 (Fitzsimmons et al., 2013). It is therefore possible that aeolian remobilisation of tephra  
 718 material may also be reflected in the Ioannina record, however, as noted, little evidence  
 719 exists of geochemical alteration of tephra which would be expected if tephra has been  
 720 remobilised from exposed environments.

721 To summarise, the consistent geochemical signal of glass shards deposited within  
 722 the I-08 core between 29.88 and 28.51 m depth suggests erosion and redeposition of  
 723 Campanian Ignimbrite tephra into the lake from the wider Ioannina catchment and the  
 724 lake basin edges. Remobilisation appears to take place in two phases representing at least  
 725 two separate processes. The shape of the shard concentration profile, which gradually  
 726 decreases, suggests that immediately above the visible I08T\_30.14 (CI) deposit, from  
 727 29.92 m through to 29.70 m depth tephra input is related to erosion of primary tephra fall  
 728 from the Campanian Ignimbrite eruption within the Ioannina catchment. Subsequently,  
 729 a hiatus in tephra deposition is interpreted as reflecting landscape stabilisation, with

730 tephra deposits are no longer exposed to processes of surface run-off. The hiatus is clear  
 731 in both the XRF data as well as the tephra glass shard concentration (Fig. 6a-c). We  
 732 suggest the I08T\_28.98 tephra marker, which is constrained to a 2 cm depth interval, is  
 733 a primary air-fall deposit associated with Tufi Biancastri volcanism at Campi Flegrei  
 734 caldera, however, we cannot yet correlate this tephra deposit to a specific eruption. From  
 735 ca. 28 m depth upwards, there is a change in the sedimentary regime at the I-08 core  
 736 site, which we interpret as a reduction in lake level resulting in the remobilisation of  
 737 tephra material from the exposed lake margins. Extra-basin inputs from either aeolian  
 738 remobilisation of exposed tephra surfaces or subsequent primary air-fall tephra inputs  
 739 cannot be ruled out, however, given hiatuses in deposition of tephra glass shards, are  
 740 unlikely to act as the dominant processes driving tephra deposition.

### 741 **5.3 Age-depth model**

742 The identification of the Pantelleria Green Tuff (Y-6) and Campanian Ignimbrite (Y-5)  
 743 tephra markers within I-08 provides an opportunity to extend the chronology of Jones et al.  
 744 (2013) back to ca. 45 ka BP. Furthermore, the identification of the Vallone del Gabbellotto  
 745 (E-1) provides an opportunity to refine the Holocene chronology of the I-08 core. Here  
 746 we present a revised I-08 age-depth model which incorporates the three new tephra ages  
 747 (Tab. 2; Fig. 10). The new full core-length age model incorporates earlier radiocarbon  
 748 dates from macrocharcoal samples and compound specific radiocarbon analysis (CSRA)  
 749 for the upper section of the core (Jones et al., 2013). The uncalibrated radiocarbon age  
 750 estimate for the E-1 marker (Caron et al., 2012) is recalibrated using IntCal20 as part  
 751 of the OxCal model. Visible tephra deposits are most likely deposited over the course  
 752 of days and weeks as opposed to years, therefore the 18 cm thick I08T\_30.14 deposit  
 753 is treated as an event horizon in the age model. The  $39.85 \pm 0.14$  ka BP age for the CI  
 754 eruption is input at the lower (30.14 m) and upper (29.96 m) bounds of the I08T\_30.14  
 755 tephra.

Ioannina Tephra	Correlative		Eruption Age (ka)	Method	Reference
	Proximal	Distal			
I08T_14.39	Vallone del Gabbellotto	E-1	$7.77 \pm 0.04$	$^{14}\text{C}$	Caron et al. (2012)
I08T_30.14	Campanian Ignimbrite	Y-5	$39.85 \pm 0.14$	$^{40}\text{Ar}/^{39}\text{Ar}$	Giaccio et al. (2017)
I08T_31.93	Pantelleria Green Tuff	Y-6	$45.7 \pm 1.00$	$^{40}\text{Ar}/^{39}\text{Ar}$	Scaillet et al. (2013)

Table 2. Ioannina core I-08 tephra layers, and most widely used dates associated with their marine and distal correlatives.  $^{14}\text{C}$  are uncalibrated.

756 The new age model provides age estimates for the uncorrelated Aeolian Island tephra  
 757 markers, I08T\_16.07 and I08T\_15.23, dated here to 12.46 to 10.21 ka BP and 10.65 to  
 758 8.52 ka BP respectively, Fig. 10b-c. The ca. 11 ka BP age for I08T\_16.07 further supports  
 759 the proposed correlation of that layer to the Ionian Sea tephra marker M25/4-12-44cm

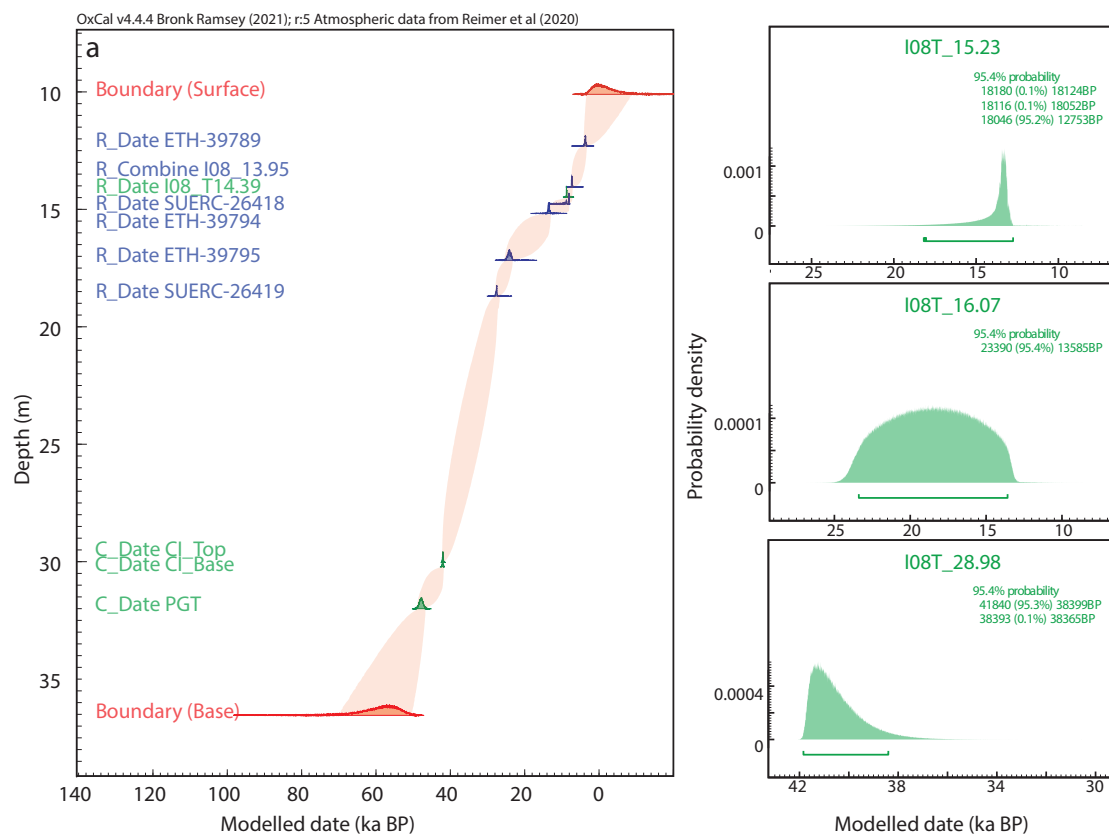


Figure 10. The new I-08 age-depth model, showing: (a) OxCal P\_sequence depositional model depth plot, incorporating radiocarbon (blue) and tephra (green) dates, and (b) posterior probability density functions for I08T\_16.07 and I08T\_15.23. Interpolation and posterior probability density functions are shown at 95.4% confidence limits.

760 Ionian Sea tephra marker, which occurs in sediments of Late Glacial age within the  
761 M25/4-12 core oxygen isotope stratigraphy (Negri et al., 1999; Albert et al., 2017).

## 762 **6 Implications of the Ioannina tephra record**

### 763 **6.1 Regional tephra correlations**

764 Three widespread tephra horizons have been identified in the Ioannina sequence: the Pan-  
765 telleria Green Tuff (PGT/Y-6), the Campanian Ignimbrite (CI/Y-5), and the Vallone del  
766 Gabellotto (VG/E-1), facilitating direct correlation of the Ioannina I-08 sequence with re-  
767 gional palaeoecological and palaeoclimatic reconstructions from different environmental  
768 contexts (Fig. 11).

769 The ca. 40 ka BP CI/Y-5 tephra layer in the Ioannina record permits correlation to  
770 key southern European terrestrial palaeoenvironmental records, such as Lago Grande di  
771 Monticchio, Italy (Allen et al., 1999; Wulf et al., 2004), Lake Ohrid, Albania/Montenegro  
772 (Vogel et al., 2010; Leicher et al., 2016) and Tenaghi Philippon, Greece (Müller et al.,  
773 2011; Wulf et al., 2018), as well as central and eastern Mediterranean marine proxy  
774 records including cores from the Ionian (Keller et al., 1978; Albert et al., 2012), Tyrre-  
775 hanian (Paterne et al., 1988), Adriatic (Bourne et al., 2010), Aegean (Keller et al., 1978;  
776 Satow et al., 2015) and Black Seas (Cullen et al., 2014). The CI/Y-5 marker can be used  
777 in inter-site comparisons of the impact of Heinrich stadial 4 (HS4; 40.2 to 38.3 ka BP,  
778 *sensu* Sanchez Goñi and Harrison 2010). High resolution analysis of the I-08 vegetation  
779 record in sediments surrounding the I08T\_30.14 tephra marker would allow the pattern  
780 and timing of the ecosystem response to HS4 at the site to be precisely evaluated and  
781 compared to other sites in the eastern Mediterranean.

782 The ca. 46 ka BP PGT/Y-6 tephra marker facilitates direct correlation to terrestrial  
783 records with palaeoenvironmental sequences including Lake Ohrid, and to marine cores  
784 from the Sicily channel (Tamburino et al., 2012) and Ionian Sea (Keller et al., 1978).  
785 Together the PGT/Y-6 and CI/Y-5 tephra layers bracket an interval of ca. 6 ka in the  
786 Ioannina, Lake Ohrid and Ionian Sea records associated with 4 Dansgaard-Oeschger  
787 events observed in the Greenland ice-core records (Rasmussen et al., 2014). Comparison  
788 of palaeoenvironmental proxies within these archives could allow both local to regional  
789 and proxy-specific responses to these climate oscillations to be explored with high  
790 precision.

791 The presence of the Campanian Ignimbrite and Pantelleria Green Tuff tephra layers  
792 also provides an exciting opportunity to link the valuable palaeoenvironmental record  
793 contained within the Ioannina sequence to regional archaeological sites. For example,  
794 CI/Y-5 deposits have been identified in the Klissoura and Franchthi sequences (Lowe  
795 et al., 2012), and the PGT/Y-6 marker has been identified at Theopetra (Karkanas et al.,  
796 2014). These tephra linkages establish a chronological framework which, going forward,

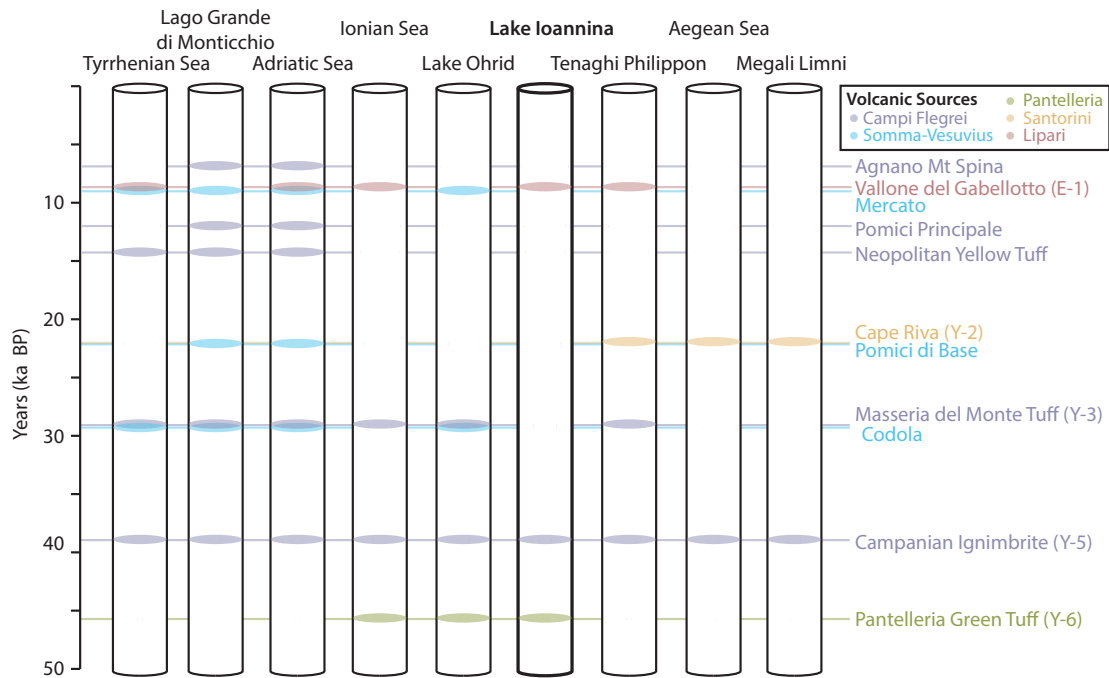


Figure 11. Simplified summary diagram of key tephra horizons within the Mediterranean tephrostratigraphic framework for the past 50 ka. Archives included here are: Tyrrhenian Sea (Paterne et al., 1988; Albert et al., 2012), Lago Grande di Monticchio (Wulf et al., 2004, 2008), Adriatic Sea (Bourne et al., 2010; Matthews et al., 2015), Ionian Sea (Keller et al., 1978; Albert et al., 2012; Insinga et al., 2014), Lake Ohrid (Wagner et al., 2008; Vogel et al., 2010; Sulpizio et al., 2010; Leicher et al., 2016), Lake Ioannina (this study), Tenaghi Philippon (Wulf et al., 2018), the Aegean Sea (Satow et al., 2015), and Megali Limni (Margari et al., 2007). Eruption ages from Bronk Ramsey et al. (2015) other than Agnano Mt Spina (Smith et al., 2011), Vallone del Gabbello (E-1) (Albert et al., 2019), Mercato (Santacroce et al., 2008) and Pantelleria Green Tuff (Y-6) (Scaillet et al., 2013). Site locations are shown in Fig. 1.

797 we hope will facilitate more thorough investigation of the environmental niches occupied  
798 by early Europeans in the region following their expansion out of Africa.

799 The identification of three cryptotephra layers correlated to Lipari between ca. 16  
800 and 14 m depth in the I-08 sequence provides the first securely dated evidence that  
801 Lipari erupted at least three times during the LGIT and Early Holocene. The Vallone  
802 del Gabellotto (E-1) isochron connects the Ioannina sequence to archives in the Ionian,  
803 Adriatic and Tyrrenian seas (Albert et al., 2017), and the terrestrial Tenaghi Philippon  
804 peat sequence (Wulf et al., 2018). Preliminary dates for the two earlier Lipari cryptotephra  
805 layers suggests two more tie points may exist between Ioannina and the Ionian Sea,  
806 however, further geochemical data is needed to confirm these findings.

## 807 **6.2 Challenges in cryptotephra analysis of the I-08 core**

808 The frequency of tephra dispersal from explosive eruptions in the Mediterranean region  
809 during the last glacial period and the geographical location of Lake Ioannina down-wind  
810 from the productive Italian Arc volcanoes, suggested that many cryptotephra layers  
811 would be found in the I-08 core sediments. However, cryptotephra analyses did not  
812 identify horizons of primary ash fall in the section of the I-08 core between 29 and 18 m.

813 The identification of discrete tephra layers from Lipari in the Late Glacial and  
814 Early Holocene sediments at Ioannina highlight the suitability of the Lake Ioannina  
815 sequence for capturing cryptotephra layers. However, during the last glacial when high  
816 concentrations of tephra were deposited in the Ioannina catchment from the voluminous  
817 Campanian Ignimbrite eruption, the swamping effect of the reworked CI/Y-5 tephra  
818 through processes of intra-basin focussing and redistribution of tephra glass shards made  
819 the detection of cryptotephra from primary air-fall impossible. Thus, even if primary  
820 air-fall tephra layers were present in the I-08 core sequence as cryptotephra horizons  
821 they would be difficult to identify against the background of reworked tephra. The  
822 challenges associated with identifying primary airfall from closely-spaced eruptions  
823 of similar geochemical composition is not a new one in tephrostratigraphic research  
824 (e.g Pyne-O'Donnell et al., 2008). In an attempt to overcome these challenges glass  
825 shard colour, grain size, and morphology were carefully considered during microscopic  
826 analysis of samples with the aim of detecting any changes in glass shard characteristics  
827 that might indicate input of tephra from different sources (McLean et al., 2018). However,  
828 as has been noted from many distal tephra archives, silicic tephra from Mediterranean  
829 sources have quite similar morphologies, so few eruptions are distinguishable on the  
830 basis of morphology alone (Bourne et al., 2010; Matthews et al., 2015). Thus, it is  
831 possible that cryptotephra layers were not found during this study because the shards  
832 from different eruptions in the Mediterranean tend to be of similar morphology and  
833 colour.

834 Unexpectedly, this study has demonstrated that the identification of reworked tephra  
835 horizons can, in supplement to other proxy data such as grain size and geochemistry,

836 provide an insight into changing processes of erosion, sediment in-wash, and reworking  
837 within a lake catchment. The value of detailed sedimentary analyses to understand  
838 tephra taphonomy has been demonstrated in this study through the combination of grain  
839 size analysis, XRF data, and tephra shard counting. Complex processes of sediment  
840 remobilisation and reworking were identified, raising questions about the integrity of the  
841 sediment record between 29 and 28.5 m depth as a primary, undisturbed, deposit. The  
842 presence of non-contemporaneous tephra within younger sediments suggests in-wash  
843 and redeposition of older material from the edge of the lake further into the lake. Deter-  
844 mining the age offset between the age of the redeposited material and contemporaneous  
845 sedimentation would be a challenge, further highlighting the importance of sediment  
846 taphonomy in Quaternary reconstructions.

847 The absence of tephra evidence for a number of widespread Quaternary eruptions in  
848 the I-08 sequence may be due to preferential deposition of tephra deposits near inflows  
849 and internal redistribution through currents (Pyne-O'Donnell et al., 2008). For example,  
850 internal processes can result in tephra deposits being reworked to below detection levels  
851 in some areas of the lake, however, such processes are complex and dynamic (Dugmore  
852 and Newton, 2012; Watson et al., 2016). Spatial variation in intra-basin focussing of  
853 tephra over time may explain why cryptotephra are present within the sequence over the  
854 Late Glacial and Early Holocene but not during other periods.

### 855 **6.3 Methodological recommendations**

856 Syn-depositional and post-depositional tephra transportation have been demonstrated  
857 in a range of studies undertaken in lake environments, often revealing large intra-basin  
858 variability in visible and/or crypto- tephra layer thickness (Mangerud et al., 1984). In the  
859 case of the Ioannina record, where tephrostratigraphic analysis was carried out only on a  
860 single core containing evidence of reworked sediment, the record of tephra deposited at  
861 lake site may not have been fully captured (Watson et al., 2016). Thus, replication of  
862 this study on future cores from the site may provide a more complete picture of tephra  
863 deposition at Ioannina.

864 The omission of key regional tephra markers (e.g. the Y-3) may be a result of small  
865 gaps between the core segments, an artefact of the coring methodology applied. Gaps  
866 in the stratigraphy mean it is possible that key isochrons may be missing (Lowe, 2011).  
867 Furthermore, gaps in the core complicate the identification of the primary ash fall layer  
868 and may results in a reworked layer being identified as a primary air-fall deposit, which  
869 can result in age attribution of an eruption age to an incorrect depth. Detailed stratigraphic  
870 analysis, facilitating the identification of horizons where reworking is likely, can help in  
871 developing a robust tephrochronology. We, therefore, highlight the importance of taking  
872 overlapping, parallel cores wherever possible, which minimise gaps in the stratigraphy.

873    **7 Conclusions**

874    The development of an extended independent chronology for the I-08 core is a step  
875    forward in the dating of an important palaeoenvironmental record. The integration of the  
876    Ioannina site into the Mediterranean tephra framework provides direct correlations with  
877    a range of Quaternary sequences in the Mediterranean region. The potential of tephra  
878    studies at Ioannina is by no means limited to the last glacial cycle, and tephrochronologies  
879    provide opportunities for dating and correlation of records over multiple glacial cycles.  
880    Importantly, tephra studies may act as independent checks of earlier, tuned chronologies  
881    for Ioannina sequences.

882    The chronology developed here also opens up opportunities for future work on the I-08 core,  
883    particularly the potential for increased resolution, sub-millennial scale study of the proxy record contained within the sediments. Pollen analysis of Ioannina core  
884    I-284 has revealed marked vegetation responses to millennial-scale climatic oscillations  
885    (Tzedakis et al., 2004). The three secure isochrons, the last glacial Campanian Ignimbrite  
886    (CI/Y-5; ca. 39.8 ka BP) and Pantelleria Green Tuff (PGT/Y-6; ca. 45.7 ka BP) and the  
887    Holocene Vallone del Gabellotto cryptotephra marker (E-1; ca. 8.3 ka BP) identified in  
888    the Ioannina sequence provide opportunities for direct correlation of this pollen record  
889    with palaeoenvironmental, palaeoclimate, and archaeological sequences throughout  
890    the eastern Mediterranean. In particular, the CI/Y-5 marker provides an opportunity  
891    to undertake detailed inter-site comparisons of the timing of ecosystem responses to  
892    Heinrich stadial 4 (40.2-38.3 ka BP *sensu*. Sanchez Goñi and Harrison 2010).

894    We have highlighted a significant challenge in Mediterranean tephra studies and,  
895    indeed, tephra studies globally, which is the identification of primary airfall cryptotephra  
896    layers against a background of sediment (and therefore tephra) reworking, particularly  
897    in areas where multiple eruptions produce huge volumes of glass shards with similar  
898    morphologies and geochemical signatures. In this work, whilst it is possible that the  
899    record contains distal deposits from multiple eruptions from Campi Flegrei, particularly  
900    those following the Campanian Ignimbrite eruption, it has not been possible to produce  
901    reliable correlations through geochemical analysis. The main barrier preventing geo-  
902    chemical attribution of these deposits to subsequent eruptions is the broad geochemical  
903    envelope of the large Campanian Ignimbrite eruption which has multiple phases (Tom-  
904    linson et al., 2012), many of which are identified at Ioannina. Refining and developing  
905    techniques which allow for the further discrimination of these different eruptions will be  
906    a crucial step in developing and expanding the Mediterranean tephra chronostratigraphic  
907    framework.

## 908 8 Acknowledgements

909 We thank Tim Jones and Vicky Cullen for supporting the work on the Holocene and  
910 Lateglacial sections of the core. We are also indebted to Chronis Tzedakis and Ian Lawson  
911 for providing the I-08 core and numerous constructive comments on the manuscript,  
912 and to Harriet Allen for her support throughout this project. Iris Buisman and Victoria  
913 Smith kindly supported EPMA analysis. AM was funded by a PhD studentship from  
914 the Department of Geography, University of Cambridge, with initial work by CSL  
915 and PGA supported via the NERC-funded project on Response of Humans to Abrupt  
916 Environmental Transitions (NE/E015670/1). We thank Sabine Wulf, Roberto Sulpizio,  
917 and Simon Blockley for their constructive feedback on the manuscript.

## 918 References

- 919 Albert, P., Hardiman, M., Keller, J., Smith, V. C., Bourne, A. J., Wulf, S., Zanchetta,  
920 G., Sulpizio, R., Müller, U. C., Pross, J., Ottolini, L., Matthews, I. P., Blockley, S. P.,  
921 and Menzies, M. A. (2015). Revisiting the Y-3 tephrostratigraphic marker: a new  
922 diagnostic glass geochemistry, age estimate, and details on its climatostratigraphical  
923 context. *Quaternary Science Reviews*, 118:105–121.
- 924 Albert, P., Tomlinson, E. L., Lane, C. S., Wulf, S., Smith, V. C., Coltelli, M., Keller, J.,  
925 Lo Castro, D., Manning, C. J., Müller, W., and Menzies, M. A. (2013). Late glacial  
926 explosive activity on Mount Etna: Implications for proximal-distal tephra correlations  
927 and the synchronisation of Mediterranean archives. *Journal of Volcanology and  
928 Geothermal Research*, 265:9–26.
- 929 Albert, P. G., Giaccio, B., Isaia, R., Costa, A., Niespolo, E. M., Nomade, S., Pereira,  
930 A., Renne, P. R., Hinchliffe, A., Mark, D. F., Brown, R. J., and Smith, V. C. (2019).  
931 Evidence for a large-magnitude eruption from Campi Flegrei caldera (Italy) at 29 ka.  
932 *Geology*, 47(7):595–599.
- 933 Albert, P. G., Tomlinson, E. L., Smith, V. C., Di Roberto, A., Todman, A., Rosi, M.,  
934 Marani, M., Muller, W., and Menzies, M. A. (2012). Marine-continental tephra  
935 correlations: Volcanic glass geochemistry from the Marsili Basin and the Aeolian  
936 Islands, Southern Tyrrhenian Sea, Italy. *Journal of Volcanology and Geothermal  
937 Research*, 229-230:74–94.
- 938 Albert, P. G., Tomlinson, E. L., Smith, V. C., Di Traglia, F., Pistolesi, M., Morris, A.,  
939 Donato, P., De Rosa, R., Sulpizio, R., Keller, J., Rosi, M., and Menzies, M. (2017).  
940 Glass geochemistry of pyroclastic deposits from the Aeolian Islands in the last 50 ka:  
941 A proximal database for tephrochronology. *Journal of Volcanology and Geothermal  
942 Research*, 336:81–107.
- 943 Allen, J. R. L., Huntley, B., Brandt, U., Brauer, A., Hubberten, H.-W., Keller, J., Kraml,  
944 M., Mackensen, A., Mingram, J., Negendank, J. F., Nowaczyk, N. R., Oberhänsli, H.,

- 945      Watts, W. A., Wulf, S., and Zolitschka, B. (1999). Rapid environmental changes in  
946      southern Europe during the last glacial period. *Nature*, 400(6746):740–743.
- 947      Andersen, K. K., Azuma, N., Barnola, J. M., Bigler, M., Biscaye, P., Caillon, N.,  
948      Chappellaz, J., Clausen, H. B., Dahl-Jensen, D., Fischer, H., Flückiger, J., Fritzsche,  
949      D., Fujii, Y., Goto-Azuma, K., Grønsvold, K., Gundestrup, N. S., Hansson, M., Huber,  
950      C., Hvidberg, C. S., Johnsen, S. J., Jonsell, U., Jouzel, J., Kipfstuhl, S., Landais, A.,  
951      Leuenberger, M., Lorrain, R., Masson-Delmotte, V., Miller, H., Motoyama, H., Narita,  
952      H., Popp, T., Rasmussen, S. O., Raynaud, D., Rothlisberger, R., Ruth, U., Samyn,  
953      D., Schwander, J., Shoji, H., Siggard-Andersen, M. L., Steffensen, J. P., Stocker,  
954      T., Sveinbjörnsdóttir, A. E., Svensson, A., Takata, M., Tison, J. L., Thorsteinsson,  
955      T., Watanabe, O., Wilhelms, F., and White, J. W. (2004). High-resolution record  
956      of Northern Hemisphere climate extending into the last interglacial period. *Nature*,  
957      431(7005):147–151.
- 958      Blaauw, M. (2012). Out of tune: the dangers of aligning proxy archives. *Quaternary  
959      Science Reviews*, 36:38–49.
- 960      Blaauw, M., Christen, J. A., Bennett, K., and Reimer, P. J. (2018). Double the dates and  
961      go for bayes — impacts of model choice, dating density and quality on chronologies.  
962      *Quaternary Science Reviews*, 188:58 – 66.
- 963      Blockley, S. P., Bourne, A. J., Brauer, A., Davies, S. M., Hardiman, M., Harding, P. R.,  
964      Lane, C. S., MacLeod, A., Matthews, I. P., Pyne-O'Donnell, S. D., Rasmussen, S. O.,  
965      Wulf, S., and Zanchetta, G. (2014). Tephrochronology and the extended intimate  
966      (integration of ice-core, marine and terrestrial records) event stratigraphy 8–128 ka  
967      b2k. *Quaternary Science Reviews*, 106:88–100.
- 968      Blockley, S. P., Pyne-O'Donnell, S., Lowe, J., Matthews, I., Stone, A., Pollard, A.,  
969      Turney, C., and Molyneux, E. (2005). A new and less destructive laboratory procedure  
970      for the physical separation of distal glass tephra shards from sediments. *Quaternary  
971      Science Reviews*, 24(16):1952–1960.
- 972      Bond, G., Broecker, W., Johnsen, S., McManus, J., Labeyrie, L., Jouzel, J., and Bonani,  
973      G. (1993). Correlations between climate records from North Atlantic sediments and  
974      Greenland ice. *Nature*, 365(6442):143–147.
- 975      Bourne, A., Albert, P., Matthews, I., Trincardi, F., Wulf, S., Asioli, A., Blockley, S.,  
976      Keller, J., and Lowe, J. (2015). Tephrochronology of core prad 1-2 from the adriatic  
977      sea: insights into italy explosive volcanism for the period 200–80 ka. *Quaternary  
978      Science Reviews*, 116:28–43.
- 979      Bourne, A. J., Lowe, J., Trincardi, F., Asioli, A., Blockley, S. P., Wulf, S., Matthews, I., ,  
980      A., and Vigliotti, L. (2010). Distal tephra record for the last ca 105,000 years from  
981      core PRAD 1-2 in the central Adriatic Sea: implications for marine tephrostratigraphy.  
982      *Quaternary Science Reviews*, 29(23-24):3079–3094.
- 983      Bronk Ramsey, C. (2009). Bayesian analysis of radiocarbon dates. *Radiocarbon*,  
984      51(1):337–360.

- 985 Bronk Ramsey, C. (2020). OxCal v4.4: <https://c14.arch.ox.ac.uk/oxcal/OxCal.html>.
- 986
- 987 Bronk Ramsey, C., Albert, P., Blockley, S. P., Hardiman, M., Lane, C. S., Lee, S.,  
988 Matthews, I. P., Smith, V. C., and Lowe, J. J. (2015). Improved age estimates for key  
989 Late Quaternary European tephra horizons in the RESET lattice. *Quaternary Science  
990 Reviews*, 118:18–32.
- 991 Buckland, H. M., Cashman, K. V., Engwell, S. L., and Rust, A. C. (2020). Sources of  
992 uncertainty in the Mazama isopachs and the implications for interpreting distal tephra  
993 deposits from large magnitude eruptions. *Bulletin of Volcanology*, 82(3):1–17.
- 994 Caron, B., Siani, G., Sulpizio, R., Zanchetta, G., Paterne, M., Santacroce, R., Tema, E.,  
995 and Zanella, E. (2012). Late Pleistocene to Holocene tephrostratigraphic record from  
996 the Northern Ionian Sea. *Marine Geology*, 311–314:41–51.
- 997 Civetta, L., Cornette, Y., Crisci, G., Gillot, P. Y., Orsi, G., and Requejo, C. S. (1984). Ge-  
998 ology, geochronology and chemical evolution of the island of Pantelleria. *Geological  
999 Magazine*, 121(6):541–562.
- 1000 Costa, A., Folch, A., Macedonio, G., Giaccio, B., Isaia, R., and Smith, V. C. (2012).  
1001 Quantifying volcanic ash dispersal and impact of the Campanian Ignimbrite super-  
1002 eruption. *Geophysical Research Letters*, 39(10):1–16.
- 1003 Cullen, V. L., Smith, V. C., and Arz, H. W. (2014). The detailed tephrostratigraphy of a  
1004 core from the south-east Black Sea spanning the last ~60 ka. *Journal of Quaternary  
1005 Science*, 29(7):675–690.
- 1006 Dansgaard, W., Clausen, H. B., Gundestrup, N., Hammer, C. U., Johnsen, S. F., Kristins-  
1007 dottir, P. M., and Reeh, N. (1982). A new greenland deep ice core. *Science*,  
1008 218(4579):1273–1277.
- 1009 Dansgaard, W., Johnsen, S. J., Clausen, H. B., Dahl-Jensen, D., Gundestrup, N. S.,  
1010 Hammer, C. U., Hvidberg, C. S., Steffensen, J. P., Sveinbjörnsdóttir, Á. E., Jouzel,  
1011 J., and Bond, G. C. (1993). Evidence for general instability of past climate from a  
1012 250-kyr ice-core record. *Nature*, 364(6434):218–220.
- 1013 Davies, S. (2015). Cryptotephras: the revolution in correlation and precision dating.  
1014 *Journal of Quaternary Science*, 30(2):114–130.
- 1015 Dominguez, L., Bonadonna, C., Forte, P., Jarvis, P. A., Cioni, R., Mingari, L., Bran, D.,  
1016 and Panebianco, J. E. (2020). Aeolian Remobilisation of the 2011-Cordón Caulle  
1017 Tephra-Fallout Deposit: Example of an Important Process in the Life Cycle of Volcanic  
1018 Ash. *Frontiers in Earth Science*, 7:343.
- 1019 Dugmore, A. and Newton, A. (2012). Isochrons and beyond: maximising the use of  
1020 tephrochronology in geomorphology. *Jökull*, 62:39–52.
- 1021 Eastwood, W., Pearce, N., Westgate, J., Perkins, W., Lamb, H., and Roberts, N. (1999).  
1022 Geochemistry of santorini tephra in lake sediments from southwest turkey. *Global and  
1023 Planetary Change*, 21(1-3):17–29.
- 1024 Engwell, S. L., Sparks, R. S., and Carey, S. (2014). Physical characteristics of tephra

- 1025 layers in the deep sea realm: The Campanian Ignimbrite eruption. *Geological Society*  
1026 *Special Publication*, 398(1):47–64.
- 1027 Fitzsimmons, K. E., Hambach, U., Veres, D., and Iovita, R. (2013). The Campanian  
1028 Ignimbrite Eruption: New Data on Volcanic Ash Dispersal and Its Potential Impact on  
1029 Human Evolution. *PLoS ONE*, 8(6):e65839.
- 1030 Frogley, M. R., Griffiths, H. I., and Heaton, T. H. E. (2009). Historical biogeography and  
1031 Late Quaternary environmental change of Lake Pamvotis , Ioannina ( north-western  
1032 Greece ): evidence from ostracods. *Journal of Biogeography*, 28(6):745–756.
- 1033 Gehrels, M. J., Lowe, D. J., Hazell, Z. J., and Newnham, R. M. (2006). A continuous  
1034 5300-yr Holocene cryptotephrostratigraphic record from northern New Zealand and  
1035 implications for tephrochronology and volcanic hazard assessment. *The Holocene*,  
1036 16(2):173–187.
- 1037 Giacco, B., Hajdas, I., Isaia, R., Deino, A., and Nomade, S. (2017). High-precision  $^{14}\text{C}$   
1038 and 40Ar/39Ar dating of the Campanian Ignimbrite (Y-5) reconciles the time-scales  
1039 of climatic-cultural processes at 40 ka. *Scientific Reports*, 7(1):45940.
- 1040 Goñi, M. F. S., Turon, J.-L., Eynaud, F., and Gendreau, S. (2000). European climatic  
1041 response to millennial-scale changes in the atmosphere–ocean system during the last  
1042 glacial period. *Quaternary Research*, 54(3):394–403.
- 1043 Hardiman, M. J. (2012). *Testing and refining the chronology and correlation of Mediter-*  
1044 *ranean pollen records of late Last Glacial age using tephrochronology*. PhD thesis,  
1045 Royal Holloway, University of London.
- 1046 Hayward, C. (2012). High spatial resolution electron probe microanalysis of tephras  
1047 and melt inclusions without beam-induced chemical modification. *The Holocene*,  
1048 22:119–125.
- 1049 Higgs, E. S., Vita-Finzi, C., Harris, D. R., and Fagg, A. E. (1967). The climate, envi-  
1050 ronment and industries of Stone Age Greece: Part III. With an appendix on a late  
1051 Quaternary pollen diagram from Ioanninae. *Proceedings of the Prehistoric Society*,  
1052 1:199–244.
- 1053 Insinga, D. D., Tamburrino, S., Lirer, F., Vezzoli, L., Barra, M., De Lange, G. J., Tiepolo,  
1054 M., Vallefuoco, M., Mazzola, S., and Sprovieri, M. (2014). Tephrochronology of the  
1055 astronomically-tuned KC01B deep-sea core, Ionian Sea: Insights into the explosive  
1056 activity of the Central Mediterranean area during the last 200ka. *Quaternary Science*  
1057 *Reviews*, 85:63–84.
- 1058 Jochum, K. P. and Willbold, M. (2006). Reference materials in geoanalytical research  
1059 -review for 2004 and 2005. *Geostandards and Geoanalytical Research*, 30(3):143–156.
- 1060 Johnsen, S. J., Clausen, H. B., Dansgaard, W., Fuhrer, K., Gundestrup, N., Hammer,  
1061 C. U., Iversen, P., Jouzel, J., Stauffer, B., and Steffensen, J. P. (1992). Irregular glacial  
1062 interstadials recorded in a new greenland ice core. *Nature*, 359(6393):311–313.
- 1063 Jones, T. D., Lawson, I. T., Reed, J. M., Wilson, G. P., Leng, M. J., Gierga, M.,  
1064 Bernasconi, S. M., Smittenberg, R. H., Hajdas, I., Bryant, C. L., and Tzedakis, P. C.

- 1065 (2013). Diatom-inferred late Pleistocene and Holocene palaeolimnological changes in  
1066 the Ioannina basin, northwest Greece. *Journal of Paleolimnology*, 49(2):185–204.
- 1067 Jordan, N. J., Rotolo, S. G., Williams, R., Speranza, F., McIntosh, W. C., Branney, M. J.,  
1068 and Scaillet, S. (2018). Explosive eruptive history of pantelleria, italy: Repeated  
1069 caldera collapse and ignimbrite emplacement at a peralkaline volcano. *Journal of  
1070 Volcanology and Geothermal Research*, 349:47 – 73.
- 1071 Karkanas, P., White, D., Lane, C. S., Stringer, C., Davies, W., Cullen, V. L., Smith, V. C.,  
1072 Ntinou, M., Tsartsidou, G., and Kyparissi-Apostolika, N. (2014). Tephra correlations  
1073 and climatic events between the MIS6/5 transition and the beginning of MIS3 in  
1074 Theopetra Cave, central Greece. *Quaternary Science Reviews*, 118:170–181.
- 1075 Keller, J., Ryan, W. B., Ninkovich, D., and Altherr, R. (1978). Explosive volcanic activity  
1076 in the Mediterranean over the past 200,000 yr as recorded in deep-sea sediments.  
1077 *Bulletin of the Geological Society of America*, 89(4):591–604.
- 1078 Lane, C. S., Chorn, B. T., and Johnson, T. C. (2013). Ash from the Toba supereruption  
1079 in Lake Malawi shows no volcanic winter in East Africa at 75 ka. *Proceedings of the  
1080 National Academy of Sciences*, 110(20):8025–8029.
- 1081 Lane, C. S., Cullen, V., White, D., Bramham-Law, C., and Smith, V. (2014). Cryptotephra  
1082 as a dating and correlation tool in archaeology. *Journal of Archaeological Science*,  
1083 42(1):42–50.
- 1084 Lawson, I. T. (2001). *The Late Glacial and Holocene Environmental History of Greece*.  
1085 PhD thesis, University of Cambridge.
- 1086 Lawson, I. T., Frogley, M., Bryant, C. L., Preece, R., and Tzedakis, P. C. (2004). The  
1087 Lateglacial and Holocene environmental history of the Ioannina basin, north-west  
1088 Greece. *Quaternary Science Reviews*, 23(14):1599–1625.
- 1089 Le Bas, M. J., Maitre, R. W., Streckeisen, A., and Zanettin, B. (1986). A chemical  
1090 classification of volcanic rocks based on the total alkali-silica diagram. *Journal of  
1091 Petrology*, 27(3):745–750.
- 1092 Leicher, N., Zanchetta, G., Sulpizio, R., Giaccio, B., Wagner, B., Nomade, S., Francke,  
1093 A., and Carlo, P. D. (2016). First tephrostratigraphic results of the DEEP site record  
1094 from Lake Ohrid (Macedonia and Albania). *Biogeosciences*, 13:2151–2178.
- 1095 Li, C. and Born, A. (2019). Coupled atmosphere-ice-ocean dynamics in Dansgaard-  
1096 Oeschger events. *Quaternary Science Reviews*, 203:1–20.
- 1097 Lowe, D. J. (2011). Tephrochronology and its application: A review. *Quaternary  
1098 Geochronology*, 6(2):107–153.
- 1099 Lowe, J., Barton, N., Blockley, S. P., Ramsey, C. B., Cullen, V. L., Davies, W., Gamble,  
1100 C., Grant, K., Hardiman, M., Housley, R., Lane, C. S., Lee, S., Lewis, M., MacLeod,  
1101 A., Menzies, M., Müller, W., Pollard, M., Price, C., Roberts, A. P., Rohling, E. J.,  
1102 Satow, C., Smith, V. C., Stringer, C. B., Tomlinson, E. L., White, D., Albert, P.,  
1103 Arienz, I., Barker, G., Boric, D., Carandente, A., Civetta, L., Ferrier, C., Guadelli,  
1104 J.-L., Karkanas, P., Koumouzelis, M., Müller, U. C., Orsi, G., Pross, J., Rosi, M.,

- 1105 Shalamanov-Korobar, L., Sirakov, N., and Tzedakis, P. C. (2012). Volcanic ash layers  
1106 illuminate the resilience of Neanderthals and early modern humans to natural hazards.  
1107 *Proceedings of the National Academy of Sciences*, 109(34):13532–7.
- 1108 Lowe, J., Rasmussen, S., Björck, S., Hoek, W., Steffensen, J., Walker, M., and Yu, Z.  
1109 (2008). Synchronisation of palaeoenvironmental events in the north atlantic region  
1110 during the last termination: a revised protocol recommended by the intimate group.  
1111 *Quaternary Science Reviews*, 27(1):6 – 17. INTegration of Ice-core, Marine and  
1112 Terrestrial records (INTIMATE): Refining the record of the Last Glacial-Interglacial  
1113 Transition.
- 1114 Lowe, J. and Walker, M. J. (2015). Measuring quaternary time: A 50-year perspective.  
1115 *Journal of Quaternary Science*, 30(2):104–113.
- 1116 Mahood, G. A. and Hildreth, W. (1986). Geology of the peralkaline volcano at Pantelleria,  
1117 Strait of Sicily. *Bulletin of Volcanology*, 48(2-3):143–172.
- 1118 Mangerud, J. a. N., Lie, E., Furnes, H., Kristiansen, I. L., and Mo, L. L. (1984). A  
1119 Younger Dryas Ash Bed in western Norway, and its possible correlations with tephra  
1120 in cores from the Norwegian Sea and the North Atlantic. *Quaternary Research*,  
1121 104:85–104.
- 1122 Margari, V., Pyle, D., Bryant, C. L., and Gibbard, P. (2007). Mediterranean tephra  
1123 stratigraphy revisited: Results from a long terrestrial sequence on Lesvos Island,  
1124 Greece. *Journal of Volcanology and Geothermal Research*, 163(1):34–54.
- 1125 Marra, F., Castellano, C., Cucci, L., Florindo, F., Gaeta, M., Jicha, B. R., Palladino, D. M.,  
1126 Sottili, G., Tertulliani, A., and Tolomei, C. (2020). Monti sabatini and colli albani: the  
1127 dormant twin volcanoes at the gates of rome. *Scientific Reports*, 10(1):8666.
- 1128 Matthews, I. P., Trincardi, F., Lowe, J. J., Bourne, A. J., MacLeod, A., Abbott, P. M.,  
1129 Andersen, N., Asioli, A., Blockley, S. P., Lane, C. S., Oh, Y. A., Satow, C. S., Staff,  
1130 R. A., and Wulf, S. (2015). Developing a robust tephrochronological framework for  
1131 Late Quaternary marine records in the Southern Adriatic Sea: New data from core  
1132 station SA03-11. *Quaternary Science Reviews*, 118:84–104.
- 1133 McLean, D., Albert, P. G., Nakagawa, T., Suzuki, T., Staff, R. A., Yamada, K., Kitaba,  
1134 I., Haraguchi, T., Kitagawa, J., and Smith, V. C. (2018). Integrating the Holocene  
1135 tephrostratigraphy for East Asia using a high-resolution cryptotephra study from Lake  
1136 Suigetsu (SG14 core), central Japan. *Quaternary Science Reviews*, 183:36–58.
- 1137 Melekestsev, I. V., Kirianov, V., and Praslov, N. D. (1984). Catastrophic eruption in the  
1138 Phlegrean Fields region (Italy) - possible source for a volcanic ash in late Pleistocene  
1139 sediments on the European part of the USSR. *Vulkanologija i Seismologija*, 3:35–44.
- 1140 Meniel, L. C., Skinner, L. C., Tarasov, L., and Tzedakis, P. C. (2020). An ice-climate  
1141 oscillatory framework for dansgaard–oeschger cycles. *Nature Reviews Earth & Envi-  
1142 ronment*, 1(12):677–693.
- 1143 Morley, M. W. and Woodward, J. C. (2011). The Campanian Ignimbrite (Y5) tephra at  
1144 Crvena Stijena Rockshelter, Montenegro. *Quaternary Research*, 75(3):683–696.

- 1145 Müller, U. C., Pross, J., Tzedakis, P. C., Gamble, C., Kotthoff, U., Schmiedl, G., Wulf,  
1146 S., and Christianis, K. (2011). The role of climate in the spread of modern humans into  
1147 Europe. *Quaternary Science Reviews*, 30(3-4):273–279.
- 1148 Negri, A., Capotondi, L., and Keller, J. (1999). Calcareous nannofossils, planktonic  
1149 foraminifera and oxygen isotopes in the late Quaternary sapropels of the Ionian Sea.  
1150 *Marine Geology*, 157(1-2):89–103.
- 1151 Neugebauer, I., Wulf, S., Schwab, M. J., Serb, J., Plessen, B., Appelt, O., and Brauer, A.  
1152 (2017). Implications of s1 tephra findings in dead sea and tayma palaeolake sediments  
1153 for marine reservoir age estimation and palaeoclimate synchronisation. *Quaternary  
1154 Science Reviews*, 170:269–275.
- 1155 Pappalardo, L., Civetta, L., D’Antonio, M., Deino, A., Di Vito, M., Orsi, G., Carandente,  
1156 A., De Vita, S., Isaia, R., and Piochi, M. (1999). Chemical and Sr-isotopical evolu-  
1157 tion of the Phlegraean magmatic system before the Campanian Ignimbrite and the  
1158 Neapolitan Yellow Tuff eruptions. *Journal of Volcanology and Geothermal Research*,  
1159 91(2-4):141–166.
- 1160 Paterne, M., Guichard, F., Duplessy, J. C., Siani, G., Sulpizio, R., and Labeyrie, J.  
1161 (2008). A 90,000-200,000 yrs marine tephra record of Italian volcanic activity in  
1162 the Central Mediterranean Sea. *Journal of Volcanology and Geothermal Research*,  
1163 177(1):187–196.
- 1164 Paterne, M., Guichard, F., and Labeyrie, J. (1988). Explosive activity of the South Italian  
1165 volcanoes during the past 80,000 years as determined by marine tephrochronology.  
1166 *Journal of Volcanology and Geothermal Research*, 34(3-4):153–172.
- 1167 Peretyazhko, I. S., Savina, E. A., Karmanov, N. S., and Shcherbakov, Y. D. (2015).  
1168 Genesis of mugearites and benmoreites of nemrut volcano, eastern turkey: Magma  
1169 mixing and fractional crystallization of trachybassaltic melt. *Petrology*, 23(4):376–403.
- 1170 Pyle, D. M., Ricketts, G. D., Margari, V., van Andel, T. H., Sinitsyn, A. A., Praslov, N. D.,  
1171 and Lisitsyn, S. (2006). Wide dispersal and deposition of distal tephra during the  
1172 Pleistocene ’Campanian Ignimbrite/Y5’ eruption, Italy. *Quaternary Science Reviews*,  
1173 25(21-22):2713–2728.
- 1174 Pyne-O’Donnell, S., Blockley, S., Turney, C., and Lowe, J. (2008). Distal volcanic ash  
1175 layers in the lateglacial interstadial (gi-1): problems of stratigraphic discrimination.  
1176 *Quaternary Science Reviews*, 27(1):72–84. INTegration of Ice-core, Marine and  
1177 Terrestrial records (INTIMATE): Refining the record of the Last Glacial-Interglacial  
1178 Transition.
- 1179 Ramsey, C. B. (2008). Deposition models for chronological records. *Quaternary Science  
1180 Reviews*, 27(1-2):42–60.
- 1181 Ramsey, C. B. and Lee, S. (2013). Recent and planned developments of the program  
1182 oxcal. *Radiocarbon*, 55(2–3):720–730.
- 1183 Rasmussen, S. O., Bigler, M., Blockley, S. P., Blunier, T., Buchardt, S. L., Clausen,  
1184 H. B., Cvijanovic, I., Dahl-Jensen, D., Johnsen, S. J., Fischer, H., Gkinis, V., Guillevic,

- 1185 M., Hoek, W. Z., Lowe, J. J., Pedro, J. B., Popp, T., Seierstad, I. K., Steffensen,  
1186 J. P., Svensson, A. M., Valletlonga, P., Vinther, B. M., Walker, M. J., Wheatley, J. J.,  
1187 and Winstrup, M. (2014). A stratigraphic framework for abrupt climatic changes  
1188 during the Last Glacial period based on three synchronized Greenland ice-core records:  
1189 refining and extending the INTIMATE event stratigraphy. *Quaternary Science Reviews*,  
1190 106:14–28.
- 1191 Reimer, P. J. (2020). The IntCal20 Northern Hemisphere radiocarbon age calculation  
1192 curve (0–55 cal kBP). *Radiocarbon*, 00:1–33.
- 1193 Romero, J. R., Kagalou, I., Imberger, J., Hela, D., Kotti, M., Bartzokas, A., Albanis,  
1194 T., Evmirides, N., Karkabounas, S., Papagiannis, J., et al. (2002). Seasonal water  
1195 quality of shallow and eutrophic lake pamvotis, greece: implications for restoration.  
1196 *Hydrobiologia*, 474(1):91–105.
- 1197 Rotolo, S. G., Scaillet, S., La Felice, S., and Vita-Scaillet, G. (2013). A revision of the  
1198 structure and stratigraphy of pre-green tuff ignimbrites at pantelleria (strait of sicily).  
1199 *Journal of Volcanology and Geothermal Research*, 250:61–74.
- 1200 Roucoux, K., Tzedakis, P. C., Frogley, M., Lawson, I. T., and Preece, R. (2008). Veg-  
1201 etation history of the marine isotope stage 7 interglacial complex at Ioannina, NW  
1202 Greece. *Quaternary Science Reviews*, 27(13):1378–1395.
- 1203 Roucoux, K. H., Shackleton, N. J., De Abreu, L., Schönfeld, J., and Tzedakis, P. C.  
1204 (2001). Combined Marine Proxy and Pollen Analyses Reveal Rapid Iberian Vegeta-  
1205 tion Response to North Atlantic Millennial-Scale Climate Oscillations. *Quaternary  
1206 Research*, 56:128–132.
- 1207 Roucoux, K. H., Tzedakis, P. C., Lawson, I. T., and Margari, V. (2011). Vegetation history  
1208 of the penultimate glacial period (Marine isotope stage 6) at Ioannina, north-west  
1209 Greece. *Journal of Quaternary Science*, 26(6):616–626.
- 1210 Sanchez Goñi, M. F. and Harrison, S. P. (2010). Millennial-scale climate variability and  
1211 vegetation changes during the Last Glacial: Concepts and terminology. *Quaternary  
1212 Science Reviews*, 29(21-22):2823–2827.
- 1213 Santacroce, R., Cioni, R., Marianelli, P., Sbrana, A., Sulpizio, R., Zanchetta, G., Donahue,  
1214 D. J., and Joron, J. L. (2008). Age and whole rock-glass compositions of proximal  
1215 pyroclastics from the major explosive eruptions of Somma-Vesuvius: A review as a  
1216 tool for distal tephrostratigraphy. *Journal of Volcanology and Geothermal Research*,  
1217 177(1):1–18.
- 1218 Satow, C., Tomlinson, E. L., Grant, K. M., Albert, P. G., Smith, V. C., Manning, C. J.,  
1219 Ottolini, L., Wulf, S., Rohling, E. J., Lowe, J. J., Blockley, S. P., and Menzies,  
1220 M. A. (2015). A new contribution to the Late Quaternary tephrostratigraphy of the  
1221 Mediterranean: Aegean Sea core LC21. *Quaternary Science Reviews*, 117:96–112.
- 1222 Scaillet, S., Vita-Scaillet, G., and Rotolo, S. G. (2013). Millennial-scale phase rela-  
1223 tionships between ice-core and Mediterranean marine records: Insights from high-  
1224 precision  $^{40}\text{Ar}/^{39}\text{Ar}$  dating of the Green Tuff of Pantelleria, Sicily Strait. *Quaternary*

- 1225      *Science Reviews*, 78:141–154.
- 1226      Shotton, F. W. (1972). An example of hard-water error in radiocarbon dating of vegetable  
1227      matter. *Nature*, 240(5382):460–461.
- 1228      Siani, G., Sulpizio, R., Paterne, M., and Sbrana, A. (2004). Tephrostratigraphy study  
1229      for the last 18,000  $^{14}\text{C}$  years in a deep-sea sediment sequence for the South Adriatic.  
1230      *Quaternary Science Reviews*, 23(23):2485–2500.
- 1231      Smith, V. C., Isaia, R., and Pearce, N. J. (2011). Tephrostratigraphy and glass composi-  
1232      tions of post-15 kyr Campi Flegrei eruptions: Implications for eruption history and  
1233      chronostratigraphic markers. *Quaternary Science Reviews*, 30(25–26):3638–3660.
- 1234      Staff, R. A., Hardiman, M., Bronk Ramsey, C., Adolphi, F., Hare, V. J., Koutsodendris, A.,  
1235      and Pross, J. (2019). Reconciling the Greenland ice-core and radiocarbon timescales  
1236      through the Laschamp geomagnetic excursion. *Earth and Planetary Science Letters*,  
1237      520:1–9.
- 1238      Sulpizio, R., Zanchetta, G., Paterne, M., and Siani, G. (2003). A review of tephrostratig-  
1239      raphy in central and southern Italy during the last 65 ka. *Alpine and Mediterranean  
1240      Quaternary*, 16(1):91–108.
- 1241      Sulpizio, R., Zanchetta, G., Vogel, H., Wagner, B., and To, C. (2010). Tephrostratigraphy  
1242      and tephrochronology of lakes Ohrid and Prespa, Balkans. *Biogeosciences*, 7:3273–  
1243      3288.
- 1244      Sun, S. S. and McDonough, W. F. (1989). Chemical and isotopic systematics of oceanic  
1245      basalts: Implications for mantle composition and processes. *Geological Society  
1246      Special Publication*, 42(1):313–345.
- 1247      Tamburino, S., Insinga, D. D., Sprovieri, M., Petrosino, P., and Tiepolo, M. (2012).  
1248      Major and trace element characterization of tephra layers offshore Pantelleria Island:  
1249      Insights into the last 200 ka of volcanic activity and contribution to the Mediterranean  
1250      tephrochronology. *Journal of Quaternary Science*, 27(2):129–140.
- 1251      Tomlinson, E. L., Arienzzo, I., Civetta, L., Wulf, S., Smith, V. C., Hardiman, M., Lane,  
1252      C. S., Carandente, A., Orsi, G., Rosi, M., Müller, W., and Menzies, M. A. (2012). Geo-  
1253      chemistry of the Phlegraean Fields (Italy) proximal sources for major Mediterranean  
1254      tephras: Implications for the dispersal of Plinian and co-ignimbritic components of  
1255      explosive eruptions. *Geochimica et Cosmochimica Acta*, 93:102–128.
- 1256      Tomlinson, E. L., Smith, V. C., Albert, P., Aydar, E., Civetta, L., Cioni, R., Çubukçu, E.,  
1257      Gertisser, R., Isaia, R., Menzies, M. A., Orsi, G., Rosi, M., and Zanchetta, G. (2015).  
1258      The major and trace element glass compositions of the productive Mediterranean  
1259      volcanic sources: tools for correlating distal tephra layers in and around Europe.  
1260      *Quaternary Science Reviews*.
- 1261      Tomlinson, E. L., Thordarson, T., Müller, W., Thirlwall, M., and Menzies, M. (2010).  
1262      Microanalysis of tephra by LA-ICP-MS — Strategies, advantages and limitations  
1263      assessed using the Thorsmörk ignimbrite (Southern Iceland). *Chemical Geology*,  
1264      279(3):73–89.

- 1265 Tryon, C. A., Logan, M. A. V., Mouralidis, D., Kuhn, S., Slimak, L., and Balkan-Atlı, N.  
1266 (2009). Building a tephrostratigraphic framework for the paleolithic of central anatolia,  
1267 turkey. *Journal of Archaeological Science*, 36(3):637–652.
- 1268 Tzedakis, P. C. (1994). Vegetation Change through Glacial-Interglacial Cycles: A Long  
1269 Pollen Sequence Perspective. *Philosophical Transactions of the Royal Society B:  
1270 Biological Sciences*, 345(1314):403–432.
- 1271 Tzedakis, P. C. (2002). Buffered Tree Population Changes in a Quaternary Refugium:  
1272 Evolutionary Implications. *Science*, 297(5589):2044–2047.
- 1273 Tzedakis, P. C., Frogley, M., Lawson, I. T., Preece, R., Cacho, I., and de Abreu, L. (2004).  
1274 Ecological thresholds and patterns of millennial-scale climate variability: The response  
1275 of vegetation in Greece during the last glacial period. *Geology*, 32(2):109–112.
- 1276 van der Bilt, W. G., Lane, C. S., and Bakke, J. (2017). Ultra-distal Kamchatkan ash on  
1277 Arctic Svalbard: Towards hemispheric cryptotephra correlation. *Quaternary Science  
1278 Reviews*, 164:230–235.
- 1279 Vogel, H., Wagner, B., Zanchetta, G., Sulpizio, R., and Rosén, P. (2010). A paleoclimate  
1280 record with tephrochronological age control for the last glacial-interglacial cycle from  
1281 Lake Ohrid, Albania and Macedonia. *Journal of Paleolimnology*, 44(1):295–310.
- 1282 Wagner, B., Wulf, S., Wessels, M., Daut, G., and Nowaczyk, N. (2008). The last 40 ka  
1283 tephrostratigraphic record of Lake Ohrid, Albania and Macedonia: a very distal archive  
1284 for ash dispersal from Italian volcanoes. *Journal of Volcanology and Geothermal  
1285 Research*, 177(1):71–80.
- 1286 Watson, E. J., Swindles, G. T., Stevenson, J. A., Savov, I., and Lawson, I. T. (2016). The  
1287 transport of Icelandic volcanic ash: Insights from northern European cryptotephra  
1288 records. *Journal of Geophysical Research: Solid Earth*, 121(10):7177–7192.
- 1289 Wulf, S., Hardiman, M. J., Staff, R. A., Koutsodendris, A., Appelt, O., Blockley, S. P.,  
1290 Lowe, J. J., Manning, C. J., Ottolini, L., Schmitt, A. K., Smith, V. C., Tomlinson,  
1291 E. L., Vakhrameeva, P., Knipping, M., Kotthoff, U., Milner, A. M., Müller, U. C.,  
1292 Christianis, K., Kalaitzidis, S., Tzedakis, P. C., Schmiedl, G., and Pross, J. (2018).  
1293 The marine isotope stage 1–5 cryptotephra record of Tenaghi Philippon, Greece:  
1294 Towards a detailed tephrostratigraphic framework for the Eastern Mediterranean  
1295 region. *Quaternary Science Reviews*, 186:236–262.
- 1296 Wulf, S., Keller, J., Satow, C., Gertisser, R., Kraml, M., Grant, K. M., Appelt, O.,  
1297 Vakhrameeva, P., Koutsodendris, A., Hardiman, M., Schulz, H., and Pross, J. (2020).  
1298 Advancing santorini's tephrostratigraphy: New glass geochemical data and improved  
1299 marine-terrestrial tephra correlations for the past 360 kyrs. *Earth-Science Reviews*,  
1300 200:102964.
- 1301 Wulf, S., Kraml, M., Brauer, A., Org Keller, J., Org, J., and Negendank, F. W. (2004).  
1302 Tephrochronology of the 100 ka lacustrine sediment record of Lago Grande di Montic-  
1303 chio (southern Italy). *Quaternary International*, 122:7–30.
- 1304 Wulf, S., Kraml, M., and Keller, J. (2008). Towards a detailed distal tephrostratigraphy in

- 1305 the Central Mediterranean: The last 20,000 yrs record of Lago Grande di Monticchio.  
1306 *Journal of Volcanology and Geothermal Research*, 177(1):118–132.
- 1307 Wutke, K., Wulf, S., Hardiman, M., Dulski, P., Luterbacher, J., and Brauer, A. (2015).  
1308 Geochemical properties and environmental impacts of seven Campanian tephra layers  
1309 deposited between 40 and 38 ka BP in the varved lake sediments of Lago Grande di  
1310 Monticchio, southern Italy. *Quaternary Science Reviews*, 118:67–83.

<sup>1</sup> This file contains supplementary figures and tables for “The tephrochronology of  
<sup>2</sup> Lake Ioannina, NW Greece, from ca.46-4 ka BP” by McGuire et al.

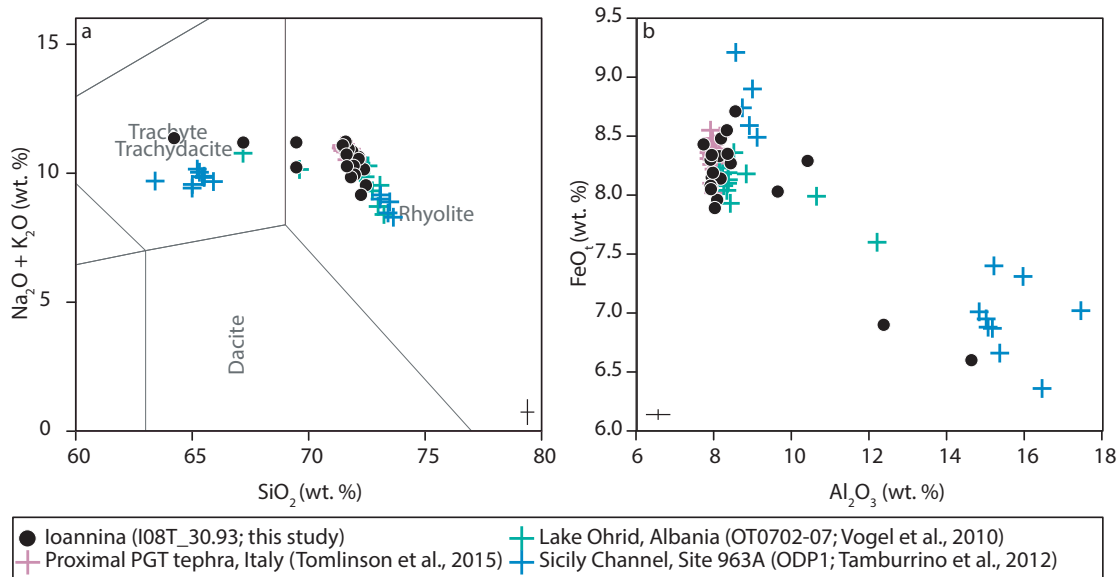


Figure S1. Major element geochemistry for tephra glass shards from visible tephra layer I08T\_30.93, showing: (a) total alkali vs. silica plot (Le Bas et al., 1986) and (b) FeOt vs  $\text{Al}_2\text{O}_3$ , plotted alongside geochemical data from proximal Pantelleria Green Tuff deposits and distal occurrences of the Y-6 tephra marker.

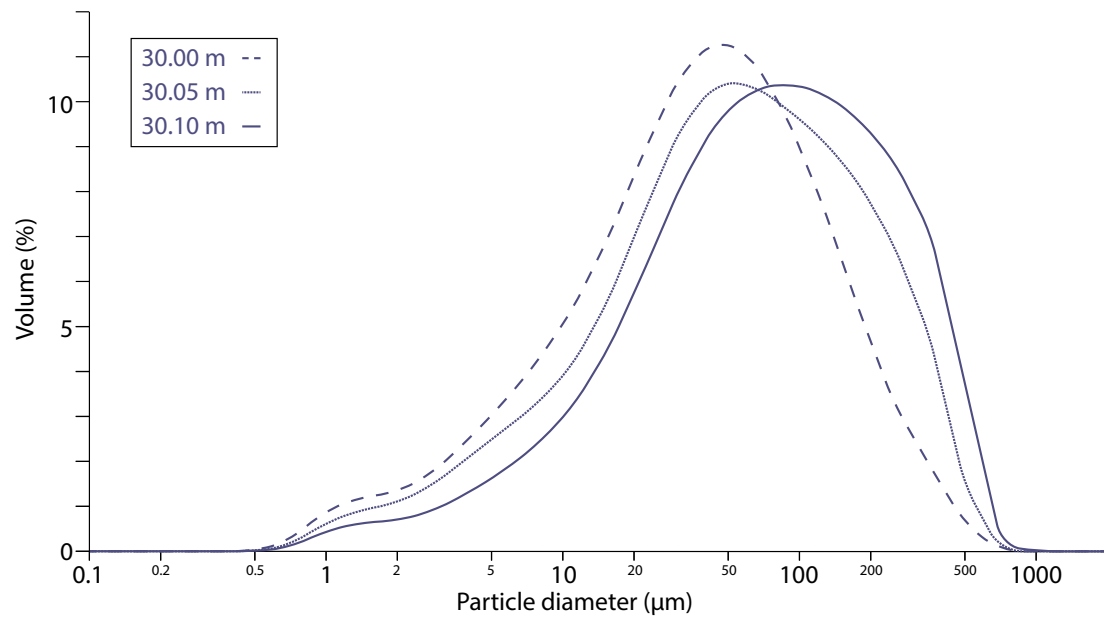


Figure S2. Particle size distributions for visible tephra layer I08T\_30.14, showing upward fining.

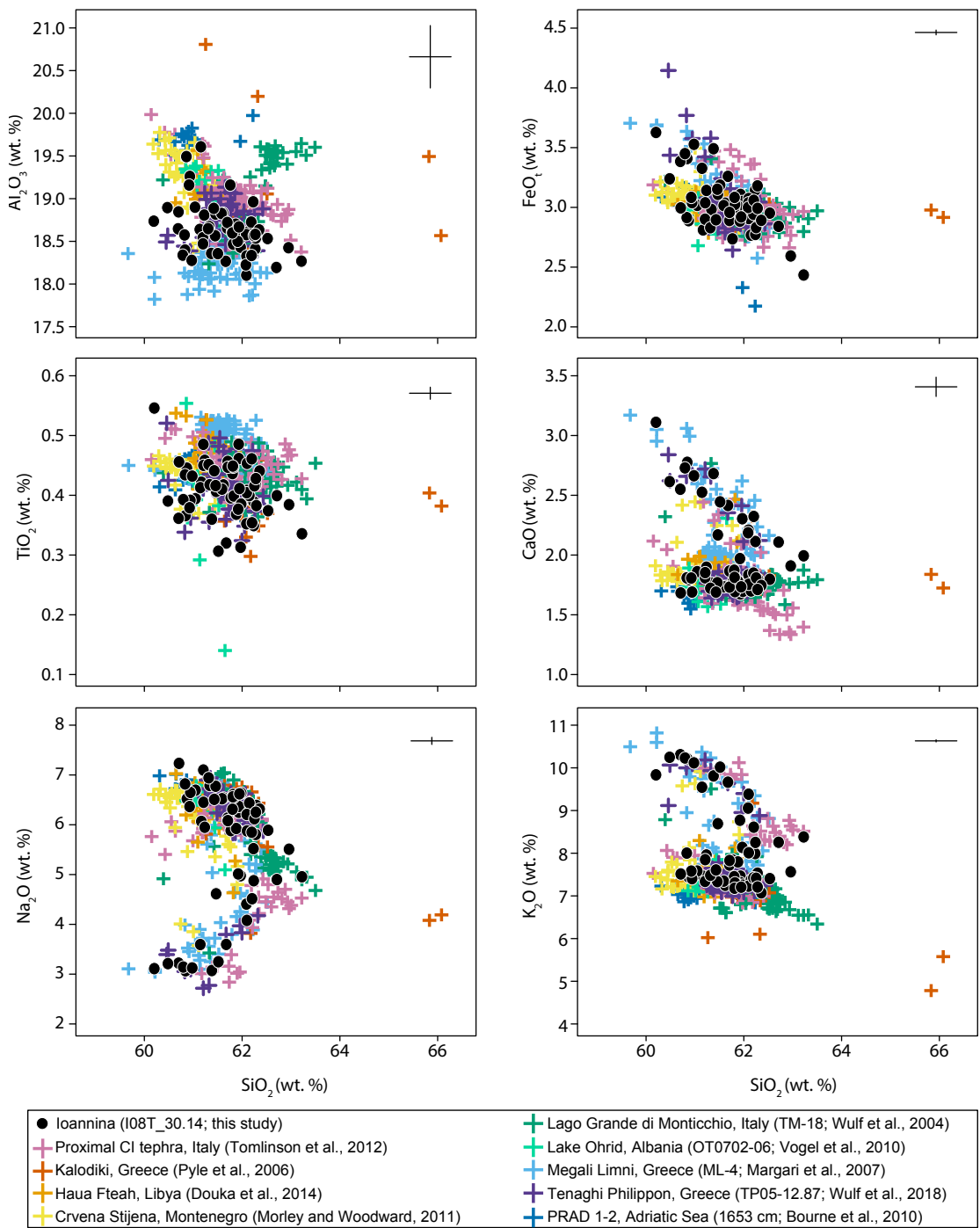


Figure S3. Major element geochemistries for tephra glass shards from visible tephra layer I08T\_30.14 plotted alongside geochemical data from proximal Campanian Ignimbrite deposits and distal occurrences of the Y-5 tephra marker.

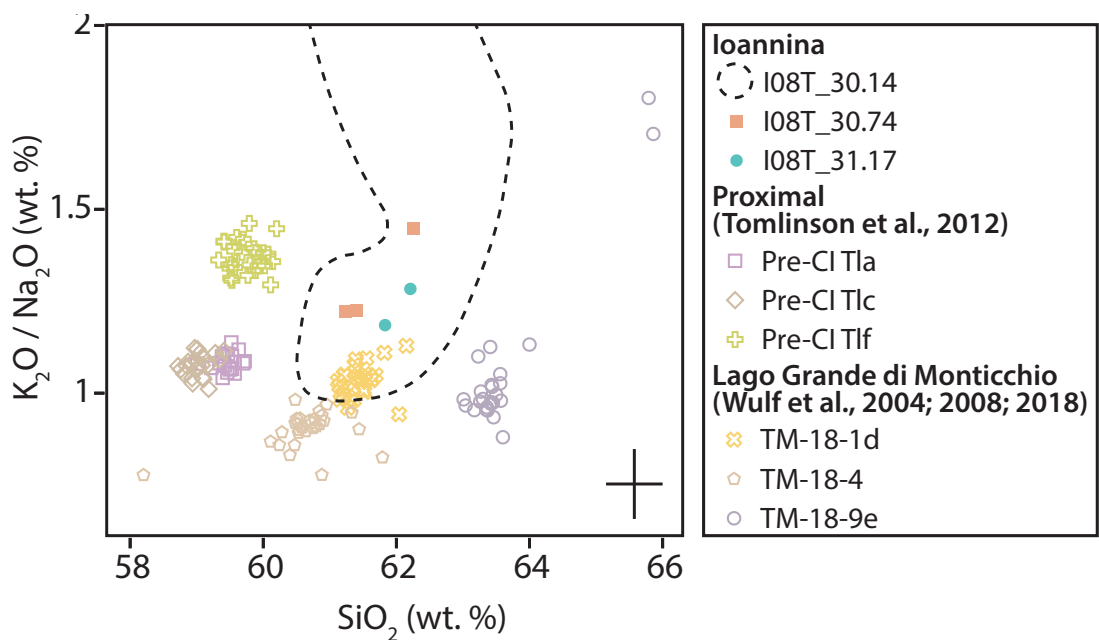


Figure S4. Biplot showing major element glass compositions of cryptotephra I08T\_31.17 and I08T\_30.74 m, showing the geochemical field of the visible I08T\_30.14 tephra marker, and medial-distal products of Campi Flegrei with a stratigraphic position below the CI.

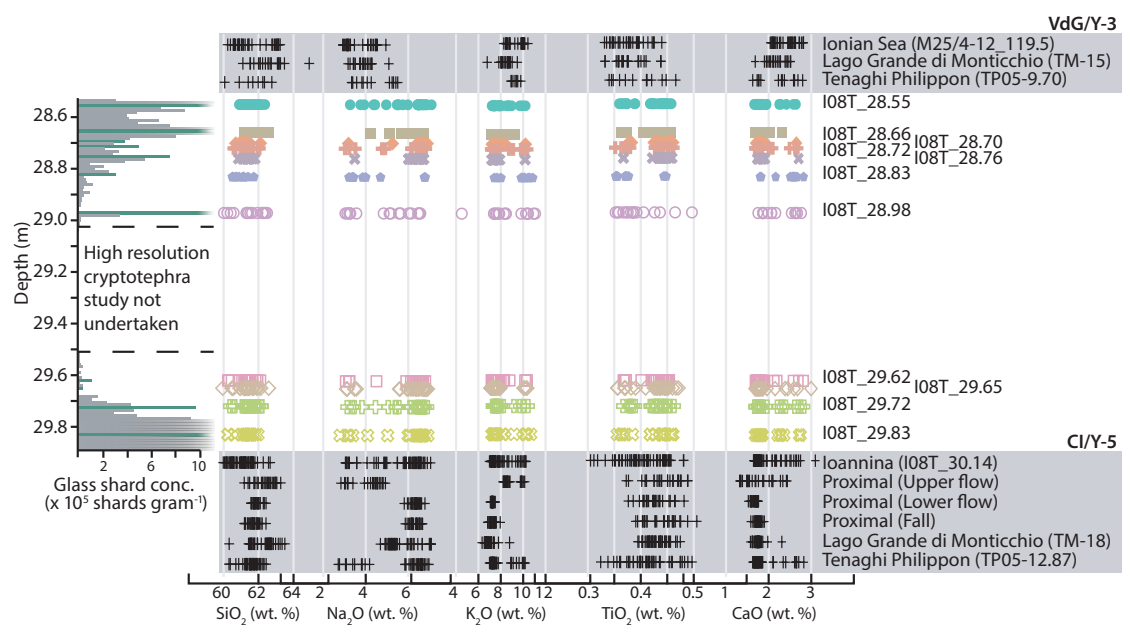


Figure S5. Major element geochemistry of tephra glass shards from I-08 cryptotephra layers between 29.88 and 28.51 m depth, showing glass shard concentrations alongside major and minor element compositions for identified peaks. Plotted for comparison are the major and minor element compositions of selected widespread tephra markers originating from Campi Flegrei including proximal (Tomlinson et al., 2015), and distal correlatives from Ionian Sea core M25/4-12 (Albert et al., 2015), Lago Grande di Monticchio (Wulf et al., 2004) and Tenaghi Philippon (Wulf et al., 2018).

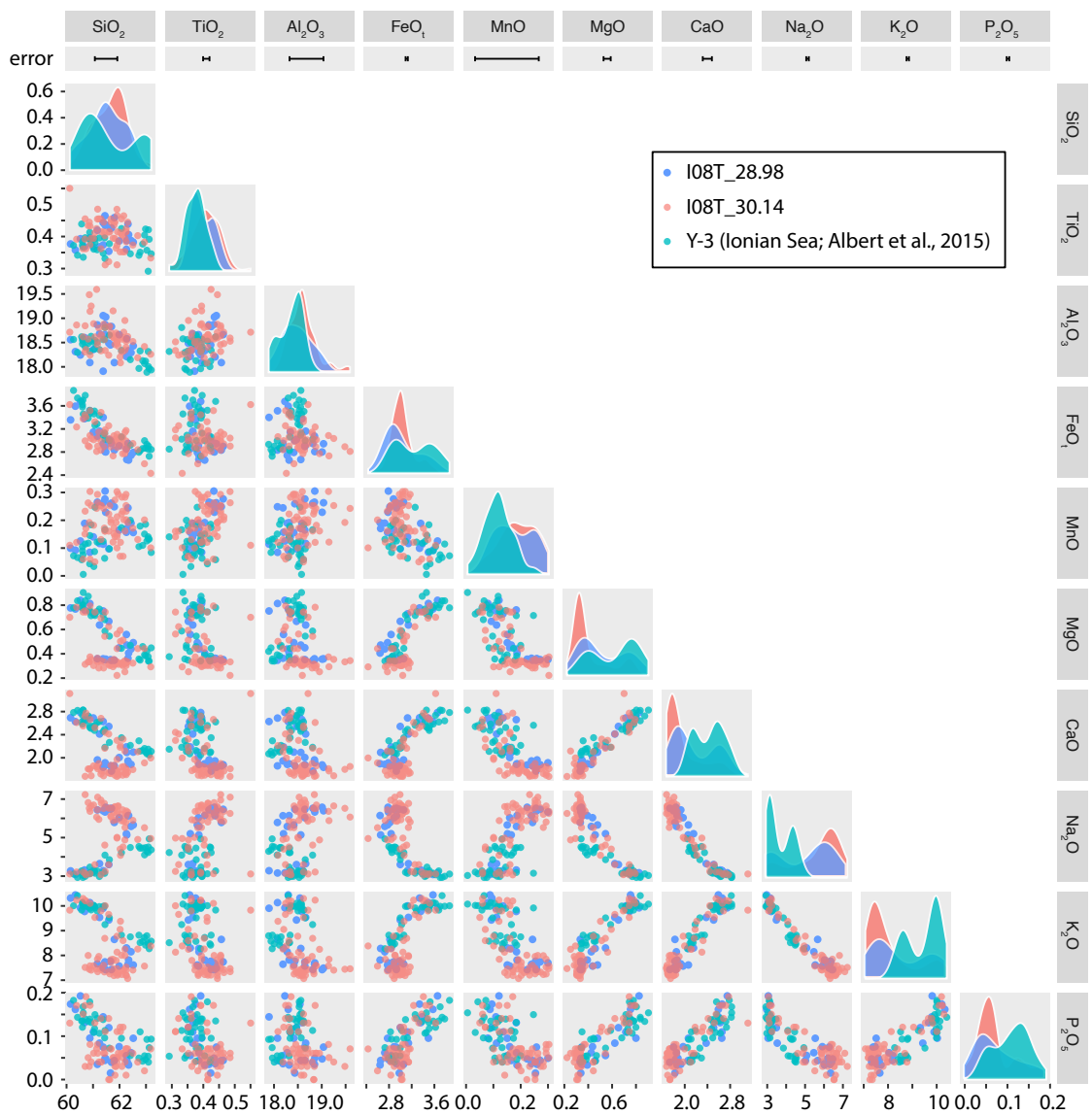


Figure S6. Scatter plot matrix showing the full (wt%) major and minor element geochemical composition of I-08 tephra layers I08T\_28.98 and I08T\_30.14, in addition to the composition of the Y-3 tephra marker from the type site in the Ionian Sea (Albert et al., 2015).

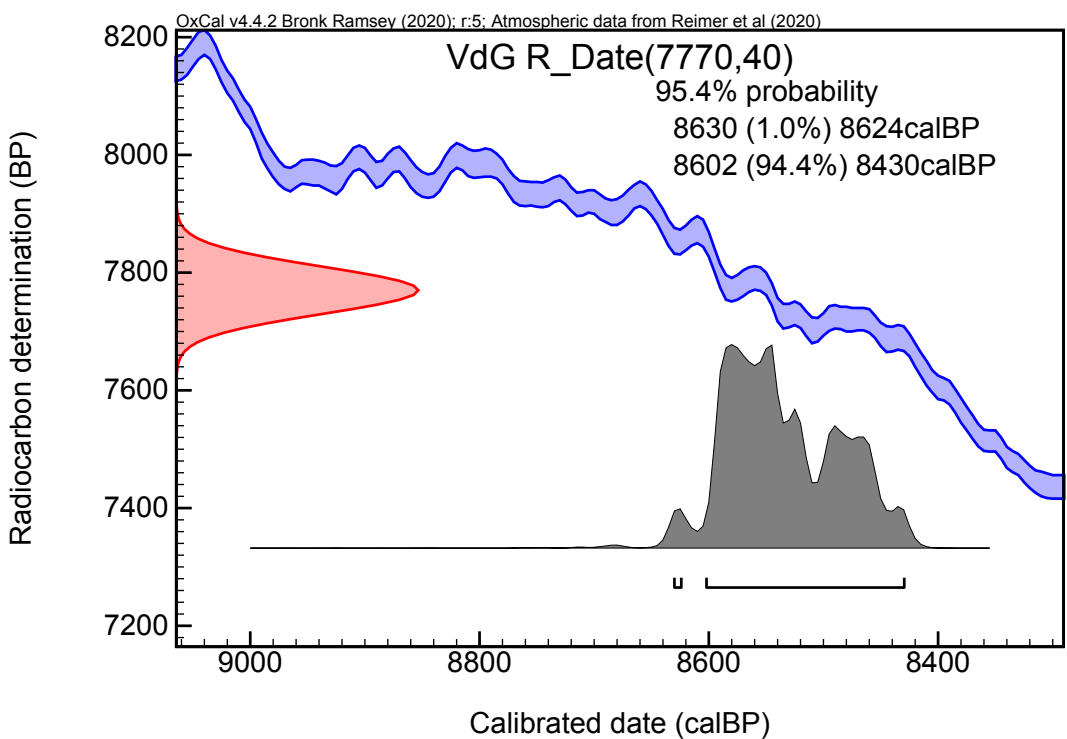


Figure S7. Probability density function for the remodelled Caron et al. (2012) age of the Vallone del Gabellotto (VdG/E-1) eruption (with 95.4% highest probability density ranges shown).

Eruption	Distal correlations	Volcano	Composition	Chronology (ka BP)
Vallone del Gabellotto	Adriatic Sea (E-1, Paterne et al. 1988; Siani et al. 2004) Ionian Sea (E-1, Paterne et al. 1988, Caron et al. 2012; M25/4-12.28cm; Albert et al. 2012)	Lipari	Italy Rhyolite (Albert et al. 2017)	8.43–8.73 ( $^{14}\text{C}$ ; Siani et al. 2004), 7.77 $\pm$ 0.04 ( $^{14}\text{C}$ ; Caron et al. 2012)
Tenaghi Philippon, Greece (TP05–5.075, Wulf et al. 2018)	Tyrrhenian Sea (E-1, Paterne et al. 1988)			
Mercato	Lago Grande di Monticchio, Italy (TM-6, Wulf et al. 2004, Somma-Vesuvius 2008)	Italy Phonolite (Tomlinson et al. 2015)	8.536 $\pm$ 0.091 ( $^{14}\text{C}$ ; Zanchetta et al. 2012)	
	Adriatic Sea (SA03-11 T363, Matthews et al. 2015)			
	Lake Ohrid, Albania and Macedonia (OT0702-3, Vogel et al. 2010; OH-DP-0027, Leicher et al. 2016)			
	Lake Prespa, Macedonia, Albania, and Greece (PT0915-2, Damaschke et al. 2013)			
Pomicci Principali	Tyrrhenian Sea (V-1, Paterne et al. 1988)	Italy Phonolite (Tomlinson et al. 2012a)	11.999 $\pm$ 0.104 ( $^{14}\text{C}$ ; Smith et al. 2011; Bronk Ramsey et al. 2015)	ca. 13 (K/Ar; Gillot and Keller, 1993)
	Lago Grande di Monticchio, Italy (TM-7b, Wulf et al. 2004, Campi Flegrei 2008)	Italy Phonolite (Tomlinson et al. 2012a)	11.999 $\pm$ 0.104 ( $^{14}\text{C}$ ; Smith et al. 2011; Bronk Ramsey et al. 2015)	ca. 13 (K/Ar; Gillot and Keller, 1993)
Upper Vancori Lago Amendoiare	Adriatic Sea (PRAD 203, Bourne et al. 2010; SA03-11 T492, Matthews et al. 2015)	Stromboli Somma-Vesuvius	Italy Trachyte (Albert et al. 2017) Phonolite, trachyte (Smith et al. 2011)	15.55 $\pm$ 0.78 (Varve counting; Wulf et al. 2008)
Casa Lentia	Lago dell'Accessa (1305 cm, Drescher-Schneider et al. 2007)	Vilcano	Italy Trachyte, rhyolite (Albert et al. 2017)	20.11
Neapolitan Yellow Tuff	Adriatic Sea (PRAD 218, Bourne et al. 2010; SA03-11 T640, Campi Flegrei 2008-2008; SA03-11 T651, Matthews et al. 2015)	Italy Phonolite, trachyte (Tomlinson et al. 2012a)	14.940 $\pm$ 1.00 ( $^{40}\text{Ar}/^{39}\text{Ar}$ ; Deino et al. 2004), 14.194 $\pm$ 0.344 ( $^{14}\text{C}$ ; Siani et al. 2004; Bronk Ramsey et al. 2015)	
N-051	Adriatic Sea (1660 cm, Drescher-Schneider et al. 2007)			
Upper Pollara	Lago Grande di Monticchio, Italy (TM-10, Wulf et al. 2004, 2008-2008; SA03-11 T651, Matthews et al. 2015)			
Biancavilla-Montalto	Fucino, Italy (TF-2, Giaccio et al. 2017b)			
Ignimbrite	Lago Grande di Monticchio, Italy (TM-8, Wulf et al. 2004, 2008)			
	Sulmona (SUL4-3 MTI, Giaccio et al. 2009b)			
	Tyrrhenian Sea (C-2, Paterne et al. 1988)			
	Nemrut	Turkey	Comendite (?)	15 $\pm$ 1 K/Ar; ?
	Salina	Italy	Rhyolite (Albert et al. 2017)	15.00–16.09 ( $^{14}\text{C}$ ; Keller, 1980)
	Mt. Etna	Italy	Trachyte (Albert et al. 2013)	16.905–17.670 ( $^{14}\text{C}$ ; Siani et al. 2004; Albert et al. 2013)
	1-1, Insinga et al. 2014)			

Continued overleaf

Table S7 – *Continued from previous page*

Eruption	Distal correlations	Volcano	Composition	Chronology (ka BP)
PRa	Lago Grande di Monticchio, Italy (TM-11, Wulf et al. 2004, 2008; 2012)	Campi Flegrei	Italy	Phonolite, trachyte (Tomlinson et al. 1999) $^{40}\text{Ar}/^{39}\text{Ar}$ ; Pappalardo et al. 2012a)
Verdoline	Adriatic Sea (PRAD 784, Bourne et al. 2010; SA03-11 T865, Somma-Vesuvius Matthews et al. 2015)	Italy	Trachyte (Tomlinson et al. 2015)	$16.1 \pm 0.2$ ( $^{40}\text{Ar}/^{39}\text{Ar}$ ; Pappalardo et al. 1999) $19.226 \pm 0.208$ ( $^{14}\text{C}$ ; Siani et al. 2004; Bronk Ramsey et al. 2015)
Sant Angelo (younger)	Lago Grande di Monticchio, Italy (TM-12, Wulf et al. 2004, 2008)	Ischia	Italy	Phonolite, trachyte (Tomlinson et al. ca. 20 (K/Ar; Civetta et al. 1991) 2015)
Solchiaro	Adriatic Sea (PRAD 845, Bourne et al. 2010)	Procida-Vivara	Italy	Basaltic, trachyanandesite (Wulf et al. 2004, 2008)
Cape Riva	Lago Grande di Monticchio, Italy (TM-14, Wulf et al. 2004, 2008)	Santorini	Greece	Basaltic, trachyanandesite (Wulf et al. 2004, 2008)
Pomice di Base	Tyrrhenian Sea (C-4, Paterno et al. 1988) Aegean Sea (Y-2, Keller et al. 1978; Aksu et al. 2008) Marmara Sea (Y-2, Aksu et al. 2008) Megali Limni, Greece (ML-1, Margari et al. 2007) Teneghi Philippon, Greece (TP05-7.61, Wulf et al. 2018) Adriatic Sea (PRAD 875, Bourne et al. 2010; SA03-11 T950, Somma-Vesuvius Matthews et al. 2015)	Lipari Santorini	Italy Greece	Rhyolite (Tomlinson et al. 2015) $21.26 \pm 1.06$ (Varve counting; Wulf et al. 2004, 2008)
Monte Guardia Cape Tripiti	Lago Grande di Monticchio, Italy (TM-13, Wulf et al. 2004, 2008; 2012)	Salina	Italy	Lattice, trachyte (Tomlinson et al. 2015) $22.081 \pm 0.346$ ( $^{14}\text{C}$ ; Siani et al. 2004; Bronk Ramsey et al. 2015)
Lower Pollara	Lago di Pergusa, Italy (T2, Narcisi 2002) Aegean Sea (Y-4, Keller et al. 1978, Aksu et al. 2008; LC21-3,776, Satow et al. 2015)	Gölcük	Turkey	Dacite, rhyolite (Albert et al. 2017) $24.65\text{--}27.10$ ( $^{14}\text{C}$ ; Siani et al. 2004) ca. 26 (Fabbro et al. 2013)
Cycle III		Campi Flegrei	Italy	Phonolite, trachyte (Tomlinson et al. 2015)
VRb		Campi Flegrei	Italy	Trachyte (Tomlinson et al. 2012a) $26.41\text{--}27.63$ ( $^{14}\text{C}$ ; Crisci et al. 1991; Albert et al. 2017)
Masseria del Monte Tuff	Ionian Sea (Y-3, Keller et al. 1978; Albert et al. 2015)			Trachyte, phonolite (Albert et al. 2015) $24$ to $70$ ka (K/Ar; Platevoet et al. 2008)
Codola	Adriatic Sea (SA03-11 T1327, Matthews et al. 2015) Lago Grande di Monticchio, Italy (TM-15, Wulf et al. 2004, 2008; 2012)			Trachyte, phonolite (Tomlinson et al. 2015) $29.250 \pm 0.960$ ( $^{14}\text{C}$ ; Alessio et al. 1974; Bronk Ramsey et al. 2015)

*Continued overleaf*

Table S7 – *Continued from previous page*

Eruption	Distal correlations	Volcano	Composition	Chronology (ka BP)
VRa	Lago Grande di Monticchio, Italy (TM-16b, Wulf et al. 2004, 2008) Lake Ohrid, Albania and Macedonia (OT0702-5, Vogel et al. 2010)	Campi Flegrei	Trachyte (Tomlinson et al. 2012a)	30.3 ± 0.2 ( $^{40}\text{Ar}/^{39}\text{Ar}$ ; Pappalardo et al. 1999)
Obrik Tepe Yali-2	Adriatic Sea (PRAD 1332, Bourne et al. 2010; Albert et al. Campi Flegrei Adriatic Sea (MAR03-24-351cm, Aksu et al. 2008; LC21-4.285, Satow et al. 2015)	Açgöl Yali	Basaltic (?) Rhyolite (Satow et al. 2015)	37.0 ± 3.0 ca. 34 (K/Ar; ?) 32.894 ± 0.502 and 32.992 ± 0.503 ka BP (Age-depth model; Satow et al. 2015)
Sant Montano	Ischia	Italy	Phonolite, trachyte (Tomlinson et al. 2015)	ca. 34 (K/Ar; Civetta et al. 1991)
Schiava Albano 7	Lago Grande di Monticchio, Italy (TM-17-2, Wulf et al. 2015) Fucino, Italy (TF-4, Giaccio et al. 2017b) Lago Grande di Monticchio, Italy (TM-17bc, Wulf et al. 2004, 2008; 2012) Sulmona (SUL4-3 Albano 7, Giaccio et al. 2009b) Adriatic Sea (SA03-11 T76Q, Matthews et al. 2015)	Somma-Vesuvius Colli Albani	Trachyte (Tomlinson et al. 2012a) Fordite (Freda et al. 2006)	ca. 36 (Stratigraphy; Giaccio et al. 2008) 37.0 ± 3.0 ( $^{40}\text{Ar}/^{39}\text{Ar}$ ; Freda et al. 2006), 33.0 ± 4.0 and 35.9 ± 0.6 ( $^{40}\text{Ar}/^{39}\text{Ar}$ ; Giaccio et al. 2009a)
TLo	Adriatic Sea (PRAD 1653, Bourne et al. 2010; SA03-11 Campi Flegrei T1598, Matthews et al. 2015) Aegean Sea (Y-5, Keller et al. 1978; Aksu et al. 2008) Fucino, Italy (TF-5a, Giaccio et al. 2017b) Ionian Sea (Y-5, Keller et al. 1978; KC01B I-4, Insinga et al. 2014) Lago Grande di Monticchio, Italy (TM-18, Wulf et al. 2004, 2008)	Campi Flegrei	Trachyte, phonolite (Tomlinson et al. 2015)	<39.85 (Stratigraphy; Tomlinson et al. 2015)
Campanian Ignimbrite	Lake Ohrid, Albania and Macedonia (OT0702-6, Vogel et al. 2010; OH-DP-0169a+b, Leicher et al. 2016) Lake Prespa, Macedonia, Albania, and Greece (PT0915-7, Damaschke et al. 2013) Levantine Sea (Y-5, Keller et al. 1978) Megali Limni, Greece (ML-2, Margari et al. 2007) Tenaghi Philippon, Greece (TP05-12.87, Wulf et al. 2018) Tyrrenian Sea (C-10, Paterne et al. 1988)	Italy	Trachyte, phonolite (Tomlinson et al. 2012a)	>39.85 (Stratigraphy; Tomlinson et al. 2015)
TLf	Campi Flegrei	Italy	Trachyte, phonolite (Tomlinson et al. 2012a)	>39.85 (Stratigraphy; Tomlinson et al. 2015)
TLc	Campi Flegrei	Italy	Trachyte, phonolite (Tomlinson et al. 2012a)	>39.85 (Stratigraphy; Tomlinson et al. 2015)
Peperino Ignimbrite Agnone	Fucino, Italy (TF-5, Giaccio et al. 2017b)	Colli Albani Ischia	Foidite (Freda et al. 2006) Phonolite, trachyte (Tomlinson et al. 2014)	41.0 ± 7.0 ( $^{40}\text{Ar}/^{39}\text{Ar}$ ; Freda et al. 2006), ca. 43 (K/Ar; Civetta et al. 1991)

*Continued overleaf*

Table S7 – *Continued from previous page*

Eruption	Distal correlations	Volcano	Composition	Chronology (ka BP)
Falcone		Lipari	Rhyolite (Albert et al. 2017)	$43 \pm 1$ (K/Ar; Forni et al. 2013)
Pantelleria Green Tuff	Ionian Sea (Y-6, Keller et al. 1978) Lake Ohrid, Albania and Macedonia (OT0702-7, Vogel et al. 2010)	Panelleria	Rhyolite (Tomlinson et al. 2015)	$45.7 \pm 1.0$ ( $^{40}\text{Ar}/^{39}\text{Ar}$ ; Scaillet et al. 2013)
	Lake Prespa, Macedonia, Albania, and Greece (PT0915-9 , Damaschke et al. 2013)			
	Levantine Sea (Y-6, Keller et al. 1978)			
Pietre Rosse	Sicily Channel (ODPI, Tamburri et al. 2012)	Ischia	Phonolite, trachyte (Tomlinson et al. 2014)	$45 \pm 6$ (Varve counting; Tomlinson et al. 2014)
Nisyros Upper Pumice		Nisyros	Rhyolite (Tomlinson et al. 2012b)	$>50.4$ (Age-depth model; Tomlinson et al. 2012b)
Schiappone		Ischia	Phonolite, trachyte (Tomlinson et al. 2014)	$50.6 \pm 2.0$ (Varve counting; Tomlinson et al. 2014; Bronk Ramsey et al. 2015)
Upper Scoriae 2		Santorini	Andesite, dacite, trachyte (Tomlinson et al. 2015)	$54 \pm 3$ ( $^{40}\text{Ar}/^{39}\text{Ar}$ ; Druitt et al. 1999)
Punta del Perciatto		Lipari	Rhyolite (Albert et al. 2017)	$<55$ (K/Ar; Forni et al. 2013)
Monte Epomeo Green Tuff	Adriatic Sea (PRAD 1870, Bourne et al. 2010)	Ischia	Phonolite, trachyte (Tomlinson et al. 2014)	$55 \pm 4$ ( $^{40}\text{Ar}/^{39}\text{Ar}$ ; Watts et al. 1996)
	Fucino, Italy (TF-7, Giaccio et al. 2017b)			
	Ionian Sea (Y-7, Keller et al. 1978; KC01B I-1, Insinga et al. 2014)			
	Lago Grande di Monicchio, Italy (TM-19, Wulf et al. 2004, 2008; 2012)			
Tla	Tyrrhenian Sea (C-18; Paterne et al. 1988)	Campi Flegrei	Phonolite (Tomlinson et al. 2012a)	$58.9 \pm 1.8$ ( $^{40}\text{Ar}/^{39}\text{Ar}$ ; Pappalardo et al. 1999)
Porticello		Ischia	Phonolite, trachyte (Tomlinson et al. 2014)	$59 \pm 2$ (Varve counting; Tomlinson et al. 2014)
Albano 3	Fucino, Italy (TF-8, Giaccio et al. 2017b)	Colli Albani	Foidite (Freda et al. 2006)	$68.6 \pm 1.1$ ( $^{40}\text{Ar}/^{39}\text{Ar}$ ; Freda et al. 2006), $73.0 \pm 3.0$ ( $^{40}\text{Ar}/^{39}\text{Ar}$ ; Giaccio et al. 2009a)
Albano 1	Fucino, Italy (TF-9, Giaccio et al. 2017b)	Colli Albani	Foidite (Freda et al. 2006)	$68.9 \pm 0.2$ and $69.4 \pm 0.6$ ( $^{40}\text{Ar}/^{39}\text{Ar}$ ; Freda et al. 2006) $72 \pm 3$ ( $^{40}\text{Ar}/^{39}\text{Ar}$ ; Giaccio et al. 2009a)

Table S7. A summary of last glacial and Early Holocene Mediterranean volcanic eruptions identified in proximal deposits, detailing the source volcano, associated distal deposits, the geochemical affinity (after Le Bas et al. 1986), and best available geochronological information

### <sup>3</sup> References

- <sup>4</sup> Aksu, A. E., Jenner, G., Hiscott, R. N., and İşler, E. B. (2008). Occurrence, stratigraphy  
<sup>5</sup> and geochemistry of Late Quaternary tephra layers in the Aegean Sea and the Marmara  
<sup>6</sup> Sea. *Marine Geology*, 252(3-4):174–192.
- <sup>7</sup> Albert, P., Hardiman, M., Keller, J., Smith, V. C., Bourne, A. J., Wulf, S., Zanchetta,  
<sup>8</sup> G., Sulpizio, R., Müller, U. C., Pross, J., Ottolini, L., Matthews, I. P., Blockley, S. P.,  
<sup>9</sup> and Menzies, M. A. (2015). Revisiting the Y-3 tephrostratigraphic marker: a new  
<sup>10</sup> diagnostic glass geochemistry, age estimate, and details on its climastratigraphical  
<sup>11</sup> context. *Quaternary Science Reviews*, 118:105–121.
- <sup>12</sup> Albert, P., Tomlinson, E. L., Lane, C. S., Wulf, S., Smith, V. C., Coltelli, M., Keller, J.,  
<sup>13</sup> Lo Castro, D., Manning, C. J., Müller, W., and Menzies, M. A. (2013). Late glacial  
<sup>14</sup> explosive activity on Mount Etna: Implications for proximal-distal tephra correlations  
<sup>15</sup> and the synchronisation of Mediterranean archives. *Journal of Volcanology and  
<sup>16</sup> Geothermal Research*, 265:9–26.
- <sup>17</sup> Albert, P. G., Giaccio, B., Isaia, R., Costa, A., Niespolo, E. M., Nomade, S., Pereira,  
<sup>18</sup> A., Renne, P. R., Hinchliffe, A., Mark, D. F., Brown, R. J., and Smith, V. C. (2019).  
<sup>19</sup> Evidence for a large-magnitude eruption from Campi Flegrei caldera (Italy) at 29 ka.  
<sup>20</sup> *Geology*, 47(7):595–599.
- <sup>21</sup> Albert, P. G., Tomlinson, E. L., Smith, V. C., Di Roberto, A., Todman, A., Rosi, M.,  
<sup>22</sup> Marani, M., Muller, W., and Menzies, M. A. (2012). Marine-continental tephra  
<sup>23</sup> correlations: Volcanic glass geochemistry from the Marsili Basin and the Aeolian  
<sup>24</sup> Islands, Southern Tyrrhenian Sea, Italy. *Journal of Volcanology and Geothermal  
<sup>25</sup> Research*, 229-230:74–94.
- <sup>26</sup> Albert, P. G., Tomlinson, E. L., Smith, V. C., Di Traglia, F., Pistolesi, M., Morris, A.,  
<sup>27</sup> Donato, P., De Rosa, R., Sulpizio, R., Keller, J., Rosi, M., and Menzies, M. (2017).  
<sup>28</sup> Glass geochemistry of pyroclastic deposits from the Aeolian Islands in the last 50 ka:  
<sup>29</sup> A proximal database for tephrochronology. *Journal of Volcanology and Geothermal  
<sup>30</sup> Research*, 336:81–107.
- <sup>31</sup> Alessio, M., Bella, F., Improta, S., Belluomini, G., Calderoni, G., Cortesi, C., and Turi,  
<sup>32</sup> B. (1974). University of Rome Carbon-14 Dates XII. *Radiocarbon*, 16(3):358–367.
- <sup>33</sup> Bourne, A. J., Lowe, J., Trincardi, F., Asioli, A., Blockley, S. P., Wulf, S., Matthews, I., ,  
<sup>34</sup> A., and Vigliotti, L. (2010). Distal tephra record for the last ca 105,000 years from  
<sup>35</sup> core PRAD 1-2 in the central Adriatic Sea: implications for marine tephrostratigraphy.  
<sup>36</sup> *Quaternary Science Reviews*, 29(23-24):3079–3094.
- <sup>37</sup> Bronk Ramsey, C., Albert, P., Blockley, S. P., Hardiman, M., Lane, C. S., Lee, S.,  
<sup>38</sup> Matthews, I. P., Smith, V. C., and Lowe, J. J. (2015). Improved age estimates for key  
<sup>39</sup> Late Quaternary European tephra horizons in the RESET lattice. *Quaternary Science  
<sup>40</sup> Reviews*, 118:18–32.
- <sup>41</sup> Caron, B., Siani, G., Sulpizio, R., Zanchetta, G., Paterne, M., Santacroce, R., Tema, E.,  
<sup>42</sup> and Zanella, E. (2012). Late Pleistocene to Holocene tephrostratigraphic record from

- 43 the Northern Ionian Sea. *Marine Geology*, 311-314:41–51.
- 44 Civetta, L., Gallo, G., and Orsi, G. (1991). Sr- and Nd-isotope and trace-element  
45 constraints on the chemical evolution of the magmatic system of Ischia (Italy) in the  
46 last 55 ka. *Journal of Volcanology and Geothermal Research*, 46(3-4):213–230.
- 47 Crisci, G. M., De Rosa, R., Esperança, S., Mazzuoli, R., and Sonnino, M. (1991).  
48 Temporal evolution of a three component system: the island of Lipari (Aeolian Arc,  
49 southern Italy). *Bulletin of Volcanology*, 53(3):207–221.
- 50 Çubukçu, H., Ulusoy, İ., Aydar, E., Ersoy, O., Şen, E., Gourgaud, A., and Guillou, H.  
51 (2012). Mt. nemrut volcano (eastern turkey): Temporal petrological evolution. *Journal  
52 of Volcanology and Geothermal Research*, 209-210:33–60.
- 53 Damaschke, M., Sulpizio, R., Zanchetta, G., Wagner, B., Böhm, A., Nowaczyk, N.,  
54 Rethemeyer, J., and Hilgers, A. (2013). Tephrostratigraphic studies on a sediment core  
55 from Lake Prespa in the Balkans. *Climate of the Past*, 9(1):267–287.
- 56 De Rosa, R., Guillou, H., Mazzuoli, R., and Ventura, G. (2003). New unspiked K-  
57 Ar ages of volcanic rocks of the central and western sector of the Aeolian Islands:  
58 Reconstruction of the volcanic stages. *Journal of Volcanology and Geothermal  
59 Research*, 120(3-4):161–178.
- 60 Deino, A. L., Orsi, G., de Vita, S., and Piochi, M. (2004). The age of the Neapolitan  
61 Yellow Tuff caldera-forming eruption (Campi Flegrei caldera - Italy) assessed by  
62 40Ar/39Ar dating method. *Journal of Volcanology and Geothermal Research*, 133(1-  
63 4):157–170.
- 64 Drescher-Schneider, R., De Beaulieu, J. L., Magny, M., Walter-Simonnet, A. V., Bossuet,  
65 G., Millet, L., Brugiaapaglia, E., and Drescher, A. (2007). Vegetation history, climate  
66 and human impact over the last 15,000 years at Lago dell'Accesa (Tuscany, Central  
67 Italy). In *Vegetation History and Archaeobotany*, volume 16, pages 279–299.
- 68 Druitt, T. H., Edwards, L., Mellors, R., Pyle, D., Sparks, R., Lanpher, M., Davies, M.,  
69 and Barreiro, B. (1999). *Santorini Volcano*. Geological Society of London, London.
- 70 Fabbro, G. N., Druitt, T. H., and Scaillet, S. (2013). Evolution of the crustal magma  
71 plumbing system during the build-up to the 22-ka caldera-forming eruption of Santorini  
72 (Greece). *Bulletin of Volcanology*, 75(12):1–22.
- 73 Forni, F., Lucchi, F., Peccerillo, A., Tranne, C. A., Rossi, P. L., and Frezzotti, M. L.  
74 (2013). Stratigraphy and geological evolution of the lipari volcanic complex (central  
75 aeolian archipelago). *Geological Society Memoir*, 37(1):213–279.
- 76 Freda, C., Gaeta, M., Karner, D. B., Marra, F., Renne, P. R., Taddeucci, J., Scarlato, P.,  
77 Christensen, J. N., and Dallai, L. (2006). Eruptive history and petrologic evolution  
78 of the Albano multiple maar (Alban Hills, Central Italy). *Bulletin of Volcanology*,  
79 68(6):567–591.
- 80 Giaccio, B., Hajdas, I., Isaia, R., Deino, A., and Nomade, S. (2017a). High-precision  $^{14}\text{C}$   
81 and 40Ar/39Ar dating of the Campanian Ignimbrite (Y-5) reconciles the time-scales  
82 of climatic-cultural processes at 40 ka. *Scientific Reports*, 7(1):45940.

- 83 Giaccio, B., Isaia, R., Fedele, F. G., Di Canzio, E., Hoffecker, J., Ronchitelli, A., Sinitsyn,  
84 A. A., Anikovich, M., Lisitsyn, S. N., and Popov, V. V. (2008). The Campanian  
85 Ignimbrite and Codola tephra layers: Two temporal/stratigraphic markers for the Early  
86 Upper Palaeolithic in southern Italy and eastern Europe. *Journal of Volcanology and*  
87 *Geothermal Research*, 177(1):208–226.
- 88 Giaccio, B., Marra, F., Hajdas, I., Karner, D. B., Renne, P. R., and Sposato, A. (2009a).  
89  $^{40}\text{Ar}/^{39}\text{Ar}$  and  $^{14}\text{C}$  geochronology of the Albano maar deposits: Implications for  
90 defining the age and eruptive style of the most recent explosive activity at Colli Albani  
91 Volcanic District, Central Italy. *Journal of Volcanology and Geothermal Research*,  
92 185(3):203–213.
- 93 Giaccio, B., Messina, P., Sposato, A., Voltaggio, M., Zanchetta, G., Galadini, F., Gori,  
94 S., and Santacroce, R. (2009b). Tephra layers from Holocene lake sediments of the  
95 Sulmona Basin, central Italy: implications for volcanic activity in Peninsular Italy and  
96 tephrostratigraphy in the central Mediterranean area. *Quaternary Science Reviews*,  
97 28(25-26):2710–2733.
- 98 Giaccio, B., Niespolo, E. M., Pereira, A., Nomade, S., Renne, P. R., Albert, P., Arienzzo,  
99 I., Regattieri, E., Wagner, B., Zanchetta, G., Gaeta, M., Galli, P., Mannella, G.,  
100 Peronace, E., Sottili, G., Florindo, F., Leicher, N., Marra, F., and Tomlinson, E. L.  
101 (2017b). First integrated tephrochronological record for the last ca. 190 kyr from the  
102 Fucino Quaternary lacustrine succession, central Italy. *Quaternary Science Reviews*,  
103 158:211–234.
- 104 Insinga, D. D., Tamburri, S., Lirer, F., Vezzoli, L., Barra, M., De Lange, G. J., Tiepolo,  
105 M., Vallefouco, M., Mazzola, S., and Sprovieri, M. (2014). Tephrochronology of the  
106 astronomically-tuned KC01B deep-sea core, Ionian Sea: Insights into the explosive  
107 activity of the Central Mediterranean area during the last 200ka. *Quaternary Science*  
108 *Reviews*, 85:63–84.
- 109 Keller, J., Ryan, W. B., Ninkovich, D., and Altherr, R. (1978). Explosive volcanic activity  
110 in the Mediterranean over the past 200,000 yr as recorded in deep-sea sediments.  
111 *Bulletin of the Geological Society of America*, 89(4):591–604.
- 112 Le Bas, M. J., Maitre, R. W., Streckeisen, A., and Zanettin, B. (1986). A chemical  
113 classification of volcanic rocks based on the total alkali-silica diagram. *Journal of*  
114 *Petrology*, 27(3):745–750.
- 115 Leicher, N., Zanchetta, G., Sulpizio, R., Giaccio, B., Wagner, B., Nomade, S., Francke,  
116 A., and Carlo, P. D. (2016). First tephrostratigraphic results of the DEEP site record  
117 from Lake Ohrid (Macedonia and Albania). *Biogeosciences*, 13:2151–2178.
- 118 Margari, V., Pyle, D., Bryant, C. L., and Gibbard, P. (2007). Mediterranean tephra  
119 stratigraphy revisited: Results from a long terrestrial sequence on Lesvos Island,  
120 Greece. *Journal of Volcanology and Geothermal Research*, 163(1):34–54.
- 121 Matthews, I. P., Trincardi, F., Lowe, J. J., Bourne, A. J., MacLeod, A., Abbott, P. M.,  
122 Andersen, N., Asioli, A., Blockley, S. P., Lane, C. S., Oh, Y. A., Satow, C. S., Staff,

- 123 R. A., and Wulf, S. (2015). Developing a robust tephrochronological framework for  
124 Late Quaternary marine records in the Southern Adriatic Sea: New data from core  
125 station SA03-11. *Quaternary Science Reviews*, 118:84–104.
- 126 Mouralis, D., Pastre, J. F., Kuzucuoğlu, C., Türkcan, A., and Guillou, H. (2019).  
127 Tephrostratigraphy and chronology of the quaternary gölludağ and acıgöl volcanic  
128 complexes (central anatolia, turkey). *Mediterranean Geoscience Reviews*, 1(2):179–  
129 202.
- 130 Narcisi, B. (2002). Tephrostratigraphy of the Late Quaternary lacustrine sediments of  
131 Lago di Pergusa ( central Sicily ). *Italian Journal of Geosciences*, 121:211–219.
- 132 Pappalardo, L., Civetta, L., D’Antonio, M., Deino, A., Di Vito, M., Orsi, G., Carandente,  
133 A., De Vita, S., Isaia, R., and Piochi, M. (1999). Chemical and Sr-isotopical evolu-  
134 tion of the Phlegraean magmatic system before the Campanian Ignimbrite and the  
135 Neapolitan Yellow Tuff eruptions. *Journal of Volcanology and Geothermal Research*,  
136 91(2-4):141–166.
- 137 Paterne, M., Guichard, F., and Labeyrie, J. (1988). Explosive activity of the South Italian  
138 volcanoes during the past 80,000 years as determined by marine tephrochronology.  
139 *Journal of Volcanology and Geothermal Research*, 34(3-4):153–172.
- 140 Platevoet, B., Scaillet, S., Guillou, H., Blamart, D., Nomade, S., Massault, M., Poisson,  
141 A., Elitok, Ö., Özgür, N., Yagmurlu, F., and Yilmaz, K. (2008). Pleistocene eruptive  
142 chronology of the Gölcük volcano, Isparta Angle, TurkeyChronologie des épisodes  
143 volcaniques pléistocènes du volcan Gölcük, Angle d’Isparta, Turquie. *Quaternaire*,  
144 2(19):147–156.
- 145 Satow, C., Tomlinson, E. L., Grant, K. M., Albert, P. G., Smith, V. C., Manning, C. J.,  
146 Ottolini, L., Wulf, S., Rohling, E. J., Lowe, J. J., Blockley, S. P., and Menzies,  
147 M. A. (2015). A new contribution to the Late Quaternary tephrostratigraphy of the  
148 Mediterranean: Aegean Sea core LC21. *Quaternary Science Reviews*, 117:96–112.
- 149 Scaillet, S., Vita-Scaillet, G., and Rotolo, S. G. (2013). Millennial-scale phase rela-  
150 tionships between ice-core and Mediterranean marine records: Insights from high-  
151 precision  $^{40}\text{Ar}/^{39}\text{Ar}$  dating of the Green Tuff of Pantelleria, Sicily Strait. *Quaternary  
152 Science Reviews*, 78:141–154.
- 153 Siani, G., Sulpizio, R., Paterne, M., and Sbrana, A. (2004). Tephrostratigraphy study  
154 for the last 18,000  $^{14}\text{C}$  years in a deep-sea sediment sequence for the South Adriatic.  
155 *Quaternary Science Reviews*, 23(23):2485–2500.
- 156 Smith, V. C., Isaia, R., and Pearce, N. J. (2011). Tephrostratigraphy and glass composi-  
157 tions of post-15 kyr Campi Flegrei eruptions: Implications for eruption history and  
158 chronostratigraphic markers. *Quaternary Science Reviews*, 30(25-26):3638–3660.
- 159 Tamburino, S., Insinga, D. D., Sprovieri, M., Petrosino, P., and Tiepolo, M. (2012).  
160 Major and trace element characterization of tephra layers offshore Pantelleria Island:  
161 Insights into the last 200 ka of volcanic activity and contribution to the Mediterranean  
162 tephrochronology. *Journal of Quaternary Science*, 27(2):129–140.

- 163 Tomlinson, E. L., Albert, P. G., Wulf, S., Brown, R. J., Smith, V. C., Keller, J., Orsi, G.,  
164 Bourne, A. J., and Menzies, M. A. (2014). Age and geochemistry of tephra layers  
165 from Ischia, Italy: Constraints from proximal-distal correlations with Lago Grande di  
166 Monticchio. *Journal of Volcanology and Geothermal Research*, 287:22–39.
- 167 Tomlinson, E. L., Arienzo, I., Civetta, L., Wulf, S., Smith, V. C., Hardiman, M., Lane,  
168 C. S., Carandente, A., Orsi, G., Rosi, M., Müller, W., and Menzies, M. A. (2012a). Geo-  
169 chemistry of the Phlegraean Fields (Italy) proximal sources for major Mediterranean  
170 tephras: Implications for the dispersal of Plinian and co-ignimbritic components of  
171 explosive eruptions. *Geochimica et Cosmochimica Acta*, 93:102–128.
- 172 Tomlinson, E. L., Kinvig, H. S., Smith, V. C., Blundy, J. D., Gottsmann, J., Müller, W.,  
173 and Menzies, M. A. (2012b). The Upper and Lower Nisyros Pumices: Revisions to the  
174 Mediterranean tephrostratigraphic record based on micron-beam glass geochemistry.  
175 *Journal of Volcanology and Geothermal Research*, 243-244:69–80.
- 176 Tomlinson, E. L., Smith, V. C., Albert, P., Aydar, E., Civetta, L., Cioni, R., Çubukçu, E.,  
177 Gertisser, R., Isaia, R., Menzies, M. A., Orsi, G., Rosi, M., and Zanchetta, G. (2015).  
178 The major and trace element glass compositions of the productive Mediterranean  
179 volcanic sources: tools for correlating distal tephra layers in and around Europe.  
180 *Quaternary Science Reviews*.
- 181 Vogel, H., Wagner, B., Zanchetta, G., Sulpizio, R., and Rosén, P. (2010). A paleoclimate  
182 record with tephrochronological age control for the last glacial-interglacial cycle from  
183 Lake Ohrid, Albania and Macedonia. *Journal of Paleolimnology*, 44(1):295–310.
- 184 Watts, W. A., Allen, J. R., and Huntley, B. (1996). Vegetation history and palaeoclimate  
185 of the last glacial period at Lago Grande di Monticchio, southern Italy. *Quaternary  
186 Science Reviews*, 15(2-3):133–153.
- 187 Wulf, S., Hardiman, M. J., Staff, R. A., Koutsodendris, A., Appelt, O., Blockley, S. P.,  
188 Lowe, J. J., Manning, C. J., Ottolini, L., Schmitt, A. K., Smith, V. C., Tomlinson,  
189 E. L., Vakhrameeva, P., Knipping, M., Kotthoff, U., Milner, A. M., Müller, U. C.,  
190 Christianis, K., Kalaitzidis, S., Tzedakis, P. C., Schmiedl, G., and Pross, J. (2018).  
191 The marine isotope stage 1–5 cryptotephra record of Tenaghi Philippon, Greece:  
192 Towards a detailed tephrostratigraphic framework for the Eastern Mediterranean  
193 region. *Quaternary Science Reviews*, 186:236–262.
- 194 Wulf, S., Kraml, M., Brauer, A., Org Keller, J., Org, J., and Negendank, F. W. (2004).  
195 Tephrochronology of the 100 ka lacustrine sediment record of Lago Grande di Montic-  
196 chio (southern Italy). *Quaternary International*, 122:7–30.
- 197 Wulf, S., Kraml, M., and Keller, J. (2008). Towards a detailed distal tephrostratigraphy in  
198 the Central Mediterranean: The last 20,000 yrs record of Lago Grande di Monticchio.  
199 *Journal of Volcanology and Geothermal Research*, 177(1):118–132.
- 200 Wutke, K., Wulf, S., Hardiman, M., Dulski, P., Luterbacher, J., and Brauer, A. (2015).  
201 Geochemical properties and environmental impacts of seven Campanian tephra layers  
202 deposited between 40 and 38 ka BP in the varved lake sediments of Lago Grande di

- 203 Monticchio, southern Italy. *Quaternary Science Reviews*, 118:67–83.
- 204 Zanchetta, G., Giraudi, C., Sulpizio, R., Magny, M., Drysdale, R. N., and Sadori, L.
- 205 (2012). Constraining the onset of the Holocene "Neoglacial" over the central Italy
- 206 using tephra layers. *Quaternary Research (United States)*, 78(2):236–247.

1 This file contains the code for the OxCal model from “The tephrochronology of Lake  
2 Ioannina, NW Greece, from ca.46-4 ka BP” by McGuire et al.

```
3 Options()
4 {
5     SD1=FALSE;
6     SD2=TRUE;
7     SD3=TRUE;
8 }
9 Plot()
10 {
11     Outlier_Model("RScaled", T(5), U(0,4), "r");
12     Outlier_Model("SSimple", N(0,2), 0, "s");
13     P_Sequence("I-08 (McGuire et al., 2020)", 100, 10, U(-2,2))
14 {
15     Boundary("Base - 36.48 m")
16 {
17     z=36.48;
18 }
19 C_Date("PGT", -45700, 500)
20 {
21     Outlier("RScaled", 0.05);
22     z=31.93;
23 }
24 C_Date("CI_Base", -39785, 140)
25 {
26     Outlier("RScaled", 0.05);
27     z=30.14;
28 }
29 C_Date("CI_Top", -39784, 140, 140)
30 {
31     Outlier("RScaled", 0.05);
32     z=29.96;
33 }
34 Date("I08T_28.98")
35 {
36     z=28.98;
37 }
38 R_Date("SUERC-26419", 23028, 168)
39 {
40     Outlier("RScaled", 0.05);
```

```

41      z=18.60;
42  } ;
43 R_Date("ETH-39795",19888,355)
44 {
45   Outlier("RScaled", 0.05);
46   z=17.08;
47 } ;
48 Date("I08_T16.07")
49 {
50   z=16.07;
51 } ;
52 Date("I08_T15.23")
53 {
54   z=15.23;
55 } ;
56 R_Date("ETH-39794",11387,194)
57 {
58   Outlier("RScaled", 0.05);
59   z=15.08;
60 } ;
61 R_Date("SUERC-26418",7091,38)
62 {
63   Outlier("RScaled", 0.05);
64   z=14.67;
65 } ;
66 R_Date("I08_T14.39",7770,40)
67 {
68   Outlier("RScaled", 0.05);
69   z=14.39;
70 } ;
71 R_Combine("I08_13.95")
72 {
73   R_Date("ETH-39792",6279,138);
74 {
75   Outlier("SSimple", 0.05);
76 } ;
77 R_Date("ETH-39793",6249,169);
78 {
79   Outlier("SSimple", 0.05);
80 } ;

```

```
81     R_Date("ETH-39791", 6141, 81);
82     {
83         Outlier("SSimple", 0.05);
84     };
85     Outlier("RScaled", 0.05);
86     z=13.95;
87 };
88 R_Date("ETH-39789", 3260, 118)
89 {
90     Outlier("RScaled", 0.05);
91     z=12.20;
92 };
93 Boundary("Surface")
94 {
95     z=10;
96 };
97 };
98 };
99
100
```